



Universidad de Valladolid



**PROGRAMA DE DOCTORADO EN TECNOLOGÍAS DE LA INFORMACIÓN Y
LAS TELECOMUNICACIONES**

TESIS DOCTORAL:

**Signal processing techniques for agro-industrial machinery
monitoring**

Presentada por Rubén Ruiz González para optar al grado de
Doctor por la Universidad de Valladolid

Dirigida por:

Jaime Gómez Gil
Francisco Javier Gómez Gil
Luis Manuel Navas Gracia

Abstract

Signal processing techniques have lately been becoming more and more important in many agro-industrial applications. This signal processing-oriented approach is enabling new perspectives for many areas in the agro-industrial environment, such as real-time machinery monitoring, among others.

The main goal of this thesis is to design, implement, and assess specific signal processing techniques enabling the monitoring of agro-industrial equipment in three senses: predictive maintenance, vehicle tracking, and measurement equipment. The proposed techniques contribute by expanding and extending, and even pioneering, current state-of-the-art techniques.

The methodology followed along this thesis in order to reach the intended goals can be divided into five stages: review of the state of the art, hypothesis formulation, development and evaluation, result analysis, and results publication. The review of the state of the art was conducted in order to learn about other already existing techniques. After that, a research hypothesis was formulated to be used as the inception point of the research. Then, in the development and evaluation stage, an experimental setup was designed to develop and assess the proposed signal processing techniques. In the result analysis stage, the obtained results were compared against the literature. From this comparison, the validity of the research hypothesis could be checked. Finally, whenever redefinition of the research hypothesis was mandatory, the methodology went back to the hypothesis formulation stage. If the hypothesis was deemed to be valid, the obtained results were published.

The aforementioned methodology was applied to three different agro-industrial problems: the predictive maintenance of an agricultural harvester, the kinematic tracking of a vehicle, and the monitoring of the flow rate through each individual nozzle in agricultural sprayers. A predictive maintenance approach, based on signal processing of the acquired mechanical vibration signals from an accelerometer placed on the chassis of an agricultural harvester, was proposed to estimate the mechanical status of several components of the machinery before it irretrievably cracks (first article of the compendium). A kinematic tracking approach, based on gathering several motion-related data and applying data fusion techniques, was proposed to enable a more accurate mechanical status estimation of a vehicle (second article of the compendium). An acoustic-based flow rate measurement approach, based on signal processing of the acquired acoustic signal gathered by a nearby microphone, was proposed to estimate, in real time, the actual flow rate coming out of each nozzle in agricultural sprayers (third article of the compendium).

Three different experimental setups were used for each one of the three aforementioned agro-industrial problems tackled in this thesis. These setups were carefully designed so as to properly assess the developed methods.

Three main features of the proposed methods highlight over the rest. The first one is that all proposed methods satisfy the intended goals with high enough accuracy. The second feature is that all proposed methods lead to affordable, inexpensive systems. The last feature is the optimization of the methods, leading to less computational needs as compared to other existing approaches. This feature enables these methods to be used in real-time applications.

The results obtained in this thesis are proof of the capability of the proposed signal processing techniques to enable monitoring of agro-industrial machinery. There are two main general conclusions that can be drawn from these results. The first one is that signal processing techniques can extract useful information related to agro-industrial problems. The second conclusion is that all proposed solutions tend to be more cost-effective, more accurate, and easier to deploy as compared to existing solutions. Three main particular conclusions, one for each of the three tackled agro-industrial problems, highlight over the rest: *(i)* signal processing techniques can successfully be applied for monitoring machinery components without removing and isolating them, even while in normal operating conditions; *(ii)* real-time monitoring of flow rate from individual nozzles in agricultural sprayers can be achieved by processing the acoustic signal in their surroundings; and *(iii)* kinematic monitoring of agro-industrial vehicles can be improved by using signal processing techniques for data fusion of GNSS and on-vehicle sensors data.

Keywords

Agricultural, classification, data fusion, industrial, monitoring, predictive maintenance (PdM), regression, signal processing, support vector machines (SVM).

Resumen

En los últimos tiempos, las técnicas de procesado de señal han ido ganando importancia dentro de numerosas aplicaciones industriales. Estos enfoques orientados al procesado de señal están abriendo nuevas perspectivas en muchas áreas del ámbito agro-industrial, destacando entre ellas la monitorización de maquinaria.

El principal objetivo de esta tesis es el diseño, implementación y evaluación de esquemas de procesado de señal específicos que permitan la monitorización de equipamiento agro-industrial en tres sentidos: mantenimiento predictivo, seguimiento de vehículos y equipos de medida. Las técnicas propuestas en esta tesis contribuyen al estado del arte, expandiendo o extendiendo técnicas existentes, e incluso proponiendo esquemas completamente novedosos.

La metodología seguida a lo largo de esta tesis, con objeto de alcanzar los objetivos marcados, se puede dividir en cinco etapas: revisión del estado del arte, formulación de hipótesis, desarrollo y evaluación, análisis de resultados y publicación de resultados. La revisión del estado del arte fue llevada a cabo para aprender sobre otras técnicas similares ya existentes. Seguidamente, se formuló la hipótesis de investigación, que fue empleada como punto de partida de esta tesis. Con ello, en la etapa de desarrollo y evaluación, se diseñó un escenario experimental en el cuál desarrollar y evaluar las técnicas de procesado de señal propuestas. En la etapa de análisis de resultados, los resultados obtenidos fueron comparados con técnicas similares disponibles en diversas fuentes bibliográficas. Esta comparación hizo posible validar la hipótesis. Cuando los resultados así lo sugerían, la hipótesis de partida era modificada y todas las etapas anteriores se repetían nuevamente. Si la hipótesis, original o modificada, era validada, los resultados eran publicados en revistas y congresos científicos.

Dicha metodología ha sido aplicada a tres problemas agro-industriales diferentes: mantenimiento predictivo de una cosechadora agrícola, seguimiento cinemático de un vehículo y monitorización del flujo a través de cada una de las boquillas en un pulverizador agrícola. Un enfoque de mantenimiento predictivo, basado en el procesado de una señal de vibración mecánica adquirida por un acelerómetro situado en el chasis de la cosechadora agrícola, fue propuesto para estimar el estado mecánico de diversos componentes de la maquinaria con el fin de evitar roturas irreparables (primer artículo del compendio). Un enfoque de seguimiento de vehículos, basado en recuperar datos relativos a su estado cinemático y fusionarlos, fue propuesto para permitir una estimación más precisa del estado cinemático de un vehículo (segundo artículo del compendio). Un enfoque de medición acústica de flujo, basado en el procesado de la señal adquirida con un micrófono próximo a la boquilla, se propuso para estimar, en tiempo real, el flujo saliente por cada una de las boquillas en un pulverizador agrícola (tercer artículo del compendio).

Tres escenarios experimentales han sido utilizados para cada uno de los tres problemas agro-industriales en los que se centra esta tesis. Estos escenarios fueron cuidadosamente diseñados para poder evaluar adecuadamente los métodos desarrollados.

Tres características principales de los métodos propuestos destacan sobre el resto. La primera es que todos los métodos satisfacen los objetivos con una precisión suficiente. La segunda característica es que todos los métodos propuestos conducen a sistemas que son asequibles y baratos. La última característica es la optimización de los métodos, que conduce a menores necesidades computacionales en comparación con otros enfoques existentes. Esta última propiedad hace que estos métodos puedan emplearse en aplicaciones con requisitos de tiempo real.

Los resultados obtenidos en esta tesis ofrecen muestras de la capacidad de monitorizar maquinaria agro-industrial ofrecida por los métodos de procesamiento de señal. Hay dos conclusiones principales que se puede extraer de estos resultados. La primera es que las técnicas de procesamiento de señal pueden obtener información útil relativa a los problemas agro-industriales abordados. La segunda conclusión es que las soluciones propuestas tienden a proporcionar mayor precisión, mejor relación efectividad-coste y son más fáciles de desplegar, en comparación con otras alternativas existentes. Tres conclusiones particulares principales, una para cada uno de los tres problemas agro-industriales abordados, destacan sobre el resto: *(i)* las técnicas de procesamiento de señal puede aplicarse de manera exitosa para la monitorización de componentes de maquinaria sin necesidad de retirarlas y aislarlas, incluso mientras la maquinaria está funcionando en condiciones normales; *(ii)* el flujo de cada boquilla de un pulverizador agrícola se puede monitorizar en tiempo real empleando procesamiento de la señal acústica adquirida en los alrededores de la boquilla; y *(iii)* se puede mejorar la monitorización cinemática de vehículos agro-industriales empleando técnicas de procesamiento de señal para fusionar datos procedentes de los sensores del vehículo con datos de posicionamiento GNSS.

Palabras clave:

Agrícola, clasificación, fusión de datos, industrial, mantenimiento predictivo (PdM), máquinas de soporte vectorial (SVM), monitorización, procesamiento de señal, regresión.

Acknowledgements

This thesis is the outcome of several (some of my closest ones may say too many) years researching at Department of Signal Theory and Communications and Telematics Engineering in the University of Valladolid. It may sound cliché, but without the help, support and effort of many many people I would have never been able to make it through this process. To everyone, it goes my gratitude and recognition.

Let's start with the obvious: without my parents I would not even exist at all. You have suffered more than anyone throughout all those years, specially my absences while being abroad. I will never get to show you how grateful I am to you. Everything I have reached is because of you. Thanks for always being such a good model for me. I love you with all of my heart!

A similar recognition is deserved by my brother and sister. We have shared so many memories together, which have shaped me into who I am nowadays, that is impossible not to credit yourselves for this accomplishment. I love you, guys!

Third, but not less important, to my better half. I could not be any more grateful than I am to research. Not just professionally, but personally. I would have never expected to meet the love of my life during a scholarship abroad. Thanks for your love, support, understanding, encouragement, believing in me, and always making me strive for better, Maiara!

A remarkable acknowledgement goes to my advisors Jaime, Francisco Javier and Luis Manuel. Thanks for your confidence and support throughout this process. Without your help and orientation I would have got lost along those years. A special mention goes to Jaime. We have shared a lot of time together and you have become not just an amazing mentor but a good friend to me. Don't ever change your humble way of being and your closeness with your students. It has been an honor to have you both as professor and an advisor during these years and it will be my pleasure to be your friend forever.

To my grandparents, for having raised such amazing parents and for the moments I could manage to share with you. Thanks for always believing in me and encouraging me. May God rest your souls in peace.

To all my lab partners. Thanks for your help during this whole process and for standing my non-stop talking from time to time.

To my friends, for supporting me, even when you didn't understand why I was dedicating my time on research, and for distracting me from my worries. I'm honored to have such a few but amazing friends.

To the undergraduate students I have advised: Carlos, Lidia, and Rubén. Thanks for letting me teach you something and for having taught me so much in exchange.

I want also to express my gratitude for the opportunity to enjoy four research stays in two international research groups. First, I have to thank the Biosystems and Agriculture Department of the University of Kentucky (USA) and Tim Stombaugh for the opportunity to do two stays to work with his research group. It was very profitable because of the chance to work with a multidisciplinary group, to use their facilities to perform experiments, to meet amazing people, and to improve my English. Second, I have to thank the Departamento de Engenharia Agrícola of the Universidade Federal de Viçosa (Brazil) for their support, allowing me to collaborate with them, meet awesome people, and learn Portuguese too. Thank you to all of you: Tim, Francisco, and Flora, as well as all the rest of the amazing people I met during my stays.

To all my students. Lecturing while doing my PhD has given me an enormous personal satisfaction. Thanks for having helped me, allowing me to change my thoughts for a while during the lessons and encouraging me to never stop learning.

I also need to express my gratitude to my university (University of Valladolid), together with Banco Santander, for the grant that has allowed me to undertake this research as well as some of my scholarships abroad.

I cannot forget about thanking Javier, who directly contributed with useful help for my entire thesis with productive and valuable feedback.

My most sincere acknowledgement also goes to the two reviewers of the thesis, who have hugely contributed to enhance the final version of this thesis.

By last, I would not want to forget about anyone who should be credited in this section: colleagues from the department who have shared my worries and frustrations and have encouraged me into succeeding, people from all over the world that I have met during all those years, etc. Some of you have become good friends, but surely none will ever be forgotten.

If I have really enjoyed so much this stage of my life is because you all, so thank you very much to you all from the bottom of my heart!

Contents

Abstract	i
Resumen	iii
Acknowledgements	v
Contents	vii
List of Figures	ix
List of acronyms	xi
I Introduction to the compendium	1
1. Contextualization.....	3
2. Algorithms involved	5
2.1. Supervised learning in machine learning	5
2.2. Data fusion.....	11
3. Motivation and hypothesis formulation.....	13
4. Objectives	15
5. Methodology.....	17
6. Articles in the compendium and their relationship.....	19
7. Results	23
7.1. Predictive maintenance monitoring	23
7.2. Vehicle tracking monitoring	24
7.3. Flow rate monitoring	25
8. Conclusions	27
9. Future work.....	31
10. Merits and diffusion of the results	33
10.1. Publications.....	33
10.2. Projects	35
10.3. Research stays.....	35
10.4. Teaching	36
10.5. Other merits	37
II Articles in the compendium	39
Article 1: Predictive maintenance monitoring	41

Article 2: Vehicle tracking monitoring..... 67

Article 3: Flow rate monitoring..... 81

III Articles out of the compendium 95

Article 4: Vehicle tracking monitoring..... 97

Article 5: Predictive maintenance monitoring..... 99

Bibliography 101

List of Figures

Figure 1. Representation of a Support-Vector Machine classifier corresponding to (a) a linearly separable pattern, where the hyperplane totally separates green circles from red squares, and (b) a non-linearly separable pattern, where no hyperplane separates all the green circles from the red squares.	8
Figure 2. Representation of a Support-Vector Machine classifier with a nonlinear kernel. Function $\varphi(\cdot)$ is the nonlinear transformation mapping vectors from (a) the input space to (b) the feature space.	9
Figure 3. Architecture of a Support-Vector Machine classifier. Inner product kernels, $K(\cdot, \cdot)$, denote the m_0 -dimensional kernel inner product of the input vector with each of the N_s Support Vectors.	10
Figure 4. Stage diagram of the Kalman filtering loop.	11
Figure 5. Block diagram of the methodological stages of this thesis and their relationships. ...	17
Figure 6. Relationship between three articles composing this thesis.	20
Figure 7. Data acquisition setup for predictive maintenance monitoring. An accelerometer was placed on the structure of the machine, connected by means of a cable to an acquisition system, and a laptop was used to register and visualize the acquired data.	24
Figure 8. Data acquisition setup for vehicle tracking monitoring. An accurate GPS receiver, shown in foreground, was placed on top of the car to use as reference for comparison of the results coming from the data fusion approach.	25
Figure 9. Data acquisition setup for flow rate monitoring. A microphone was placed close to the nozzle to acquire the acoustic signal while water was flowing out of it. The signal acquired by the microphone was digitalized by an acquisition system, and a laptop was used to record the data.	26

List of acronyms

ANN	<i>Artificial Neural Network</i>
CFD	<i>Computational Fluid Dynamics</i>
EKF	<i>Extended Kalman Filter</i>
GNSS	<i>Global Navigation Satellite System</i>
IMU	<i>Inertial Measurement Unit</i>
IoT	<i>Internet of Things</i>
KF	<i>Kalman Filter</i>
LS	<i>Least Squares</i>
OBD	<i>On-Board Diagnostics</i>
PdM	<i>Predictive Maintenance</i>
RBF	<i>Radial Basis Functions</i>
SVM	<i>Support-Vector Machine</i>

I Introduction to the compendium

The first chapter of this document presents an introduction for this doctoral thesis by compendium of publications. The first section presents a general overview for the reader to understand the underlying research context. The second section briefly introduces the main processing algorithms employed throughout this thesis. The third section formulates the research hypothesis guiding this whole thesis. The fourth section deals with the addressed objectives. The fifth section presents the methodology employed to reach the intended objectives. The sixth section focuses on clarifying the links between the articles comprising this thesis. The seventh section summarizes the results obtained during the thesis. The eighth section presents the main conclusions of this thesis. The ninth section suggests some possible future work to do after this thesis. Finally, the tenth section briefly presents all the activities done during this thesis and the main results obtained from it.

1. Contextualization

More and more areas are benefiting from signal processing techniques since its inception steps. From medicine (Unser & Aldroubi, 1996) to economics (White, 1988), including many other more related areas, almost all imaginable areas can make substantial profit from using signal processing techniques.

Signal processing techniques have been becoming increasingly important in the agro-industrial field in the recent years (Jardine, Lin, & Banjevic, 2006; Liakos, Busato, Moshou, Pearson, & Bochtis, 2018; Staszewski, 2002). The introduction of this kind of techniques in the agro-industrial environment is enabling new perspectives for many areas (Smith & Shankar, 2018), such as machinery monitoring, drones and IoT for crop monitoring, remote sensing, precision spraying, robotics, machine learning, among others.

In this context, this thesis aims at investigating and proposing new signal processing-based approaches for machinery monitoring in the agricultural and industrial fields. In particular, this thesis focuses on three subareas of one of such areas, namely machinery monitoring: predictive maintenance, vehicle tracking, and measurement instrument. Agro-industrial equipment demands for ways to monitor its behavior, so as to enable the machinery operator to adjust in real time while working (Zhang, Wang, & Wang, 2002).

Agro-industrial machinery has many components that require an accurate monitoring so as to perform well when conducting their work. Some prototypical examples of magnitudes that need for accurate estimations while operating are kinematic properties, namely, position, speed, and so on. However, there exist other important magnitudes that are relevant to achieve the goals of precision agriculture, such as sprayed chemicals, rotating components status, among others.

Agro-industrial machinery is prone to suffer from wear due to its use, being advisable a proper early supervision in order to avoid large expenditures in maintenance. Thus, machinery predictive maintenance is compulsory whenever an efficient handling is desired. Inspections performed by qualified operators have traditionally been the most common way to undertake those maintenance tasks. Nevertheless, lately, new automatic procedures have appeared thanks to signal processing techniques (Han & Yang, 2006). Those approaches, though, need for component isolation before analyzing its condition. A new method, enabling automatic predictive maintenance of all components simultaneously while operating, seems to be in much need.

Agro-industrial vehicles do also require an accurate estimation of their kinematic properties. A well-known example is automatic guidance in agricultural tasks (Keicher & Seufert, 2000). Nevertheless, systems merely based on GNSS data are prone to suffer from inaccuracies or even outages, which could be catastrophic. As a consequence, current systems employ a data fusion scheme to incorporate IMU sensors (Caron, Duflos, Pomorski, & Vanheeghe, 2006) or other relevant sources of information. On-vehicle sensors accessible via OBD-II communication standard is a viable and economic option.

Agro-industrial machinery exhibits other equipment demanding for measuring devices. Those measuring devices are employed to control other magnitudes that are paramount for proper operation in precision agriculture. The sprayed quantity of chemicals is a variable of great importance when spreading pesticides, fungicides or herbicides on a crop (Tellaeché, BurgosArtizzu, Pajares, Ribeiro, & Fernández-Quintanilla, 2008). A mistaken quantity may lead to damaging the crops or reducing the yield. The flow rate measurement devices currently used are expensive, making completely unaffordable to employ one for each nozzle in an agricultural sprayer with over sixteen nozzles. Thus, an acoustics-based device, requiring an inexpensive microphone, could be used instead, realizing that the nearby acoustic signal depends on the flow rate coming out of the nozzle.

In this context, this thesis focuses on the application of signal processing techniques to solve the three aforementioned problems in the agricultural and industrial fields, namely: predictive maintenance, vehicle tracking, and measurement devices.

2. Algorithms involved

Several well-known algorithms are involved in the proposed signal processing techniques from this thesis. This section deals with a brief summary of them to serve as a basic introduction for the interested reader.

2.1. Supervised learning in machine learning

Machine learning, as a sub-field of artificial intelligence, deals with intelligent systems that can modify their behavior in accordance with the input data. Those intelligent systems must have the capability of deducing the function that best fits the input data, in order to learn from the data. Supervised learning is a branch of machine learning. Supervised learning builds an input to output mapping based on sample known input-output pairs. It is opposed to unsupervised learning, where learning happens without being given any known input-output mapping. Supervised learning algorithms employ training data in order to generate an inferred function or mapping. This generated function is to be used for future mapping of new data. Learning algorithms are required to generalize well to possible data discrepancies in the test set.

2.1.1. Regression

Regression is a branch of supervised learning, even though classical approaches appeared before machine learning techniques even existed. It aims at estimating the relationships between a dependent variable and one or more independent variables. Regression helps understand how the dependent variable depends on the independent variables.

Regression involves the following variables and parameters:

- The unknown parameters, denoted as $\boldsymbol{\beta}$.
- The independent variables, denoted as \boldsymbol{x} .
- The dependent variable, denoted as \boldsymbol{y} .

Regression relates \boldsymbol{y} to a function (f) of \boldsymbol{x} and $\boldsymbol{\beta}$, i.e. $\boldsymbol{y} \approx f(\boldsymbol{x}, \boldsymbol{\beta})$. This function, f , is typically chosen to fit well the underlying relationship between data, but generic adaptable polynomial functions are also commonly used when no prior knowledge about this relationship is at hand.

There exist several methods to accomplish regression, as can be seen in the literature (Sheather, 2009). As far as this thesis is involved, nonlinear regression with data linearization was employed. More specifically, a square root-like function was fitted by means of data linearization plus least squares (LS) technique.

$$y = \sqrt[n]{(a + b \cdot x)^m} \quad (1)$$

with m and n being known constants, and a and b being the parameters to be fitted.

It can be rearranged so that LS fitting can be performed between y' and x :

$$y' = y^{\frac{n}{m}} = a + b \cdot x \quad (2)$$

2.1.2. Classification

Classification, as a branch of supervised learning, is defined as the process of identifying the class to which a previously unseen observation belongs, based on previous knowledge given by a training dataset that contains instances the category membership of which is certain. Any algorithm which performs classification tasks –i.e. the mapping of input data to an assigned class– is called a classifier.

Classifiers must be trained, based on previous knowledge, in order to function properly. The training process makes use of a sample of N observations, the corresponding classes of which are certain. This sample of N observations is typically divided into two subsamples: the training and the test datasets. Firstly, the training dataset is used in the process of computing a classifier that is well-adapted to these data. Then the test dataset is used to assess the generalization capability of the previously computed classifier.

Both the misclassification rate and the success rate in the test dataset are commonly used as quality measurements to assess classifier performance. The misclassification rate is defined as the proportion of observations which are wrongly assigned to an incorrect class. It is expressed as follows:

$$MR = \frac{\text{Number of Incorrect Classifications}}{\text{Total Number of Classifications}} \quad (3)$$

Alternatively, the success rate (also called the hit rate) is defined as the proportion of observations that are properly assigned to the corresponding class and is calculated as follows:

$$SR = \frac{\text{Number of Correct Classifications}}{\text{Total Number of Classifications}} = 1 - MR \quad (4)$$

The *k-fold cross-validation* is an enhanced method of evaluating classifier performance, especially with small training and test datasets. In this method, the original sample of N observations is randomly partitioned into k subsamples of equal size. From those k subsamples, a single subsample is retained as the test dataset, and the remaining $k - 1$ subsamples are used as the training dataset. The *k-fold cross-validation* repeats this training and test process k times, using each of the k subsamples only once as the test dataset. Cross-validation accuracy is

calculated as the average of the success rate obtained for each of the k different test datasets. When $k=N$, k -fold cross-validation is also known as *leave-one-out cross-validation*.

Many different classifiers have been proposed in the literature (Jain, Duin, & Mao, 2000; Kotsiantis, 2007). Some of the main ones include k -nearest neighbor classifier, Bayes classifier, logistic regression, Fisher's linear discriminant, decision tree, Artificial Neural Networks (ANN), and Support-Vector Machine (SVM). SVM classifier is described in greater detail in subsection 2.1.3.

2.1.3. Support Vector Machines (SVM)

Support-Vector Machine (SVM) is a statistical supervised machine learning technique, used both for classification and for regression purposes. Originally proposed by Vapnik and Cortes (Cortes & Vapnik, 1995; Vapnik, 1998), in 1995, although its principles and derivation differ from those of Artificial Neural Networks (ANN), some authors sometimes consider SVMs as a special kind of ANN (Haykin, 1998). However, many authors refuse to do so, due to essential differences between SVM and ANN techniques (Ren, 2012). While SVM mechanisms are mainly based on a rigorous geometrical and statistical approach, ANNs try to emulate the behavior of the human brain and its neural system.

The original SVM proposal was aimed at both the binary classification problem, considering only two possible classification classes, and the multiclass classification problem, which considers more than two classification classes.

Binary linear SVM classification performs the calculation of the optimal hyperplane decision boundary, separating one class from the other, on the basis of a training dataset. Optimality can be understood, depending on whether perfect classification of the training dataset is feasible and desired, in two separate ways:

- If perfect separability of training dataset classes can be achieved, a Hard Margin optimality can be used. In this case, the hyperplane decision boundary is chosen to maximize the distance from the hyperplane to the nearest training data point.
- If perfect classification is not desired or if it is impossible, a Soft Margin optimality is used. In this case, the hyperplane selection is a customizable tradeoff between minimizing the misclassification rate and maximizing the distance to the nearest properly classified training point.

The decision boundary hyperplane in SVM classification is calculated by employing the training dataset. This decision boundary is completely determined by the so-called Support Vectors, a subset of training input vectors which by themselves alone lead to the same decision boundary. After this hyperplane is determined, the SVM classifier is ready to be used with a different dataset from the one used in the training stage. The assigned class, labeled either +1 or -1, depends on the side of the decision boundary on which the input vector falls. Figure 1 represents a graphical example of linear SVM-based classification, both in the case of linearly separable classes and non-linearly separable classes.

SVM multiclass classification usually tackles the classification and computation of the decision boundary, by reducing the problem to a set of binary classification problems. The main such approaches are *pairwise* and *one-versus-all* classification methods (Hsu & Lin, 2002). Compact multiclass reformulations of the binary classification problem have also been proposed (Hsu & Lin, 2002).

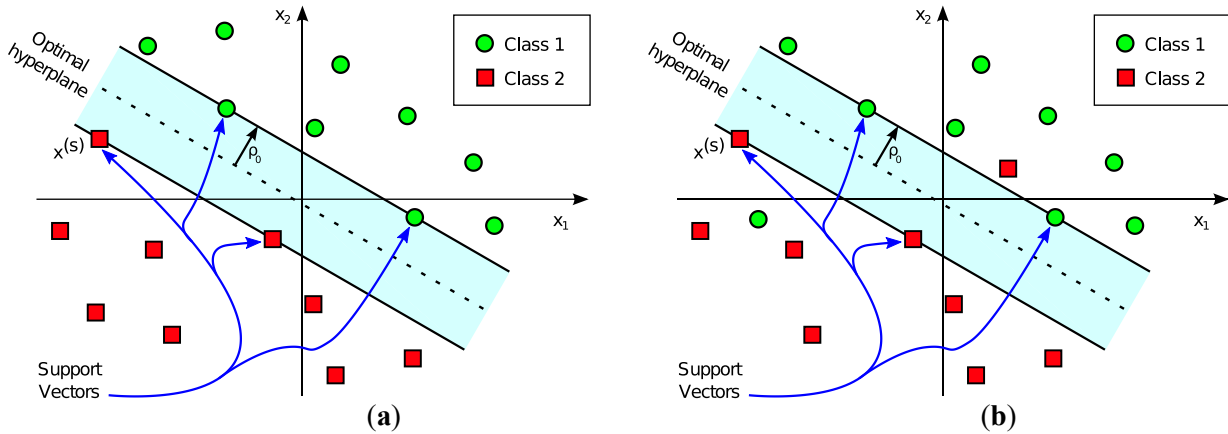


Figure 1. Representation of a Support-Vector Machine classifier corresponding to (a) a linearly separable pattern, where the hyperplane totally separates green circles from red squares, and (b) a non-linearly separable pattern, where no hyperplane separates all the green circles from the red squares.

To be mathematically rigorous, the most general SVM linear binary classification problem can be stated as follows:

“Given a training dataset, $\{\mathbf{x}_i, d_i\}_{i=1}^N$, the goal is to compute the optimal weight vector \mathbf{w} , bias b , and slack variables ξ , such that satisfy the following constraints:

$$\begin{aligned} d_i(\mathbf{w}^T \mathbf{x}_i + b) &\geq 1 - \xi_i, \forall i = 1, 2, \dots, N \\ \xi_i &\geq 0, \forall i = 1, 2, \dots, N \end{aligned} \quad (5)$$

and such that the following cost function is minimized:

$$\Phi(\mathbf{w}, \xi) = \frac{1}{2} \mathbf{w}^T \mathbf{w} + C \sum_{i=1}^N \xi_i \quad (6)$$

where, $\mathbf{x}_i \in \mathbb{R}^{m_0}$ denotes the i -th input vector, $d_i \in \{-1, 1\}$ denotes the class corresponding to the i -th input vector, $\xi = \{\xi_i\}_{i=1}^N$ represents the slack variables, and the constant C is a user-specified parameter that determines the tradeoff between misclassification and maximum inter-class margin.”

In practice, most classification problems cannot be solved by using a simple hyperplane as the decision boundary. In such cases a more complex and elaborate decision boundary is required. SVM achieves this goal by increasing the dimensionality of the input space, of dimension m_0 , by applying a nonlinear transformation, denoted by $\boldsymbol{\varphi}(\cdot)$, into a feature space of dimension $m_f > m_0$ (Figure 2). This transformation, $\boldsymbol{\varphi}(\cdot)$, serves to reduce the

misclassification probability in the transformed feature space. The most typical transformation functions, as in the case of ANNs, are radial basis functions, higher-order polynomials, and sigmoid functions. Figure 2 represents a graphical example of an SVM nonlinear classification.

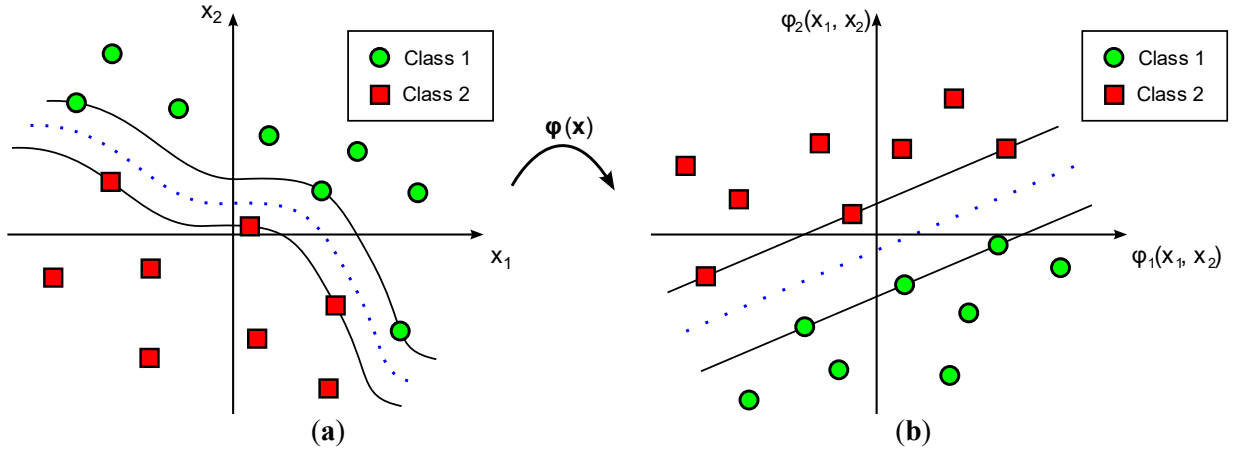


Figure 2. Representation of a Support-Vector Machine classifier with a nonlinear kernel. Function $\boldsymbol{\varphi}(\cdot)$ is the nonlinear transformation mapping vectors from (a) the input space to (b) the feature space.

The boundary in the nonlinear classification problem is still a hyperplane, not in the original input space but in the feature space, and can be expressed as the points $\boldsymbol{\varphi}(\mathbf{x})$ that satisfy that:

$$\mathbf{w}^T \boldsymbol{\varphi}(\mathbf{x}) + b = 0 \quad (7)$$

where, $\mathbf{x} \in \mathbb{R}^{m_0}$ and $\boldsymbol{\varphi}(\mathbf{x}) \in \mathbb{R}^{m_f}$.

Following the application of the Lagrange multipliers method, it has been shown that the optimal weight vector can be expressed as (Haykin, 1998):

$$\mathbf{w} = \sum_{i=1}^N \alpha_i d_i \boldsymbol{\varphi}(\mathbf{x}_i) \quad (8)$$

where, α_i stands for the Lagrange multiplier coefficients.

So, the optimal decision boundary can be rewritten as:

$$\sum_{i=1}^N \alpha_i d_i \boldsymbol{\varphi}(\mathbf{x}_i)^T \boldsymbol{\varphi}(\mathbf{x}) + b = 0 \quad (9)$$

Renaming $u_i = \alpha_i d_i$ and $K(\mathbf{x}_i, \mathbf{x}) = \boldsymbol{\varphi}(\mathbf{x}_i)^T \boldsymbol{\varphi}(\mathbf{x}) = \boldsymbol{\varphi}(\mathbf{x})^T \boldsymbol{\varphi}(\mathbf{x}_i) = K(\mathbf{x}, \mathbf{x}_i)$, the decision function, y , can be expressed as:

$$y = \sum_{i=1}^N u_i K(\mathbf{x}, \mathbf{x}_i) + b \quad (10)$$

In case of linear classifiers, $K(\mathbf{x}, \mathbf{x}_i)$ is the conventional Euclidean inner product of the input vector \mathbf{x} with the Support Vector \mathbf{x}_i . In case of nonlinear classifiers, $K(\mathbf{x}, \mathbf{x}_i)$ is the

conventional Euclidean inner product of the nonlinear transformation $\boldsymbol{\varphi}(\mathbf{x})$ of the input vector \mathbf{x} with the nonlinear transformation $\boldsymbol{\varphi}(\mathbf{x}_i)$ of the Support Vector \mathbf{x}_i .

The decision function in Eq. (10) results in the architecture depicted in Figure 3, once the proper weights and Support Vectors have been computed in the training stage. Only the Support Vectors have to be considered, as they are the only vectors that generate non-zero α_i coefficients (Haykin, 1998).

Classification is therefore performed by identifying the sign of the output value, y , in Eq. (10). If $\text{sign}(y) = +1$, then this input is labeled as class +1 and if otherwise as class -1.

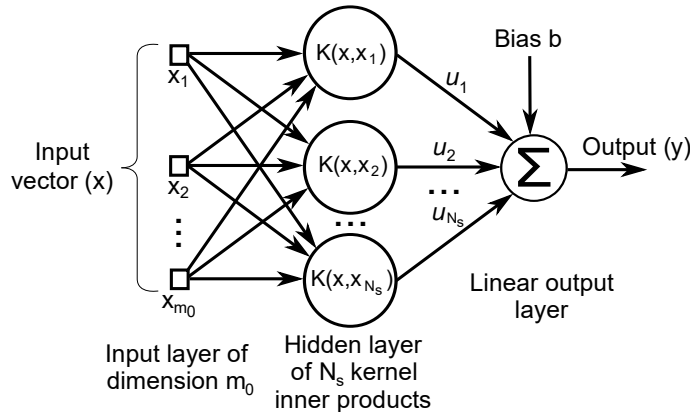


Figure 3. Architecture of a Support-Vector Machine classifier. Inner product kernels, $K(\cdot, \cdot)$, denote the m_0 -dimensional kernel inner product of the input vector with each of the N_s Support Vectors.

The most well-known and widely used nonlinear kernels are *radial basis functions (RBF)*, *sigmoids*, and *polynomials*. The *RBF kernel* can be expressed as $K(\mathbf{x}, \mathbf{y}) = \exp(-\gamma \|\mathbf{x} - \mathbf{y}\|^2)$, where γ is a user-defined parameter; the *sigmoidal kernel* can be expressed as $K(\mathbf{x}, \mathbf{y}) = \tanh(\gamma \mathbf{x}^T \mathbf{y} + c_0)$, where $\gamma > 0$ and $c_0 < 0$ are user-defined parameters; and, the *d -order polynomial kernel* can be expressed as $K(\mathbf{x}, \mathbf{y}) = (\gamma \mathbf{x}^T \mathbf{y} + c_0)^d$, where γ and c_0 are user-defined parameters and where d denotes the polynomial degree. Other kernels may also be found, in addition to those listed above.

The underlying SVM training process undertakes the problem of minimizing a quadratic functional subject to linear constraints. This problem, known as *Quadratic Programming*, has a closed solution. Although the solution can be analytically computed by applying the Lagrange multipliers method, other computational methods are typically used, especially when the dimensionality of the problem becomes high. Some of these methods include, among others, *Interior Point* methods (Ferris & Munson, 2006), the *Sequential Minimal Optimization (SMO)* algorithm (B. Schölkopf, C. J. C. Burges & A. J. Smola, Platt, 1998; Platt, April 1998), *Incremental* methods (Shilton, Palaniswami, Ralph, & Tsoi, 2005), and the *Kernel-Adatron (KA)* algorithm (Campbell & Cristianini, 1998). More information about the SVM training process has been gathered by Campbell and Ying (R. J. Brachman & T. Dietterich, Campbell & Ying, 2011).

Those readers eager to discover the rigorous mathematical statement and solution of the problem underlying Support Vector Machines are encouraged to read the comprehensive

introduction to SVM provided by Haykin (Haykin, 1998) or the in-depth work by Steinwart and Christmann (Steinwart & Christmann, 2008).

2.2. Data fusion

2.2.1. Kalman Filter (KF)

The Kalman filter (Kalman, 1960) is an efficient, recursive, mathematical algorithm that processes, at each step, inaccurate observation input data and generates a statistically optimal estimate of the subjacent real system state, by employing a prediction model and an observation model.

The basic functioning of the filter is conceptualized into two stages. The first stage is called the prediction stage, as it produces an *a priori* system state estimate from the previous state, by using a system evolution prediction model. The second stage, known as the update stage, takes into account measurements in the system to produce an *a posteriori* state estimate, by correcting the previous *a priori* estimate. This two-stage process starts with an initial estimated state, $\hat{\mathbf{x}}_0^-$, and is repeated in a loop recursively until filtering ends (Figure 4).

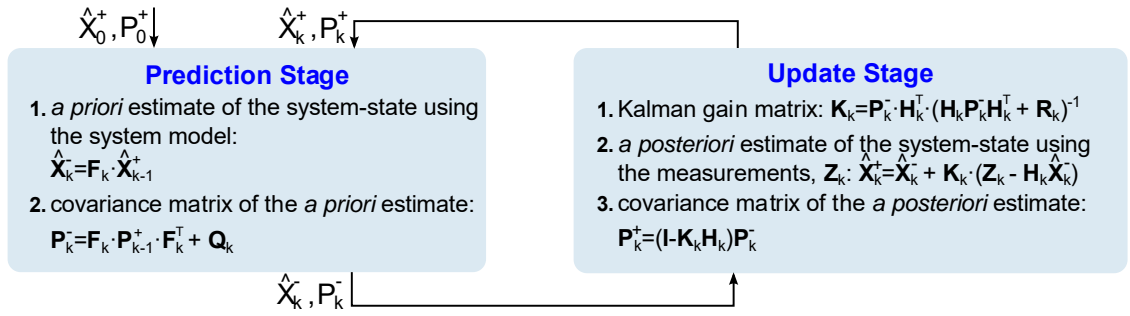


Figure 4. Stage diagram of the Kalman filtering loop.

Figure 4 summarizes the steps in each stage of the Kalman filtering process and it presents the matrices that are involved and the steps followed to implement the Kalman filter. \mathbf{F}_k is the state transition model matrix, which performs the prediction model. \mathbf{H}_k is the observation model matrix, which maps the state vector space into the measurements vector space. $\hat{\mathbf{x}}_k^-$ is the *a priori* state estimate vector, resulting from the prediction stage. $\hat{\mathbf{x}}_k^+$ is the *a posteriori* state estimate vector, derived from the measurements update stage. \mathbf{z}_k is the measurements vector obtained from the system sensors. \mathbf{K}_k is the optimal Kalman gain matrix, which weights the importance of the innovation that introduces the measurements vector \mathbf{z}_k in the update stage. \mathbf{P}_k^- is the *a priori* state covariance matrix, which provides the *a priori* estimation error covariance after the prediction stage. \mathbf{P}_k^+ is the *a posteriori* state covariance matrix, containing the *a posteriori* estimation error covariance, given after the update stage. \mathbf{Q} is the process noise covariance matrix of the prediction stage noise, which somehow ponders the weight of the process estimates. \mathbf{R} is the observation noise covariance matrix of the update stage noise, which in a way ponders the degree of confidence in each one of the measurements. The relative weights become greater as the covariance matrix elements become smaller, meaning that the quantities involved are increasingly reliable.

2.2.2. Extended Kalman Filter (EKF)

The extended Kalman filter (EKF) is a nonlinear version of the Kalman filter (KF), that is to say, linear relationships between quantities can become nonlinear. The following changes have to be applied to Figure 4 to generalized KF into EKF.

- F_k and H_k , state transition and observation matrices, respectively, are replaced by f and h , nonlinear state transition and observation functions.
- The *a priori* estimate (prediction stage) is computed now as:

$$\hat{\mathbf{x}}_k^- = f(\hat{\mathbf{x}}_{k-1}^+) \quad (11)$$

- F_k matrix is computed as the Jacobian matrix derived from f .

$$F_k = \left. \frac{\partial f}{\partial \mathbf{x}} \right|_{\hat{\mathbf{x}}_{k-1}^+} \quad (12)$$

- H_k matrix is computed as the Jacobian matrix derived from h .

$$H_k = \left. \frac{\partial h}{\partial \mathbf{x}} \right|_{\hat{\mathbf{x}}_k^-} \quad (13)$$

- The *a posteriori* estimate (update stage) is computed now as:

$$\hat{\mathbf{x}}_k^+ = \hat{\mathbf{x}}_k^- + K_k(\mathbf{z}_k - h(\hat{\mathbf{x}}_k^-)) \quad (14)$$

3. Motivation and hypothesis formulation

The inception point of this thesis was the observation of the need for simpler mechanisms to enable less complex but still highly accurate machinery monitoring. Based on the state-of-the-art literature, signal processing techniques have traditionally fit very well to this aim and have shown promising results in the past few years.

From this observation, the following **general research hypothesis** was established: *–signal processing techniques applied to raw acquired signals coming from different sensors can let us gather useful information from agro-industrial machinery, thus enabling its accurate monitoring*". Therefore, this information, that is somehow hidden otherwise, can be used for monitoring agro-industrial machinery.

This hypothesis is based on previous studies from the literature (Jardine, et al., 2006; Liakos, et al., 2018; Staszewski, 2002) and widely supported by the academic community.

The general research hypothesis can be divided into three sub-hypothesis, related to the three tackled agro-industrial problems and intimately related to the specific objectives intended to be reached in this thesis:

- *–Signal processing techniques enable effective predictive maintenance monitoring of agricultural machinery components based on the vibration signal acquired with an accelerometer*".
- *–Signal processing techniques enable effective positioning data fusion for monitoring vehicles based on relative and absolute positioning sources*".
- *–Signal processing techniques enable flow rate monitoring in agricultural sprayers based on the acoustic signal acquired with a microphone*".

4. Objectives

Developing, implementing, and assessing signal processing-based techniques for monitoring agricultural and industrial machinery based on raw data coming from different kinds of sensors is the main objective of this thesis. In addition, five particular sub-objectives have been posed for this thesis:

- **To design, implement, and evaluate signal processing techniques that enable the prediction of the status of the rotating components of machinery without removing and isolating them, using as an input the vibration signal acquired by an accelerometer.**

Previous work had tackled monitoring and predictive maintenance of small components isolated (gears, engine, bearings, etc.). These components had to be extracted from the machine in order to analyze its operation. The objective of this thesis is to consider the whole machinery without needing to remove them from the machine they form part. Therefore, monitoring simplifies greatly.

- **To design, implement, and evaluate signal processing techniques that enable the prediction of the status of the rotating components of machinery while in normal operating conditions, using as an input the vibration signal acquired by an accelerometer.**

Another objective of this thesis is to consider machinery working in normal operation too, in addition to machinery working at controlled conditions. This way, real-time monitoring can be performed without requiring performing any particular monitoring setup.

- **To design, implement, and evaluate signal processing techniques that enable monitoring flow rate from individual nozzles in agricultural sprayers, using as an input the acoustic signal acquired by a nearby microphone.**

No previous work had been done before in this area. Other somewhat similar acoustic approaches had been used for pipes, taps, and faucets. The goal of this thesis is to focus on each individual nozzle to reach a flow rate measurement device that merely requires a microphone and signal processing.

- **To design, implement, and evaluate signal processing techniques that enable monitoring kinematic quantities for agro-industrial vehicles tracking, using data coming from several on-board sensors.**

Previous work had tackled data fusion using a different set of sensors and kinematic quantities. This thesis focuses on fusing data from global navigation satellite systems (GNSS) with other kinematic information available through the on-vehicle sensors. The intention of this data fusion scheme is to keep track of vehicle when outages occur and also improving low-quality GNSS positioning.

- **To design, implement, and evaluate signal processing techniques with good performance in terms of processing time and computational load in order to work in real time.**

The developed methods in this thesis intend to reduce the amount of variables needed and try to avoid including complex processing algorithms.

- **To design machinery monitoring methods that are low-cost, in order to ease the widespread adoption by local farmers.**

The proposed methods should have a low cost associated, as compared to existing expensive alternatives. To this end, low-cost sensors and computing platforms should be used to be able to achieve this objective.

5. Methodology

The following methodological steps were followed in this thesis in order to achieve the objectives explained in the previous section. The methodology was designed to match the objectives presented in the previous section. The proposed methodology is composed of five stages: literature review, hypothesis formulation, development and evaluation, result analysis, and results publication. The relationships among these stages are represented in Figure 5.

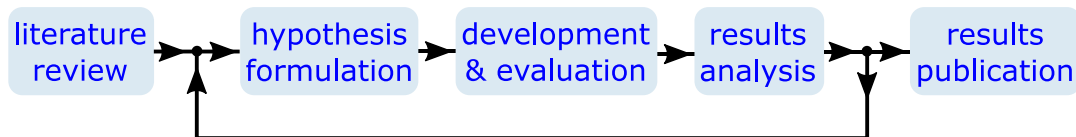


Figure 5. Block diagram of the methodological stages of this thesis and their relationships.

The **first stage of the methodology**, namely literature review, involved the study of the state of the art. This stage was mandatory so as to gain the necessary knowledge to tackle the research in this thesis. This stage of the methodology encompasses both documentation about signal processing techniques as well as other published articles and previous work on the subject. The documentation about signal processing techniques focused on supervised learning, data fusion techniques, and the rest of employed signal processing techniques (filtering, data acquisition, mechanical vibration, etc.). For its part, documentation about previous studies related to the topic of this thesis included several sources, from literature review to discussions with knowledgeable experts.

The **second stage of the methodology** undertook the formulation of the research hypothesis. The research hypothesis formulation was done after the first stage using the acquired knowledge and after having identified the research question for this thesis. This hypothesis was refined several times and, after its final version was reached, allowed for the definition of the objectives in this thesis.

The **third stage of the methodology** consisted of the development and evaluation of the signal processing techniques proposed for accomplishing the intended goals. First, the particular signal processing models were designed for each problem, focusing on defining an adaptive approach that could be refined after its assessment when needed until successful results were achieved. Furthermore, in this stage, the experimental setups were defined and data acquisition was performed. The experimental setups, which were designed so as to enable proper data acquisition to guarantee meaningful data for the later stages, consisted on placing the sensors in appropriate locations for later data acquisition. It involved removing or controlling noise sources as well as a pre-analysis of the data to check its correctness. The data acquisition was undertaken after having properly deployed the experimental setup. The acquired data was subsequently used for analyzing the adequacy of the proposed models as well as for their validation.

The **fourth stage of the methodology** focused on assessing the proposed hypothesis. This assessment was mainly based on comparing the obtained results against other methods from other articles in the literature. This stage allowed for the validation and redefinition of the

research hypothesis formulated in stage number two. Whenever the results showed that the research hypothesis could be validated, publication of the obtained results followed (last stage of the methodology). In contrast, when the results showed that the research hypothesis should be reformulated, the methodology went back to the second stage in order to try to offer a new valid hypothesis.

The **fifth stage of the methodology** was the publication of the obtained results. This publication consisted of journal and conference articles, divulging the work of each experiment. The articles produced as a result of this thesis have been submitted to peer-reviewed scientific journals and conferences, trying to facilitate its diffusion in academia and looking forward to validating the research from this thesis.

6. Articles in the compendium and their relationship

This thesis comprises three articles for compendium of publications; all of them published in JCR indexed journals belonging to first quartile (Q1) in their respective categories. Each of these articles will be respectively named hereinafter as:

Article 1. Predictive maintenance monitoring

Ruiz-Gonzalez, R.; Gomez-Gil, J.; Gomez-Gil, F.; Martínez-Martínez, V. (2014). An SVM-Based Classifier for Estimating the State of Various Rotating Components in Agro-Industrial Machinery with a Vibration Signal Acquired from a Single Point on the Machine Chassis. *Sensors* 14 (11): 20713-20735. Impact factor: 2.245 (Q1)

Article 2. Vehicle tracking monitoring

Melendez-Pastor, C.; Ruiz-Gonzalez, R.; Gomez-Gil, J. (2017). A data fusion system of GNSS data and on-vehicle sensors data for improving car positioning precision in urban environments. *Expert Systems with Applications* 80: 28-38. Impact factor: 3.768 (Q1)

Article 3. Flow rate monitoring

Ruiz-Gonzalez, R.; Stombaugh, T.S.; Martínez-Martínez, V.; Gomez-Gil, J. (2017). An acoustic method for flow rate estimation in agricultural sprayer nozzles. *Computers and Electronics in Agriculture* 141: 255-266. Impact factor: 2.427 (Q1)

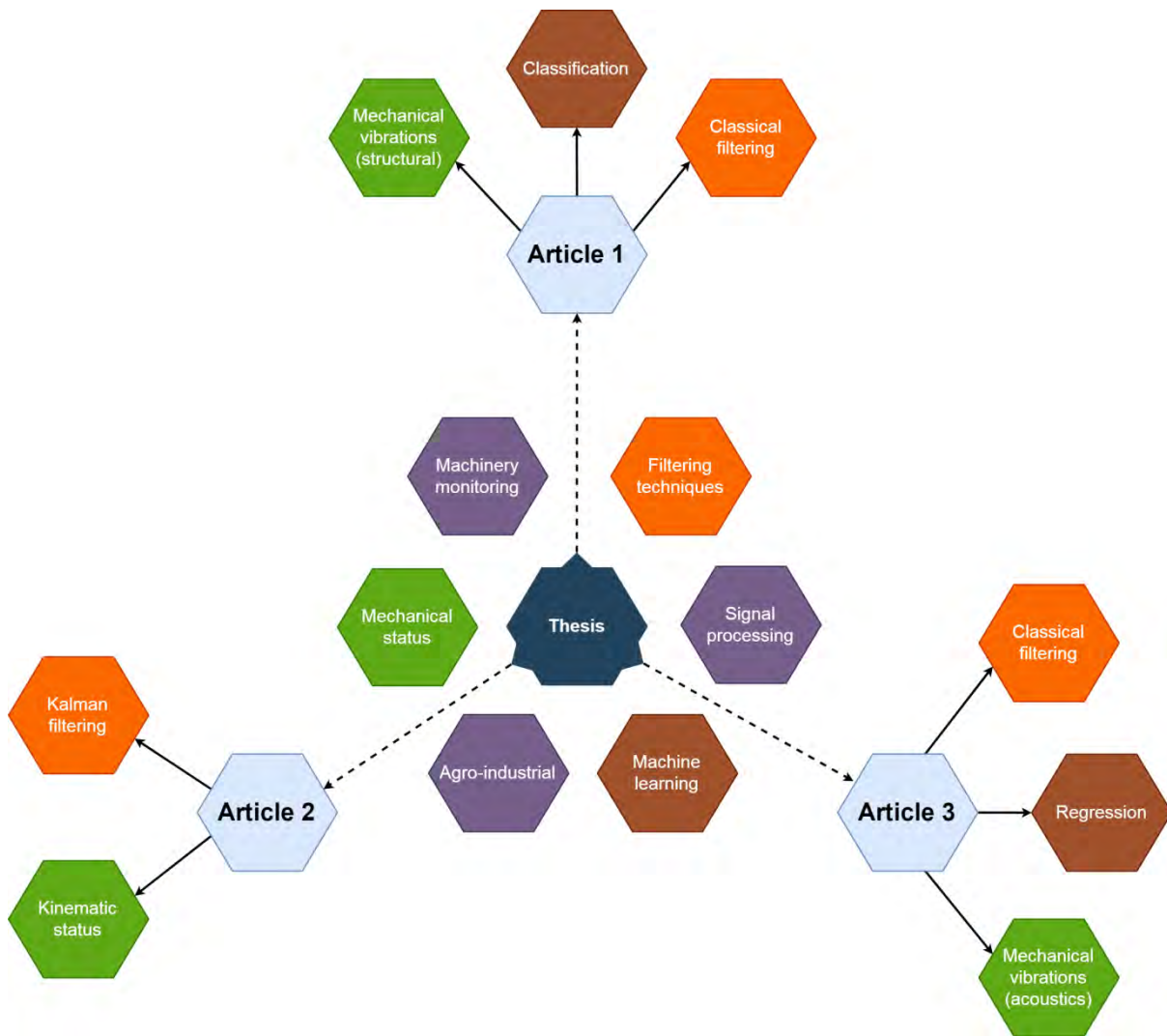


Figure 6. Relationship between three articles composing this thesis.

Figure 6 summarizes the relationship between the articles comprising this thesis. A further explanation is provided in the subsequent paragraphs.

All three articles comprising this thesis deal with three different agro-industrial monitoring problems by employing signal processing techniques. This section intends to further clarify the relationships among all of them as a unique topic.

All of the articles included for compendium undertake relevant problems within the agricultural and industrial areas. Since existing solutions are not fully satisfactory in terms of cost or accuracy, alternative approaches are posed in this thesis. The methods proposed in all three articles contribute by incorporating new knowledge into previous literature.

Moreover, all the approaches in this thesis rely on signal processing techniques to achieve the intended objectives. Both the first and third article use a common methodology to achieve the intended goals, based on similar filtering and classification schemes, while the second article employs a different approach, based on data fusion techniques.

As can clearly be observed by an eager reader, the three articles focus on monitoring agro-industrial machinery. The first article focuses on estimating the statuses of several components

of the agricultural harvester. The second article focuses on monitoring a general vehicle (which could be used for tractors, harvesters, cultivators, seeders, sprayers, etc.), by improving the estimation of its kinematic properties. The third article focuses on agricultural sprayers, by proposing a novel estimation method for flow rate on individual nozzles.

Moreover, the first and second articles propose two methods to monitor the mechanical and kinematic status of machinery, respectively. There exists an obvious relationship between the kinematics of the machinery and the rotation speed of certain components of the machinery. Therefore, estimation of both statuses is highly related and merging together the information from both methods could further improve the accuracies of both of them.

The first and third articles have a lot of similarities, as can be easily appreciated. They both work with mechanical vibrations, whether propagated along the chassis of the machinery or in the air. Moreover, the developed methods both deal with agricultural machinery components. In addition, the proposed preprocessing approach is quite analogous, mainly differing in the latest stages of the processing.

The second and third articles are also intimately related as part of accurate spraying systems in precision agriculture environments. The magnitude under monitoring in the third article, namely the flow rate, is typically being controlled so as to perform a spraying of chemicals while agricultural machinery is moving along a plot of land. Thus, by making use of both the data fusion approach from the second article and the per-nozzle flow rate measurement device, a more accurate control of the quantity being sprayed can be achieved.

7. Results

The main results of this thesis are three signal processing methods presented in the three articles comprising the compendium of publications. Each of these methods undertakes a different agro-industrial problem.

In this thesis, the three agricultural and industrial problems considered for proposing solutions employing signal processing methods were: predictive maintenance of an agricultural machine, kinematic tracking of an agro-industrial vehicle, and flow rate estimation of an agricultural sprayer. The following paragraphs briefly detail each of these problems.

7.1. Predictive maintenance monitoring

- Problem to be solved: Machinery rotating components generate mechanical vibration signals that propagate along the machinery structure. Therefore, the status of machinery components is expected to be estimable by acquiring from a single point of the machinery chassis. The status of several rotating components of an agricultural harvester machine was to be estimated by applying signal processing techniques to the vibration signal acquired by an accelerometer.
- Proposed solution: A signal processing approach, consisting of feature extraction and selection plus classification, was employed to predict the status of the rotating components. This method can be applied while in normal operating conditions, thus avoiding the disadvantages of other alternative techniques. This solution can accurately estimate the status of three rotating components of the machinery in real time.
- Original contributions: The proposed system was the first system in the literature capable of diagnosing the status of several rotating components in agricultural machinery while in normal operation, without needing to remove or isolate the components from the rest of the machinery. The same problem as in the first article of this compendium (predictive maintenance monitoring) was undertaken while the agricultural sprayer was harvesting sunflower under normal working operating conditions (E. Velasco Sánchez, Ruiz González, Gómez Gil, Gómez Gil, Meléndez Pastor, & Feijoo García, 2016). The results obtained in this scenario yielded similar accuracies as when machinery was not moving, i.e. under well-controlled conditions.

Figure 7 depicts the experimental setup employed to acquire the data acquisition related to this problem. Further details can be found in the original article (Ruiz-Gonzalez, Gomez-Gil, Gomez-Gil, & Martínez-Martínez, 2014).

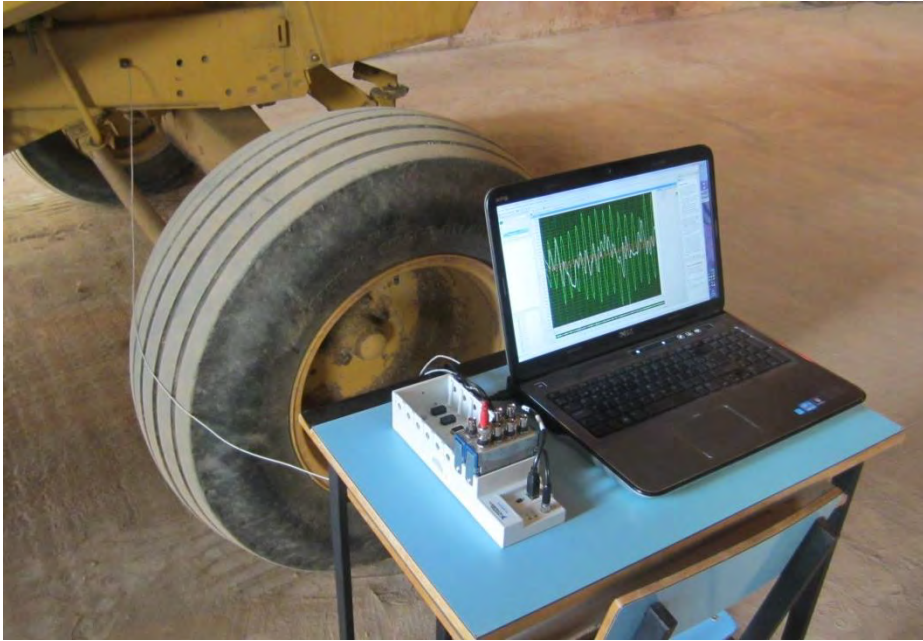


Figure 7. Data acquisition setup for predictive maintenance monitoring. An accelerometer was placed on the structure of the machine, connected by means of a cable to an acquisition system, and a laptop was used to register and visualize the acquired data.

7.2. Vehicle tracking monitoring

- Problem to be solved: Vehicle tracking suffers from inaccuracies when operating in environments with poor GNSS coverage. Therefore, incorporating other sources of positioning can considerably improve the accuracies achieved. Several techniques, incorporating relative positioning data, have been widely used in the literature when trying to improve accuracy in keeping track of vehicle's kinematic information. This thesis dealt with data fusion of GNSS data with other sources of relative positioning data. In particular, this thesis copes with employing relative positioning data coming from on-vehicle sensors accessible via OBD-II standard communication.
- Proposed solution: A data fusion model, employing the extended Kalman filter (EKF), was proposed. Absolute positioning data, coming from GNSS receiver, was fused with relative positioning data, obtained via OBD-II from the on-vehicle sensors. Ackermann steering model was used for simplifying the underlying vehicle kinematics too.
- Original contributions: The proposed model employed to describe the state of car systems has not been previously used. New relationships between the measured variables were derived, based on Ackermann steering model. The proposed system was capable of fusing data coming from on-vehicle sensors with GNSS data, allowing for accurate positioning when GNSS accuracy worsens and even for short times of complete GNSS signal outages. Moreover, data fusion in this article is performed requiring less overall variables than other counterpart alternatives, thus being more efficient. The proposed system performs positioning data fusion as a single EKF-based stage and is, thus, more flexible to the addition of new on-vehicle sensors as input or measured data and being less computationally complex.

Figure 8 depicts the experimental setup employed to acquire the data acquisition related to this problem. Further details can be found in the original article (Melendez-Pastor, Ruiz-Gonzalez, & Gomez-Gil, 2017).



Figure 8. Data acquisition setup for vehicle tracking monitoring. An accurate GPS receiver, shown in foreground, was placed on top of the car to use as reference for comparison of the results coming from the data fusion approach.

7.3. Flow rate monitoring

- Problem to be solved: Employing traditional flow rate measurement devices for each nozzle is quite expensive in an agricultural sprayer, and per-nozzle accurate measurements are mandatory when aiming at precision agriculture spraying. Based on the observation that the nearby acoustic signal varies as flow rate coming out of the nozzle does, an acoustics-based signal processing method seems to be useful to tackle this problem.
- Proposed solution: An acoustics-based signal processing method was developed in order to estimate flow rate through the nozzles. The method employed several stages including frequency domain analysis, in-band power calculation, normalization, and nonlinear regression.
- Original contributions: The proposed system was the first-ever method in the literature capable of accurately measuring flow rate in real-time in an agricultural sprayer by means of processing the acoustic signal acquired nearby. In addition, the proposed system is low-cost when compared to traditional flow rate measurement devices. Moreover, most suitable frequency bands were analyzed in the frequency domain as well as the influence of distance and quality of microphone device.

Figure 9 depicts the experimental setup employed to acquire the data acquisition related to this problem. Further details can be found in the original article (Ruiz-Gonzalez, Stombaugh, Martínez-Martínez, & Gomez-Gil, 2017).

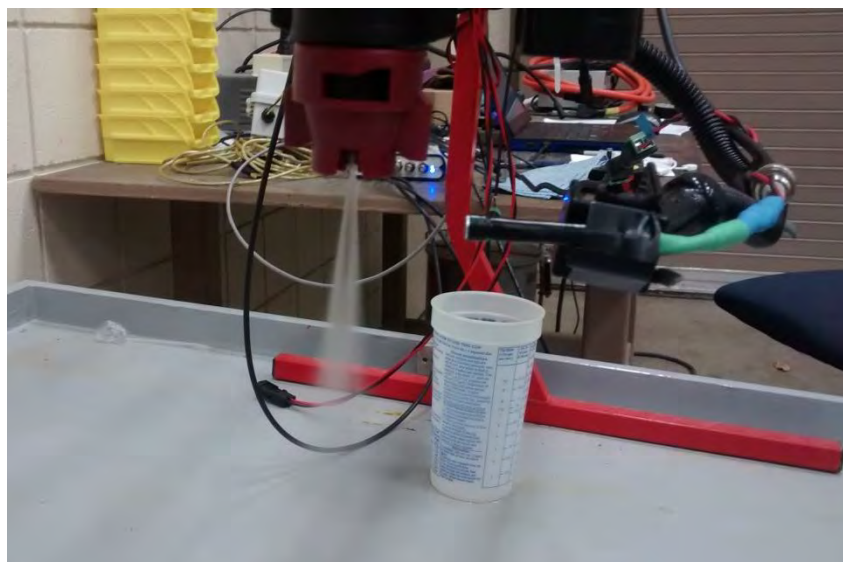


Figure 9. Data acquisition setup for flow rate monitoring. A microphone was placed close to the nozzle to acquire the acoustic signal while water was flowing out of it. The signal acquired by the microphone was digitalized by an acquisition system, and a laptop was used to record the data.

8. Conclusions

The results derived from this thesis, summarized in the previous section and available as an annex in the following chapter, suggest the next conclusions. Two general conclusions are posed together with four particular conclusions, which are associated with the sub-objectives of this thesis.

- The **first general conclusion** is that it is feasible to develop and implement signal processing-based techniques for monitoring agricultural and industrial machinery. This conclusion is supported by the results from all three articles composing this thesis by compendium. The work conducted in all three articles composing this thesis show that signal processing techniques enable feasible solutions for the undertaken problems in the agricultural and the industrial fields. It is expected that other particular problems, within the area of monitoring agricultural and industrial machinery, can also benefit from similar signal processing techniques.
- The **second general conclusion** is that all proposed solutions tend to be more cost-effective, more accurate, and easier to deploy as compared to existing solutions. When compared to the literature, the proposals made in this thesis have a lower cost, achieve accuracies otherwise unreachable, and do not require complex procedures to deploy the associated system. The results from all three articles give evidence supporting this conclusion. All three methods proposed in this thesis employ low-cost sensors for its operation, as opposed to alternative systems, and only require cheap commodity computing platforms to work in real time. Further details are given in all three articles.
- The **third general conclusion** is that all proposed solutions can operate in real time. Due to the processing optimization leading to low computational power requirements, all three methods proposed in this thesis could be deployed for real-time operation. Therefore, this enables effective machinery monitoring while it is being used instead of those alternative methods that just perform monitoring *a posteriori*. The advantage of that lies in the ability to detect improper statuses beforehand, just right after they happen. The results from all three articles give evidence supporting this conclusion.
- The **first particular conclusion** is that signal processing techniques can be employed for monitoring machinery components, using as an input the vibration signal acquired by an accelerometer, without removing and isolating them, even while in normal operating conditions. The results from the first article of this compendium (predictive maintenance), provides proof of this. This conclusion can be further subdivided into the following conclusions:
 - Accurate estimation of the status of various rotating components in agro-industrial machinery is possible by processing the vibration signal acquired from a single point on the machine structure. The results reveal the potential of this method to estimate the status of distant components by processing vibration signals from a unique sensor located at a fixed position, midway along the harvester chassis, because a mean cross-validation accuracy higher than 85% was obtained.

- Analyzing the individual cross-validation accuracy obtained for each rotating component, the suitability of the SVM classifier for estimating each separate machinery status is evident. On the one hand, the rotating component status with the best cross-validation accuracy was the engine speed, with a cross-validation accuracy of 100% in all cases. On the other hand, the worst cross-validation accuracy was obtained for threshing cylinder balance status, for which the cross-validation accuracy was between 63.41% and 87.49%. These values are perfectly valid for deploying a predictive maintenance system, since it can detect unbalances in certain components, thus alerting the operator of the machinery to perform some corrective maintenance on this component.
 - The vibration signal can be acquired with a uniaxial accelerometer, the orientation of which does not significantly affect the classification accuracy. The comparison of the results of cross-validation accuracy along the three accelerometer axes supports this conclusion. The higher differences observable for the threshing cylinder balance status shows differences of around 20%. However, almost no differences in accuracy were appreciated for the rest of the states, which were lower than 10% in all cases. Although vibrations are usually generated in a specific direction, the results obtained here suggest that the machine structure spreads them along all of the axes, making the use of an arbitrary axis for their detection possible.
 - The accelerometer sensor does not need to be placed very close to the rotating components, which makes the acquisition stage simple and non-intrusive. Previous work in the scientific literature has only analyzed isolated mechanical components, using one accelerometer for each isolated component.
 - The proposed approach, using feature extraction plus feature selection, only requires a maximum of seven features as input for the SVM classifier. This way, the subsequent classifier is simpler and more efficient than other existing alternatives requiring a much larger set of features.
 - No significant improvements are noted between the use of either nonlinear or linear kernels, when using an SVM classifier. For the undertaken problem, no significant improvements appeared when introducing more complex nonlinear kernels.
 - Real-time monitoring of the machinery can be performed thanks to the ability of the proposed system to operate in normal working conditions, *i.e.* while the harvester is working harvesting in the field.
 - The proposed method provides a low-cost way of estimating the status of the machinery, just requiring an accelerometer and low-cost computing platform in order to achieve high accuracies. The low cost of this method contrasts with existing alternative methods that require expensive transportation of the machinery to inspection facilities.
- The **second particular conclusion** is that real-time monitoring of flow rate from individual nozzles in agricultural sprayers can be achieved by processing the acoustic signal in their surroundings. The results from the third article of this compendium (flow rate monitoring) are proof of this.
 - The nozzle-generated acoustic signal contains enough information to enable accurate flow rate estimation. It is evident, from the achieved results, that the generated

acoustic signal contains information related to the flow rate through the nozzle tip, and many processing techniques can be proposed for this end.

- The proposed method can be used to estimate the flow rate of individual nozzles in a low-cost way with a high accuracy in a laboratory environment. The flow rate estimation accuracies obtained with the proposed acoustic method are close enough to some of the traditionally used flowmeters, whose relative RMSE errors can reach 4%.
- The flow rate estimation becomes more difficult, *i.e.* the errors increase, for either very low or very high flow rates, when operating outside the flow range recommended by the nozzle manufacturer. One possible explanation for this behavior is the fact that the spray deposition pattern and output droplet size distribution of the nozzles changes appreciably outside of the manufacturer recommended range, which will consequently change the acoustic signature. The increased difficulty in estimation could also be due to the acoustic signals being more similar in these extreme cases. This effect is even more noticeable for low flow rates due to the inherently lower intensity of the nozzle-generated signal. This lower intensity leads to the acoustic noise floor being relatively stronger with respect to the signal of interest, thus making the estimation more difficult.
- The proposed method can work in real time. When executed in post-processing in MATLAB®, it requires less than five seconds to process the 61-second-long recordings for 10 flow rates, where the reported times were obtained in a Dell Latitude E6400 laptop. This execution time, less than 0.01 seconds for each single epoch, shows the feasibility of performing all the necessary tasks between the acquisitions of two consecutive epochs, which is 0.5 seconds. It is worth remarking that no explicit code optimization was done and the computational efficiency of the method could be further improved for real-time operation.
- Consistent results, with neither significant improvements nor detriments, can be obtained when using a high-end or a low-end microphone. The results prove that the high-end microphone does not outperform the low-end microphone. Furthermore, the measurements provided by both are coherent, since moderate (0.40–0.59), strong (0.60–0.79) or very strong (0.80–1.0) positive correlations were found. Additionally, the reported *p*-values from the Welch's t-test showed no statistically significant differences between both microphones for two out of the three tested nozzles. The fact that the proposed method is highly independent of microphone quality makes it economically feasible to replicate flow sensors across a large boom with many nozzles.
- The frequency band between 1450 Hz and 1950 Hz provided the best accuracies. Several bandwidths were tested, and a bandwidth of 500 Hz was found to be the best because it gave acceptable accuracies and was narrow enough to avoid excessive wideband interferences. Looking over the frequencies from 0 Hz to 50 kHz, the band from 1450 Hz to 1950 Hz contained more information than any other related to the flow rate.
- The method accuracy does not depend too much on the nozzle-to-microphone distance. The results show a tendency of a slow but progressive accuracy degradation as distance is increased. Only distances over 6 cm were tested in order to prevent the microphones from getting wet and thus being damaged. Moreover, since specific calibrations are required for each distance, it is worth noting that the proposed method will require strict control of microphone location while operating. However, a simple straightforward calibration can be used in this case, requiring just the determination of the in-band power for highest and lowest flow rates for the normalization stage.

- The proposed method presents a low-cost design, requiring for its deployment only a low-end microphone and a microcontroller-based computing platform.
 - There is an oscillatory behavior in the estimated flow rates, which highlights the possibility of the integral errors in flow rate compensating over time. Thus, an even lower error can be achieved in terms of the cumulative volume applied to the whole plot of land that is being sprayed.
 - Each nozzle tip requires its own calibration since no singular curve could be fitted accurately for all nozzle tips.
 - These studies were conducted in a relatively controlled laboratory environment; thus, the reproducibility of these accuracies in real agricultural settings has yet to be verified.
- The **third particular conclusion** is that kinematic monitoring of agro-industrial vehicles can be improved by using signal processing techniques for data fusion of GNSS and on-vehicle sensors data. The results from the second article of this compendium (vehicle tracking monitoring) support this conclusion with evidence.
 - On-vehicle sensors data can be employed through the proposed data fusion system for improving the car positioning precision provided by a standalone low-cost GNSS receiver. Positioning errors can be reduced by half in terms of the RMSE and the 95th-percentile of the distance error distribution, and up to one fourth in terms of the maximum distance error.
 - The best precision improvements are expected to be achieved in urban or forest areas, where tall buildings or trees hinder the effectiveness of GNSS systems. It is expected that the proposed system could be of great value in the event of short-term GNSS signal outages, which are prevalent in cities with tall buildings and skyscrapers or in forests-like environments. Wherever the GNSS receiver provides high accuracies, the proposed system becomes less effective. Thus, all scenarios where GNSS accuracies worsen can take more profit from the proposed system.
 - The proposed system requires less variables than other existing alternatives, thus being more efficient. Previously proposed approaches, also employing EKF, required several stages and intermediate variables, which yielded to much more complex systems, both in computational terms and as far as tuning of covariance matrices is involved.
 - The proposed system can be easily adapted to incorporate new variables and sensors, since the EKF allows for simple addition of new sensed variables into the model. Merely deriving the mathematical relationship between sensed variables and state variables is enough for system update as well as covariance matrices tuning too.
 - This method presents a low cost due to the use of low-cost GPS and a set of sensors that is currently incorporated on-board of the agro-industrial vehicles.

9. Future work

In this thesis several solutions were satisfactorily proposed for three particular agro-industrial problems. All along the research performed in this thesis, several lines of future work appeared.

The following future work lines, among others, have been identified.

- Related to the **predictive maintenance monitoring**: A currently live project is working on replacing feature extraction stage by a frequency selection approach, so as to identify most suitable frequencies and trying to relate them to rotating speed with the help of an expert person. Another future line could be working on continuous estimation of the speed of the rotating components by processing the vibration signal, enabling real-time monitoring of the speed of certain rotating components. In addition, diagnostics and prognostics, in the sense of estimating the level of damage and predicting its future evolution, could be tackled too.
- Related to the **vehicle tracking monitoring**: The employed data fusion approach did not consider dynamic tuning of the covariance matrices. Since sensor accuracy varies, especially for GNSS receivers as coverage improves or worsens, a modified method, which relies more or less on each sensor based on their accuracy at each time instant, could outperform the proposed approach.
- Related to the **flow rate monitoring**: Since the experiments in this thesis were conducted on a well-controlled laboratory environment, where acoustic interferences and noises were avoided, testability on a real environment would be necessary. It is expected that, as a result, a new refined approach becomes necessary after that testing in the real field. An exhaustive study about optimal microphone location could be another possible line of future research. Another line of research could further delve into acoustics generation in agricultural sprayer nozzles, probably using Computational Fluid Dynamics (CFD) for simulations.

In addition to those particular lines of future work, a more general line of research could focus on how to properly incorporate all the systems proposed in this thesis into a whole system, which could lead to complete systems of great usefulness in precision agriculture tasks. For example, by employing accurate kinematic data together with accurate flow rate measurements, a very accurate control of chemicals spraying could be achieved.

Additional future work could focus on trying to develop an abstract framework, valid for any particular agro-industrial problem, which examines signals in order to provide an *a priori* likelihood of success without the need of proposing a particular signal processing technique beforehand.

10. Merits and diffusion of the results

This section presents a summary of the merits obtained during the research process of this thesis and the diffusion of the obtained results: the scientific publications, the granted patents, the participation in research projects, the research stays in other international research groups, the courses lectured, and other merits.

10.1. Publications

This subsection presents the articles sent to peer-reviewed international journals and conferences, which has been published or accepted for publication.

10.1.1. Publications in JCR-indexed international journals

The articles published in JCR-indexed international journals are presented below. Moreover, Table 1 shows the main quality parameters of the journals where these articles were published:

- Gomez-Gil, J.; Ruiz-Gonzalez, R.; Alonso-Garcia, S.; Gomez-Gil, F.J. (2013). A Kalman filter implementation for precision improvement in Low-Cost GPS positioning of tractors. *Sensors* 13 (11): 15307-15323.
- Ruiz-Gonzalez, R.; Gomez-Gil, J.; Gomez-Gil, F.; Martínez-Martínez, V. (2014). An SVM-Based Classifier for Estimating the State of Various Rotating Components in Agro-Industrial Machinery with a Vibration Signal Acquired from a Single Point on the Machine Chassis. *Sensors* 14 (11): 20713-20735.
- Martínez-Martínez, V.; Gomez-Gil, F.J.; Gomez-Gil, J.; Ruiz-Gonzalez, R. (2015). An Artificial Neural Network based expert system fitted with Genetic Algorithms for detecting the status of several rotary components in agro-industrial machines using a single vibration signal. *Expert Systems with Applications* 42 (17–18): 6433-6441.
- Melendez-Pastor, C.; Ruiz-Gonzalez, R.; Gomez-Gil, J. (2017). A data fusion system of GNSS data and on-vehicle sensors data for improving car positioning precision in urban environments. *Expert Systems with Applications* 80: 28-38.
- Ruiz-Gonzalez, R.; Stombaugh, T.S.; Martínez-Martínez, V.; Gomez-Gil, J. (2017). An acoustic method for flow rate estimation in agricultural sprayer nozzles. *Computers and Electronics in Agriculture* 141: 255-266.

Journal	ISSN	Year	Impact Factor	Journal Ranking
Sensors	1424-8220	2013	2.048	<ul style="list-style-type: none"> • Q1 on <i>Instruments & Instrumentation</i> (10/57) • Q2 on <i>Chemistry, Analytical</i> (36/76) • Q3 on <i>Electrochemistry</i> (15/27)
		2014	2.245	<ul style="list-style-type: none"> • Q1 on <i>Instruments & Instrumentation</i> (10/56) • Q2 on <i>Chemistry, Analytical</i> (31/74) • Q3 on <i>Electrochemistry</i> (14/28)
Computers and Electronics in Agriculture	0168-1699	2017	2.427	<ul style="list-style-type: none"> • Q1 on <i>Agriculture, Multidisciplinary</i> (7/57) • Q2 on <i>Computer Science, Interdisciplinary Applications</i> (39/105)
Expert Systems with Applications	0957-4174	2015	2.981	<ul style="list-style-type: none"> • Q1 on <i>Operations Research & Management Science</i> (6/82) • Q1 on <i>Engineering, Electrical & Electronic</i> (27/257) • Q1 on <i>Computer Science, Artificial Intelligence</i> (19/130)
		2017	3.768	<ul style="list-style-type: none"> • Q1 on <i>Operations Research & Management Science</i> (8/84) • Q1 on <i>Engineering, Electrical & Electronic</i> (42/260) • Q1 on <i>Computer Science, Artificial Intelligence</i> (20/132)

Table 1: Quality parameters of the JCR-indexed journals where articles have been published.

10.1.2. Publications in international conference proceedings

This subsection presents the works presented in international conferences and international workshops:

- Ruiz-Gonzalez, R.; Gomez-Gil, J.; Gomez-Gil, F.J.; Navas-Gracia, L.M. Blind 3D localization and separation of multiple vibration and acoustic sources simultaneously active. The 18th IEEE Conference on Sensors, IEEE Sensors 2017, Glasgow, Scotland (United Kingdom), October 29th to November 1st 2017.

10.1.3. Publications in national conference proceedings

This subsection presents the works presented in national conferences:

- Ruiz González, R. A Kalman filter based system for relative positioning improvement in low-cost GPS receivers. Congreso para la Difusión de la Producción Científica e Innovadora (CODIPROCIN). January 14th -15th 2015.

- Ruiz González, R.; Gómez Gil, F.J.; Gómez Gil, J.; Meléndez Pastor, C.; Feijoo García, F. Estimación del estado mecánico de maquinaria agrícola en funcionamiento mediante el análisis automático de vibraciones. XXI Congreso Nacional de Ingeniería Mecánica, Elche, Alicante (Spain). November 9th -11th 2016.
- Feijoo García, F.; Gómez Gil, F. J.; Ruiz Calvo, J.; Peláez Vara, J.; Martínez Martínez, A.; R. Ruiz González. Análisis espectral de desequilibrios rotantes en maquinaria agrícola. XXI Congreso Nacional de Ingeniería Mecánica, Elche, Alicante (Spain). November 9th -11th 2016.

10.2. Projects

This subsection presents information about a project in which I have participated during my PhD thesis:

- Simplificación del diagnóstico de la apnea del sueño infantil mediante nuevas técnicas de procesado de señales cardiorrespiratorias (SIMPLICITY):
 - Reference: DPI2017-84280-R
 - Starting date: January, 2018.
 - Finishing date: December, 2020.
 - Duration: 36 months.
 - Funding entity: Ministerio de Economía y Competitividad (Ministry of Economy and Competitiveness, Spain).
 - Participant entities: Grupo de Investigación Biomédica (Biomedical Engineering Research Group), University of Valladolid.
 - Principal investigator: Roberto Hornero Sánchez.
 - Role: Investigator.

10.3. Research stays

This subsection presents information about the four research stays done in this thesis:

- First stay:
 - Organization: University of Kentucky.
 - Center: Department of Biosystems & Agricultural Engineering.
 - Location: Lexington (Kentucky), USA.
 - Start of the stay: September, 2015.
 - Duration: 3.5 months.
 - Funding entity: University of Valladolid (Spain).
 - Stay purpose: Research for a CNH Industrial company project about estimating the flux of water through nozzles by means of the acoustic signal.

- Second stay:
 - Organization: University of Kentucky.
 - Center: Department of Biosystems & Agricultural Engineering.
 - Location: Lexington (Kentucky), USA.
 - Start of the stay: September, 2016.
 - Duration: 3.5 months.
 - Funding entity: University of Valladolid (Spain).
 - Stay purpose: Research for a CNH Industrial company project about estimating the flux of water through nozzles by means of the acoustic signal.

- Third stay:
 - Organization: Universidade Federal de Viçosa.
 - Center: Departamento de Engenharia Agrícola.
 - Location: Viçosa (Minas Gerais), Brazil.
 - Start of the stay: April, 2017.
 - Duration: 2 months.
 - Funding entity: Banco Santander, by means of the —Beas Iberoamérica. Jóvenes profesores e investigadores. Santander Universidades” grant.
 - Stay purpose: Research about the macaw palm fruit-stem system: anisotropic viscoelastic modeling and structural analysis.

- Fourth stay:
 - Organization: Universidade Federal de Viçosa.
 - Center: Departamento de Engenharia Agrícola.
 - Location: Viçosa (Minas Gerais), Brazil.
 - Start of the stay: January, 2018.
 - Duration: 6 months.
 - Funding entity: None.
 - Stay purpose: Research about the macaw palm fruit-stem system: anisotropic viscoelastic modeling and structural analysis.

10.4. Teaching

This subsection presents information about the four courses lectured during this thesis:

- Redes y Servicios Telemáticos
 - Type of course: Undergraduate.
 - Date: February-June 2016.
 - Place: Departamento de Teoría de la Señal y Comunicaciones e Ingeniería Telemática – Escuela Técnica Superior de Ingenieros de Telecomunicación (ETSIT) – Universidad de Valladolid (UVa), Valladolid, Spain.
 - Teaching load: 20 hours.

- Desarrollo de Aplicaciones Distribuidas
 - Type of course: Undergraduate.
 - Date: September 2017-January 2018.
 - Place: Departamento de Teoría de la Señal y Comunicaciones e Ingeniería Telemática – Escuela Técnica Superior de Ingenieros de Telecomunicación (ETSIT) – Universidad de Valladolid (UVa), Valladolid, Spain.
 - Teaching load: 15 hours.

- Desarrollo de Aplicaciones Distribuidas
 - Type of course: Undergraduate.
 - Date: September 2018-January 2019.
 - Place: Departamento de Teoría de la Señal y Comunicaciones e Ingeniería Telemática – Escuela Técnica Superior de Ingenieros de Telecomunicación (ETSIT) – Universidad de Valladolid (UVa), Valladolid, Spain.
 - Teaching load: 30 hours.

- Operación, Administración y Mantenimiento de Redes Telemáticas
 - Type of course: Master degree.
 - Date: September 2018-January 2019.
 - Place: Departamento de Teoría de la Señal y Comunicaciones e Ingeniería Telemática – Escuela Técnica Superior de Ingenieros de Telecomunicación (ETSIT) – Universidad de Valladolid (UVa), Valladolid, Spain.
 - Teaching load: 15 hours.

10.5. Other merits

This subsection presents information about other merits obtained during this thesis:

- Registration of a patent with the next information:
 - Name: Sistema de asistencia al conductor y métodos de adquisición y procesado de datos asociados.
 - Country: Spain.
 - Patent number: P201600489.
 - Authors: MARTÍNEZ MARTÍNEZ, Victor; MELÉNDEZ PASTOR, Carlos; RUIZ GONZÁLEZ, Rubén.
 - Owner: Universidad de Valladolid (University of Valladolid).
 - Issue date: September 18th, 2018.

- Obtained a prize with the next information:
 - Name of the prize: Premio Prometeo 2015.
 - Founding entity: Fundación General Universidad de Valladolid.
 - Date: June 2015.
 - Name of the project: Sistema para la asistencia al conductor empleando sensores inerciales y de automoción.
 - Authors: Carlos Meléndez Pastor, Rubén Ruiz González, Víctor Martínez Martínez.

- Co-directed a Bachelor Final Project with the next information:
 - Title of the project: Diseño, implementación y testeo de un Sistema de fusión de datos de posicionamiento GPS y datos de sensores, empleando filtro de Kalman extendido y sistema de comunicación OBDII, para la mejora de la precisión de posicionamiento de un vehículo.
 - Degree: Ingeniero Superior de Telecomunicación, Universidad de Valladolid.
 - Date: July 2015.
 - Author: Carlos Meléndez Pastor.
 - Directors: Rubén Ruiz González, Víctor Martínez Martínez, Jaime Gómez Gil.

- Co-directed a Bachelor Final Project with the next information:
 - Title of the project: Sistema para la detección del estado de funcionamiento de los elementos rotantes de una cosechadora a partir del procesado de vibraciones: análisis de las frecuencias más relevantes mediante algoritmos evolutivos.
 - Degree: Grado en Ingeniería de Tecnologías Específicas de Telecomunicación: Sistemas de Telecomunicación, Universidad de Valladolid.
 - Date: September 2019.
 - Author: Lidia Martínez Martínez.
 - Directors: Rubén Ruiz González, Víctor Martínez Martínez, Jaime Gómez Gil.

- Co-directed a Bachelor Final Project with the next information:
 - Title of the project: Avanzando hacia una red auto-adaptativa: simulación de redes definidas por software (SDN) mediante el simulador GNS3.
 - Degree: Grado en Ingeniería de Tecnologías de Telecomunicación, Universidad de Valladolid.
 - Date: July 2019.
 - Author: Rubén Blanco Pérez.
 - Directors: Rubén Ruiz González, Jaime Gómez Gil.

II Articles in the compendium

The second chapter of this document presents the articles that take part of this thesis as a compendium of publications. It is divided into three sections; each one related to one of the three articles included in the compendium. The three articles of this compendium have been published in JCR-indexed peer-reviewed journals of the first quartile of their category. Each one of the next sections contains an introduction to the article, some bibliographic information, and a version of the published article.

Article 1: Predictive maintenance monitoring

The first article tackles the **predictive maintenance monitoring** problem, previously described in chapter “Introduction to the compendium”. The main bibliographic data about this article is shown below:

- Title: An SVM-Based Classifier for Estimating the State of Various Rotating Components in Agro-Industrial Machinery with a Vibration Signal Acquired from a Single Point on the Machine Chassis.
- Authors: Ruben Ruiz-Gonzalez; Jaime Gomez-Gil; Francisco Javier Gomez-Gil; Víctor Martínez-Martínez
- Journal: Sensors
- Editor: MDPI
- Impact factor: 2.245 (2014)
- Journal Ranking:
 - Q1 on *Instruments & Instrumentation* (10/56).
 - Q2 on *Chemistry, Analytical* (31/74).
 - Q3 on *Electrochemistry* (14/28).
- Date of publication: November 3rd, 2014.
- ISSN: 1424-8220.
- Volume (Issue): 14 (11).
- Pages: 20713-20735.
- DOI: 10.3390/s141120713.
- URL: <https://www.mdpi.com/1424-8220/14/11/20713>.
- Number of cites: 18.

The article presented below is a version of the original article published in the previously mentioned journal. This version of the article has been authorized by the journal editor to be included in this PhD thesis as a compendium of publications.

Sensors **2014**, *14*, 20713–20735; doi:10.3390/s141120713

OPEN ACCESS

sensors

ISSN 1424-8220

www.mdpi.com/journal/sensors

Article

An SVM-Based Classifier for Estimating the State of Various Rotating Components in Agro-Industrial Machinery with a Vibration Signal Acquired from a Single Point on the Machine Chassis

Ruben Ruiz-Gonzalez ^{1,*}, Jaime Gomez-Gil ¹, Francisco Javier Gomez-Gil ² and Víctor Martínez-Martínez ¹

¹ Department of Signal Theory, Communications and Telematics Engineering, University of Valladolid, Valladolid 47011, Spain; E-Mails: jgomez@tel.uva.es (J.G.-G.); vmarmar@ribera.tel.uva.es (V.M.-M.)

² Department of Electromechanical Engineering, University of Burgos, Burgos 09006, Spain; E-Mail: fjggil@ubu.es

* Author to whom correspondence should be addressed; E-Mail: rruigon@ribera.tel.uva.es; Tel.: +34-6366-81022; Fax: +34-9834-23667.

External Editor: Gonzalo Pajares Martinsanz

Received: 9 September 2014; in revised form: 20 October 2014 / Accepted: 23 October 2014 / Published: 3 November 2014

Abstract: The goal of this article is to assess the feasibility of estimating the state of various rotating components in agro-industrial machinery by employing just one vibration signal acquired from a single point on the machine chassis. To do so, a Support Vector Machine (SVM)-based system is employed. Experimental tests evaluated this system by acquiring vibration data from a single point of an agricultural harvester, while varying several of its working conditions. The whole process included two major steps. Initially, the vibration data were preprocessed through twelve feature extraction algorithms, after which the *Exhaustive Search* method selected the most suitable features. Secondly, the SVM-based system accuracy was evaluated by using *Leave-One-Out* cross-validation, with the selected features as the input data. The results of this study provide evidence that (i) accurate estimation of the status of various rotating components in agro-industrial machinery is possible by processing the vibration signal acquired from a single point on the machine structure; (ii) the vibration signal can be acquired with a uniaxial accelerometer, the orientation of which does not significantly affect the classification

accuracy; and, (iii) when using an SVM classifier, an 85% mean cross-validation accuracy can be reached, which only requires a maximum of seven features as its input, and no significant improvements are noted between the use of either nonlinear or linear kernels.

Keywords: Support Vector Machine (SVM); predictive maintenance (PdM); agricultural machinery; condition monitoring; fault diagnosis; vibration analysis; feature extraction and selection; pattern recognition

1. Introduction

Agro-industrial machinery has a high initial investment and requires regular maintenance if further expensive repairs are to be avoided [1]. The need for machine maintenance programs and their appropriateness is a well-argued topic in the industry, which is reflected in the literature [2]. Early detection of a mechanical component that is malfunctioning will lead to its prompt replacement, thereby avoiding more costly repairs in the future.

Nowadays, many predictive maintenance techniques are employed, in order to reduce hazards and subsequent failures of machinery [1–3]. According to Scheffer *et al.* [4], the main such techniques are vibration monitoring, acoustic emission, oil analysis, particle analysis, corrosion monitoring, thermography, and performance monitoring.

Vibration analysis is a non-intrusive method that is widely employed in machinery status inspections, mainly on rotating equipment including engines, turbines, and compressors, among others [4–6]. In the case of machinery with no vibration isolation, the vibration signal propagates throughout the whole structure of the machine with moderate attenuation. The propagation of these vibrations makes it possible to monitor certain rotating components by placing an accelerometer at a different point on the machine structure [7]. However, the propagation of vibrations has a disadvantage, in so far that it transmits various vibration signals from various other machine components, in addition to the signal of interest, making it more difficult to identify the relevant signal [8].

Vibration signals from rotating components are usually analyzed in the frequency domain, because significant peaks in the signal spectrum appear at frequencies that are related to the rotation frequency of the component [4]. Various authors have performed this analysis using fast Fourier transform [9], short-time Fourier transform [10], the wavelet transform [11–15], the S-transform [16], and the Hilbert-Huang transform [17–20], among others. Due to the relationship between the rotation frequency of the machine component and the highest peaks in the spectrum signal, experts can estimate the status of machine components by looking for patterns in the spectrum signal. Nevertheless, doing so requires expert analysis of the vibration signal spectrum, which implies detailed knowledge of the machine, the way it functions and full information on the rotation speed of the component. Automated systems have been proposed to estimate the status of machine components using frequency analysis in the absence of expert analysis [19,21]. These systems incorporate knowledge of the machine component to extract characteristics from the spectrum signal and to estimate its status on the basis of these characteristics.

A Support Vector Machine (SVM) [22] is a supervised learning model widely used in the discipline of pattern recognition for classifying purposes. Due to its learning and generalization capabilities it is well suited for the implementation of estimation methods, which are widely required in automated diagnosis systems. According to the literature, many SVM-based applications have successfully been implemented [23], both for classification [24] and nonlinear regression [25]. Numerous improvements have been proposed over recent years that focus specifically on vibration monitoring in machinery fault diagnosis [26,27]. Widodo and Yang [28] offered a very thorough review of the latest major advances in the field of SVM-based vibration analysis for predictive maintenance.

Although a good deal of research has previously examined SVMs in machinery predictive maintenance [21,28], to the best of our knowledge, automatic prediction of the state of various rotating components in an agro-industrial machine by employing only one vibration signal acquired from a single point on the machine chassis, has not been conducted in previous research.

The purpose of this article is to present evidence to assess the feasibility of estimating the state of various rotating components in agro-industrial machinery by employing one vibration signal acquired from a single point on the machine chassis as the system input. The following five rotating component states in an agricultural harvester were selected to assess that estimation capability: (1) engine speed status (*high speed/low speed*); (2) threshing cylinder operating status (*on/off*); (3) threshing cylinder balance status (*balanced/unbalanced*); (4) straw chopper operating status (*on/off*); and (5) straw chopper balance status (*balanced/unbalanced*).

2. Background

This section comprises some fundamentals about vibration analysis in agro-industrial machinery, classification in supervised machine learning, feature extraction and selection, and SVM-based classification.

2.1. Vibrations in Agro-Industrial Machinery

Vibration can be defined as the repeated motion of a certain component back and forth from a given position. Accelerometers are sensors that measure proper acceleration. These devices are the most widely used for capturing vibration signals in rotating machinery applications. Typical accelerometers capture signals in frequency ranges from 1 Hz to 10 kHz [4].

The most common defects causing high vibration levels in machinery, in accordance with Scheffer *et al.* [4], are: unbalance of rotating parts, misalignment of couplings and bearings, bent shafts, worn or damaged gears and bearings, bad drive belts and chains, torque variations, electromagnetic forces, aerodynamic forces, hydraulic forces, looseness, rubbing, and resonance. When machinery rotating components operate at high speeds or under harsh operating conditions for a long time, some of these defects start to appear.

Vibrations can reveal the presence of machinery defects. Usually, vibrations on rotating components appear at specific frequencies, which are characteristic of each specific component and also depend on the component rotation speed and other properties [19,21]. Traditionally, depending on the vibration amplitude at those specific frequencies, the severity of the defects can be assessed.

Therefore, plenty of information on the condition of a component, e.g., possible deterioration, can be detected by analyzing the vibration characteristics of isolated components [4].

In addition, the vibration signals of a specific machine component can be acquired from almost any point on the machine structure, even though the signals will be slightly attenuated, due to their propagation throughout the machine structure and the imperfect isolation of the main sources of vibration. Propagation complicates data processing and the extraction of useful information, because information from several machine components is mixed. It nevertheless greatly simplifies the data acquisition stage, as just a sensor may be installed at a single point on the machine.

2.2. Classification in Supervised Machine Learning

Machine learning, as a sub-field of artificial intelligence in computer science, deals with intelligent systems that can modify their behavior in accordance with the input data. Intelligent systems must have the capability of deducing the function that best fits the input data, in order to learn from the data. Machine learning can be divided into unsupervised and supervised learning, depending on the information that is available for the learning process. Unsupervised machine learning undertakes the inference process by using an unlabeled training set, *i.e.*, without any information on the desired output, and it seeks to deduce relationships by looking for similarities in the dataset. Meanwhile, supervised machine learning assumes that a labeled training set, for which the desired output is completely known, is available.

Classification, as a branch of supervised learning, is defined as the process of identifying the class to which a previously unseen observation belongs, based on previous knowledge given by a training dataset that contains instances the category membership of which is certain. Any algorithm which performs classification tasks, *i.e.*, the mapping of input data to an assigned class, is called a classifier.

Classifiers must be trained, based on previous knowledge, in order to function properly. The training process makes use of a sample of N observations, the corresponding classes of which are certain. This sample of N observations is typically divided into two subsamples: the training and the test datasets. Firstly, the training dataset is used in the process of computing a classifier that is well-adapted to these data. Then the test dataset is used to assess the generalization capability of the previously computed classifier.

Both the misclassification rate and the success rate in the test dataset are commonly used as quality measurements to assess classifier performance. The misclassification rate is defined as the proportion of observations which are wrongly assigned to an incorrect class. It is expressed as follows:

$$MR = \frac{\text{Number of Incorrect Classifications}}{\text{Total Number of Classifications}}$$

Alternatively, the success rate (also called the hit rate) is defined as the proportion of observations that are properly assigned to the corresponding class and is calculated as follows:

$$SR = \frac{\text{Number of Correct Classifications}}{\text{Total Number of Classifications}} = 1 - MR$$

The *k-fold cross-validation* is an enhanced method of evaluating classifier performance, especially with small training and test datasets. In this method, the original sample of N observations is randomly partitioned into k subsamples of equal size. From those k subsamples, a single subsample is retained as the test dataset, and the remaining $k - 1$ subsamples are used as the training dataset. The *k-fold cross-validation* repeats this training and test process k times, using each of the k subsamples only once as the test dataset. Cross-validation accuracy is calculated as the average of the success rate obtained for each of the k different test datasets. When $k = N$, *k-fold cross-validation* is also known as *leave-one-out cross-validation*.

Many different classifiers have been proposed in the literature [29,30]. Some of the main ones include *k*-nearest neighbor classifier, Bayes classifier, logistic regression, Fisher's linear discriminant, decision tree, Artificial Neural Networks (ANN), and Support Vector Machines (SVM). An SVM classifier is used in this article and hence SVM is described in greater detail in Section 2.4.

2.3. Feature Extraction and Selection for Classification

Machine learning systems, including classifiers, are typically required to process large volumes of information. The application of dimensionality reduction techniques to the input data prevents the classifier from processing too much data and improves its performance. Dimensionality reduction, within statistical machine learning field, is defined as the process of reducing the number of variables of a dataset while retaining most of its degrees of freedom, thereby simplifying the subsequent classification problem. Feature extraction and selection are methods to accomplish dimensionality reduction.

Feature extraction [29] consists in reducing the dimensions of a d -dimensional input data vector by transforming it into a new m -dimensional output data vector, where $m < d$. The resulting m -dimensional vector, called feature vector, should retain from the original vector most of the useful information for the subsequent classification stage. This property is often referred as *degrees of freedom preservation*. Attending to their data type, features can be categorical, ordinal, integer-valued, or real-valued. A very wide variety of feature extraction algorithms have been proposed in the literature [31–34]. A taxonomy of these algorithms exists on the basis of their relationship to specific mathematical fields. The most popular such categories are nonlinear, statistical and transformed-domain based. Some of the nonlinear feature extraction algorithms are *Correlation Dimension* [35], *Kolmogorov Complexity* [36], *Lempel-Ziv Complexity* [31,37], *Approximate Entropy* [38], and *Sample Entropy* [39]. Classical time-domain based methods of statistical feature extraction include *Mean Value*, *Standard Deviation*, *Skewness*, *Kurtosis*, *Average Power*, and *Shannon Entropy* [40]. Some of the notable frequency domain feature extraction techniques are *Spectral Entropy* [32], *Median Frequency* [33,41], *Bandwidth Containing 90% of the Signal Energy*, and *Relative Wavelet Packet Energy* [34].

Feature selection [29] involves choosing, among an original set of features of size m , the subset of size n that best represents the original set and that yields the smallest classification error. The feature selection process can be conducted, among other methods by means of *Exhaustive Search* or *Sequential Forward/Backward Floating Search* [29]. On the one hand, *Exhaustive Search* explores all the possible subsets, *i.e.*, 2^m if n is a free parameter, or $\binom{m}{n}$ if n is a preset constant. This method therefore guarantees the selection of the best subset, although its use of computational resources is

excessive. On the other hand, *Sequential Forward/Backward Floating Search* restricts the search to a smaller subtree by only allowing feature deletion and addition at each step. Consequently, this method presents a more affordable computational load, but it fails to guarantee optimal subset selection, even though it has been proven to yield suboptimal results that are almost optimal.

The performance improvements offered by feature extraction and selection techniques are linked to: (i) dimension reduction that mitigates the ‘curse of dimensionality’ problem and therefore reduces the risk of over-fitting [29,42]; and (ii) simplification of the resulting classifier, which results in using less memory and fewer computational resources [29].

2.4. Support Vector Machines for Classification

Support Vector Machines (SVM) is a statistical supervised machine learning technique, used both for classification and for regression purposes. Originally proposed by Vapnik and Cortes [22,43], in 1995, although its principles and derivation differ from those of *Artificial Neural Networks* (ANN), some authors sometimes consider SVMs as a special kind of ANN [44]. However, many authors refuse to do so, due to essential differences between SVM and ANN techniques [45]. While SVM mechanisms are mainly based on a rigorous geometrical and statistical approach, ANNs try to emulate the behavior of the human brain and its neural system.

The original SVM proposal was aimed at both the binary classification problem, considering only two possible classification classes, and the multiclass classification problem, which considers more than two classification classes.

Binary linear SVM classification performs the calculation of the optimal hyperplane decision boundary, separating one class from the other, on the basis of a training dataset. Optimality can be understood, depending on whether perfect classification of the training dataset is feasible and desired, in two separate ways:

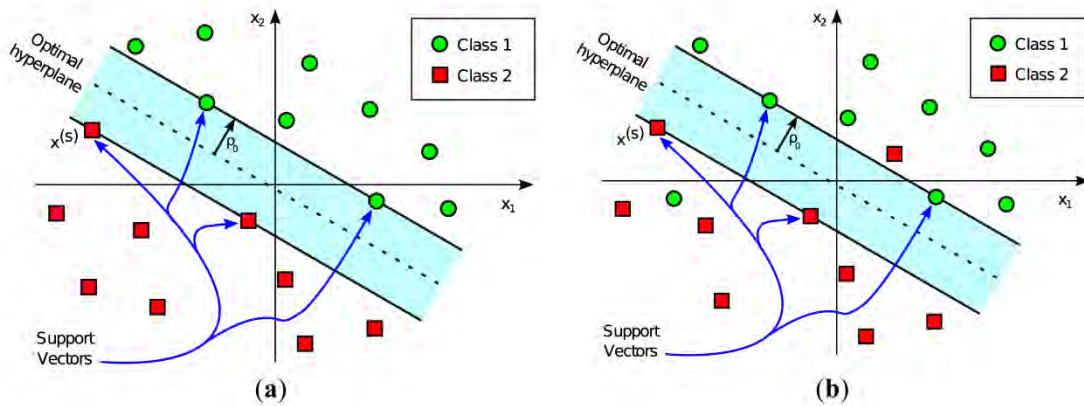
- If perfect separability of training dataset classes can be achieved, a Hard Margin optimality can be used. In this case, the hyperplane decision boundary is chosen to maximize the distance from the hyperplane to the nearest training data point.
- If perfect classification is not desired or if it is impossible, a Soft Margin optimality is used. In this case, the hyperplane selection is a customizable tradeoff between minimizing the misclassification rate and maximizing the distance to the nearest properly classified training point.

The decision boundary hyperplane in SVM classification is calculated by employing the training dataset. This decision boundary is completely determined by the so-called Support Vectors, a subset of training input vectors which by themselves alone lead to the same decision boundary. After this hyperplane is determined, the SVM classifier is ready to be used with a different dataset from the one used in the training stage. The assigned class, labeled either +1 or -1, depends on the side of the decision boundary on which the input vector falls. Figure 1 represents a graphical example of linear SVM-based classification, both in the case of linearly separable classes and non-linearly separable classes.

SVM multiclass classification usually tackles the classification and computation of the decision boundary by reducing the problem to a set of binary classification problems. The main such approaches are

pairwise and one-versus-all classification methods [46]. Compact multiclass reformulations of the binary classification problem have also been proposed [46].

Figure 1. Representation of a Support Vector Machine (SVM) classifier corresponding to (a) a linearly separable pattern, where the hyperplane totally separates green circles from red squares; and (b) a non-linearly separable pattern, where no hyperplane separates all the green circles from the red squares.



To be mathematically rigorous, the most general SVM linear binary classification problem can be stated as follows:

“Given a training dataset, $\{\mathbf{x}_i, d_i\}_{i=1}^N$, the goal is to compute the optimal weight vector \mathbf{w} , bias b , and slack variables ξ , such that satisfy the following constraints:

$$d_i(\mathbf{w}^T \mathbf{x}_i + b) \geq 1 - \xi_i, \forall i = 1, 2, \dots, N$$

$$\xi_i \geq 0, \forall i = 1, 2, \dots, N$$

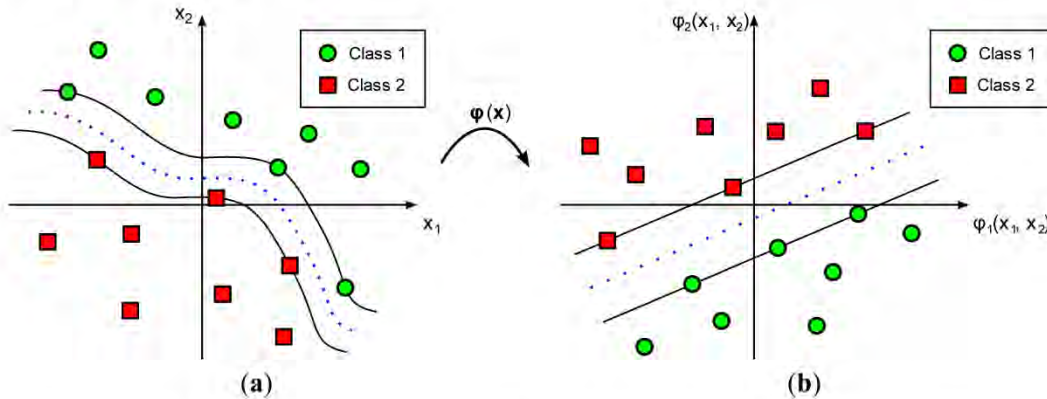
and such that the following cost function is minimized:

$$\Phi(\mathbf{w}, \xi) = \frac{1}{2} \mathbf{w}^T \mathbf{w} + C \sum_{i=1}^N \xi_i$$

where, $\mathbf{x}_i \in \mathbb{R}^{m_0}$ denotes the i -th input vector, $d_i \in \{-1, 1\}$ denotes the class corresponding to the i -th input vector, $\xi = \{\xi_i\}_{i=1}^N$ represents the slack variables, and the constant C is a user-specified parameter that determines the tradeoff between misclassification and maximum inter-class margin.”

In practice, most classification problems cannot be solved by using a simple hyperplane as the decision boundary. In such cases a more complex and elaborate decision boundary is required. SVM achieves this goal by increasing the dimensionality of the input space, of dimension m_0 , by applying a nonlinear transformation, denoted by $\varphi(\cdot)$, into a feature space of dimension $m_f > m_0$ (Figure 2). This transformation, $\varphi(\cdot)$, serves to reduce the misclassification probability in the transformed feature space. The most typical transformation functions, as in the case of ANNs, are *radial basis functions*, *higher-order polynomials*, and *sigmoids*. Figure 2 represents a graphical example of an SVM nonlinear classification.

Figure 2. Representation of a Support Vector Machine classifier with a nonlinear kernel. Function $\varphi(\cdot)$ is the nonlinear transformation mapping vectors from (a) the input space to (b) the feature space.



The boundary in the nonlinear classification problem is still a hyperplane, not in the original input space but in the feature space, and can be expressed as the points $\varphi(\mathbf{x})$ that satisfy that:

$$\mathbf{w}^T \varphi(\mathbf{x}) + b = 0 \tag{1}$$

where, $\mathbf{x} \in \mathbb{R}^{m_0}$ and $\varphi(\mathbf{x}) \in \mathbb{R}^{m_f}$.

Following the application of the Lagrange multipliers method, it has been shown that the optimal weight vector can be expressed as [44]:

$$\mathbf{w} = \sum_{i=1}^N \alpha_i d_i \varphi(\mathbf{x}_i) \tag{2}$$

where, α_i stands for the Lagrange multiplier coefficients.

Therefore, the optimal decision boundary can be rewritten as:

$$\sum_{i=1}^N \alpha_i d_i \varphi(\mathbf{x}_i)^T \varphi(\mathbf{x}) + b = 0 \tag{3}$$

Renaming $u_i = \alpha_i d_i$ and $K(\mathbf{x}_i, \mathbf{x}) = \varphi(\mathbf{x}_i)^T \varphi(\mathbf{x}) = \varphi(\mathbf{x})^T \varphi(\mathbf{x}_i) = K(\mathbf{x}, \mathbf{x}_i)$, the decision function, y , can be expressed as:

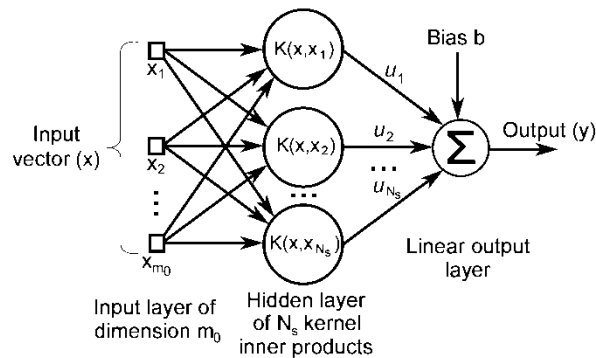
$$y = \sum_{i=1}^N u_i K(\mathbf{x}, \mathbf{x}_i) + b \tag{4}$$

In case of linear classifiers, $K(\mathbf{x}, \mathbf{x}_i)$ is the conventional Euclidean inner product of the input vector \mathbf{x} with the Support Vector \mathbf{x}_i . In case of nonlinear classifiers, $K(\mathbf{x}, \mathbf{x}_i)$ is the conventional Euclidean inner product of the nonlinear transformation $\varphi(\mathbf{x})$ of the input vector \mathbf{x} with the nonlinear transformation $\varphi(\mathbf{x}_i)$ of the Support Vector \mathbf{x}_i .

The decision function in Equation (4) results in the architecture depicted in Figure 3, once the proper weights and Support Vectors have been computed in the training stage. Only the Support Vectors have to be considered, as they are the only vectors that generate non-zero α_i coefficients [44].

Classification is therefore performed by identifying the sign of the output value, y , in Equation (4). If $\text{sign}(y) = +1$, then this input is labeled as class +1 and if otherwise as class -1.

Figure 3. Architecture of a Support Vector Machine classifier. Inner product kernels, $K(\cdot, \cdot)$, denote the m_0 -dimensional kernel inner product of the input vector with each of the N_s Support Vectors.



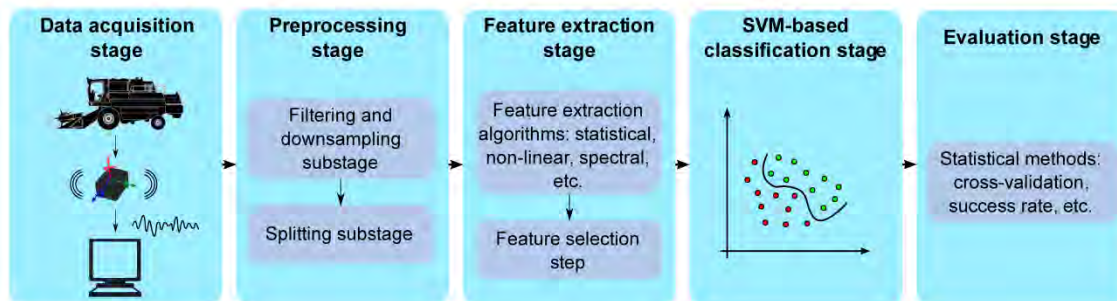
The most well-known and widely used nonlinear kernels are *radial basis functions (RBF)*, *sigmoids*, and *polynomials*. The *RBF kernel* can be expressed as $K(\mathbf{x}, \mathbf{y}) = \exp(-\gamma \|\mathbf{x} - \mathbf{y}\|^2)$, where γ is a user-defined parameter; the *sigmoidal kernel* can be expressed as $K(\mathbf{x}, \mathbf{y}) = \tanh(\gamma \mathbf{x}^T \mathbf{y} + c_0)$, where $\gamma > 0$ and $c_0 < 0$ are user-defined parameters; and, the *d -order polynomial kernel* can be expressed as $K(\mathbf{x}, \mathbf{y}) = (\gamma \mathbf{x}^T \mathbf{y} + c_0)^d$, where γ and c_0 are user-defined parameters and where d denotes the polynomial degree. Other kernels may also be found, in addition to those listed above.

The underlying SVM training process undertakes the problem of minimizing a quadratic functional subject to linear constraints. This problem, known as *Quadratic Programming*, has a closed solution. Although the solution can be analytically computed by applying the Lagrange multipliers method, other computational methods are typically used, especially when the dimensionality of the problem becomes high. Some of these methods include, among others, *Interior Point* methods [47], the *Sequential Minimal Optimization (SMO)* algorithm [48,49], *Incremental* methods [50], and the *Kernel-Adatron (KA)* algorithm [51]. More information about the SVM training process has been gathered by Campbell and Ying [52].

Those readers eager to discover the rigorous mathematical statement and solution of the problem underlying Support Vector Machines are encouraged to read the comprehensive introduction to SVM provided by Haykin [44] or the in-depth work by Steinwart and Christmann [53].

3. Materials and Methods

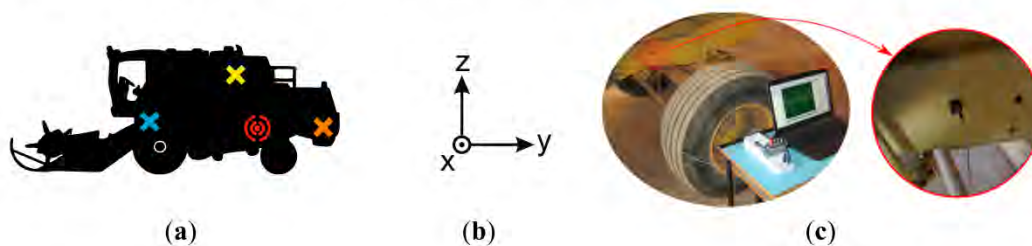
The main processing stages performed in this study can be conceptualized as follows: (i) the data acquisition stage (Section 3.1); (ii) the preprocessing stage (Section 3.2); (iii) the feature extraction and selection stage (Section 3.3); (iv) the SVM-based classification stage (Section 3.4); and (v) the evaluation stage (Section 3.5). Figure 4 summarizes the main processing stages and contains a high-level description of the methods, which are explained in greater detail in the remainder of this section.

Figure 4. Overall block diagram summarizing the main processing stages.

3.1. Data Acquisition Stage

Vibration data were experimentally obtained from an eleven-year-old New Holland TC56 harvester that had clocked 3800 working hours. Vibration signals were acquired from a stationary harvester operating in threshing mode. A Kistler 8690C50 triaxial accelerometer was used to measure the vibration signals on transverse, longitudinal and vertical axes (Figure 5). After several trial and error tests, the accelerometer sensor was placed on the left hand side of the harvester chassis, neither very close nor very far away from the rotating components under analysis (Figure 5). The sensor was positioned by using an adhesive mounting following the guidelines in Scheffer *et al.* [4]. This mounting method was selected because the frequency analysis in this article was bandlimited below 200 Hz and it permits accurate measurements within this frequency range [4]. Vibration signals were acquired using the *NI Sound and Vibration Assistant* software and a *National Instruments (NI) data acquisition (DAQ) system*. The data acquisition system was composed of an *NI 9234 data acquisition module for analog input signals* and an *NI compact DAQ chassis NI cDAQ-9172*, to connect the DAQ module to a laptop.

Figure 5. (a) Harvester schematic in which the red symbol represents the precise location of the accelerometer sensor on the chassis, the yellow cross represents the location of the engine, the blue cross represents the location of the threshing cylinder, and the orange cross represents the location of the straw chopper; (b) The coordinate axes of the accelerometer in this study were as follows: the x axis was transverse to the front direction of the harvester, the y axis pointed to the reverse direction of the harvester, and the z axis was upward vertical with respect to the ground; (c) The experimental setup for data acquisition and a close up of the position of the Kistler 8690C50 triaxial accelerometer.



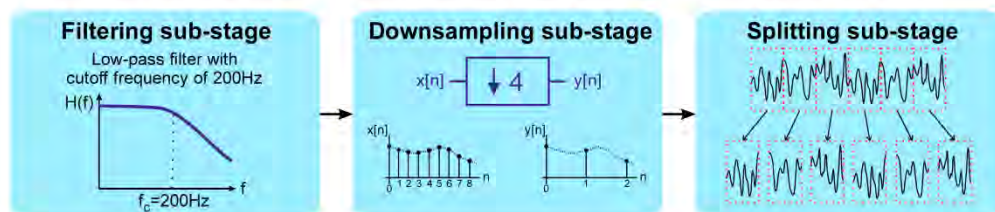
A total of 18 different data acquisition processes were performed to acquire data on all the combinations of the following harvester working conditions: (i) engine speed status (*high speed/low speed*); (ii) threshing cylinder operating status (*on/off*); (iii) threshing cylinder balance status (*balanced/unbalanced*) in the *on* operating status; (iv) straw chopper operating status (*on/off*); and (v) straw chopper balance status (*balanced/unbalanced*) in the *on* operating status. The straw chopper was unbalanced on purpose by the breakage of a blade. The unbalance was provoked in this way, because blade breakage against stones is a frequent cause of unbalances. The unbalance was provoked in this way, because blade breakage against stones is a frequent cause of unbalances. The threshing cylinder was unbalanced by adding an eccentric weight to it. The unbalance was provoked in this way, because the threshing cylinder can typically become unbalanced when its bars suffer from non-uniform wear, due to usage and an eccentric weight simulates the same effect.

Sixty-second long epochs or frames of machine operation were recorded for each of the 18 acquisition processes, using a sampling frequency of 1706.48 Hz, which generated a total of 99,120 samples per epoch.

3.2. Preprocessing Stage

The acquired acceleration time-series data were first preprocessed in order to adapt them to the subsequent feature extraction stage. The entire preprocessing stage was divided into the following three sub-stages (Figure 6): (i) a low-pass filtering sub-stage; (ii) a downsampling sub-stage; and (iii) a splitting sub-stage.

Figure 6. Block diagram representing the three preprocessing sub-stages.



In the first sub-stage, low-pass filtering took place. A digital IIR elliptic low-pass filter, with a cutoff frequency of 200 Hz, was applied to the input signal. The vibration frequencies of interest, which are the main harmonics of the components rotation speeds, are located within the range from 0 to 200 Hz. This filtering was performed in order to remove noise and unwanted interferences to achieve a better performance.

Next, after filtering, the downsampling sub-stage took place. The input signal was decimated, in order to reduce the sampling frequency by a factor of N_{fs} , where $N_{fs} \in \mathbb{N}$ is the decimation ratio. In this article, a value of $N_{fs} = 4$ was chosen, taking into account the frequency range of interest. Therefore, the effective sampling frequency was reduced after downsampling from 1706.5 Hz, the one originally employed in the acquisition stage, to 426.625 Hz.

Finally, the splitting sub-stage was conducted. The downsampled signal, coming from the second sub-stage, was then split into six epochs of about ten seconds, which was the frame size considered sufficient for keeping meaningful information on the vibration signal for the posterior feature

extraction steps and for ensuring good frequency resolution in the subsequent FFT analysis. In this way, a total of 4130 samples per epoch were obtained.

All these preprocessing tasks were performed with *MATLAB*[®] program.

3.3. Feature Extraction and Selection Stage

This stage involves the dimensionality reduction of the input data-series coming from the previous stage. It is divided into two sub-stages: feature extraction and feature selection.

Firstly, the preprocessed data from the previous stage were brought in the feature extraction sub-stage, in order to achieve a simpler classifier. Then, the input signal for this stage, denoted as $x[n]$, where $n = 1, 2, \dots, N = 4130$, was used to extract the following features:

- (1) *Average Power (P)*, defined as $\bar{P} = \frac{1}{N} \sum_{n=1}^N x[n]^2$. This feature quantifies the overall vibration intensity.
- (2) *Sample Entropy (SampEn)*, computed using the definition provided by Richman *et al.* [39]. This feature is a measurement of signal regularity that assigns higher values to more random data; for instance when multiple vibration sources are superposed.
- (3) *Spectral Entropy (SpecEn)*, computed in the same way as by Hornero *et al.* [33]. This feature was employed because of its capability to quantify the flatness of the spectrum. The more frequency peaks the signal has, the greater this feature becomes.
- (4) *Mean Value (\bar{x})*, calculated as $\bar{x} = \frac{1}{N} \sum_{n=1}^N x[n]$. It reflects the amplitude of low frequency background vibrations.
- (5) *Median frequency (MF)*, computed as the frequency which divides the power spectrum into two halves, each of which contains the same energy. It was calculated in the same way as by Hornero *et al.* [33].
- (6) *Standard Deviation (σ)*, calculated by using the mean value \bar{x} that has previously been defined, as the square root of the unbiased estimator of the variance, *i.e.*, $\sigma = \sqrt{\frac{1}{N-1} \sum_{n=1}^N (x[n] - \bar{x})^2}$. This feature provides information on the width of the amplitude histogram distribution, supplying additional information on the shape of the vibration signal.
- (7) *Skewness (s_0)*, calculated as the unbiased estimator $s_0 = \frac{\sqrt{N(N-1)}}{N-2} \frac{\frac{1}{N} \sum_{n=1}^N (x[n] - \bar{x})^3}{\left(\frac{1}{N} \sum_{n=1}^N (x[n] - \bar{x})^2\right)^{3/2}}$.

Skewness, which is a measure of histogram distribution asymmetry around its mean, can reflect vibration asymmetries due to mechanical faults.

- (8) *Kurtosis (k_0)*, calculated as the unbiased estimator $k_0 = \frac{N-1}{(N-2)(N-3)} \left((N+1)k_1 - 3(N-1) \right) + 3$, where $k_1 = \frac{\frac{1}{N} \sum_{n=1}^N (x[n] - \bar{x})^4}{\left(\frac{1}{N} \sum_{n=1}^N (x[n] - \bar{x})^2\right)^2}$. This feature reflects the peakedness of the histogram, giving information on the distribution of the vibrations amplitude.

- (9) *Central Tendency Measurement (CTM)*. In the first place, the first-order differences scatter plot is constructed, representing $x[n+1] - x[n]$ on the *X* axis against $x[n+2] - x[n+1]$ on the *Y* axis. The proportion of points lying inside a circle of a certain fixed radius is then returned as a measurement of signal regularity. A radius of 0.05 g was selected in this study,

which is an appropriate one for distinguishing the related classification classes. This feature offers a measurement of the randomness of the vibration signal, where a low value of this feature implies sharp changes in the vibration signal. Sharp changes in vibration signals may be caused both by high frequency vibrations or sudden transitions due to mechanical faults.

- (10) *Correlation coefficient (r) from the first-order differences scatter plot.* As with the previous feature, the first-order differences scatter plot is constructed first, obtaining both $X[n]$ and $Y[n]$ vectors. Then the Pearson's linear correlation coefficient between both vectors is computed as: $r = \frac{\sum_{n=1}^N (x[n]-\bar{X})(y[n]-\bar{Y})}{\sqrt{\sum_{n=1}^N (x[n]-\bar{X})^2} \sqrt{\sum_{n=1}^N (y[n]-\bar{Y})^2}}$, where \bar{X} and \bar{Y} are the mean values of $X[n]$

and $Y[n]$, respectively. This feature offers a measurement of the unpredictability of the signal from the previous data; the higher the measure of $|r|$ the more predictable the signal is.

- (11) *Lempel-Ziv Complexity (LZC)*, computed as by Hornero *et al.* [33]. This feature offers a notion of complexity in a statistical sense. It characterizes the average information quantity within a signal and can therefore reflect the superposition of several vibration sources.

- (12) *Crest Factor (C)*, calculated as $C = \frac{\max|x[n]|}{\sqrt{\frac{1}{N} \sum_i x[n]^2}}$, where N is the number of samples of the time-series $x[n]$. This feature reflects the spikiness of the signal with respect to its RMS value and is therefore useful to assess the presence of mechanical faults.

All of the above algorithms were selected on the basis of the previous literature on vibration analysis [21,54–56] and by extrapolating ideas from studies in other fields [33,37,39].

Secondly, after having extracted these features from the preprocessed data-series, the most suitable features from among them all were selected in the feature selection sub-stage. The feature selection process was undertaken by using the *Exhaustive Search* method, which explores all of the possible feature subsets. With each of the explored subsets, linear SVM *leave-one-out* cross-validation was performed to assess the goodness of this subset. The feature subset with highest cross-validation accuracy was selected. The value of parameter C , involved in the SVM classification problem, was prefixed at 1 in all cases. Cross-validation accuracy was calculated for each classifier undertaking each of the five classification problems, corresponding to the five rotating component states of the agricultural harvester under consideration: (1) engine speed status (*high speed/low speed*); (2) threshing cylinder operating status (*on/off*); (3) threshing cylinder balance status (*balanced/unbalanced*); (4) straw chopper operating status (*on/off*), and (5) straw chopper balance status (*balanced/unbalanced*).

The choice of the *Exhaustive Search* method was possible due to the relatively small number of twelve features that were involved, as mentioned above. If more features were to be explored, it would be advisable to use *Sequential Forward/Backward Floating Search* for computational efficiency [29].

All the tasks of this stage were performed in the *MATLAB*[®] programming environment using the *LIBSVM* library [57,58].

3.4. SVM-Based Classification Stage

The classification stage took place once the previous processing stages had been performed. Among the huge variety of classifiers available, SVM classification was selected in this work because

of its: (i) great generalization ability; (ii) low overtraining risk due to small datasets; and (iii) low computational load.

A different SVM-based classifier was employed for each of the five related classification problems, corresponding to the following five rotating component states of the agricultural harvester: (1) engine speed status (*high speed/low speed*); (2) threshing cylinder operating status (*on/off*); (3) threshing cylinder balance status (*balanced/unbalanced*); (4) straw chopper operating status (*on/off*); and (5) straw chopper balance status (*balanced/unbalanced*). The input of each classifier was the subset of features that led to maximum cross-validation accuracy (Section 3.3). If more than one subset led to the maximum value, only one of them was selected for the sake of simplicity. Each classifier provided one of the two classes associated with the input feature vector as its output.

For each of the five classifiers, the *linear* kernel and the *radial basis function* (RBF), the *sigmoidal*, and the *third-order polynomial* nonlinear kernels were employed, providing a comparison between their accuracy. These SVM kernels were selected, because they are the most typical and widely used. The C parameter, involved in the SVM classification formulation, and the γ and c_0 parameters, involved in the kernel, were optimized by conducting an exponential grid-search on these parameters [59]. The parameters that led to the highest cross-validation accuracy were selected.

The *LIBSVM* toolbox [57,58], running in the *MATLAB*[®] programming environment, was once again employed for classification tasks.

3.5. Classifier Performance Evaluation Stage

The *leave-one-out* cross-validation accuracy (Section 2.2), for each of the five individual classification problems under consideration, was computed to assess the goodness of the proposed classifying system. These five cross-validation accuracies, as well as the overall mean cross-validation accuracy, were used as a measurement of the accuracy of the SVM-based estimation method for each of the five aforementioned harvester states.

4. Results

The experimental results of the feature selection and classifier performance evaluation stages are presented in this section.

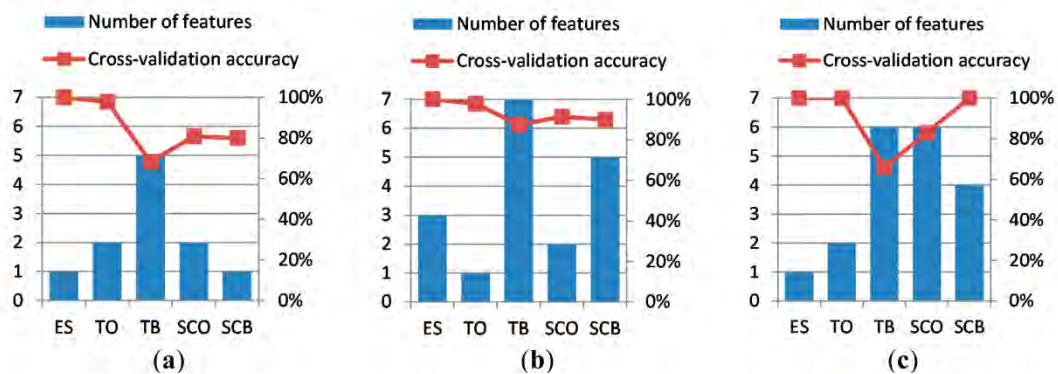
4.1. Feature Selection

The selection of the best features, following the methods explained in Section 3.3, led to the best cross-validation accuracies and best particular chosen features shown in Table 1. It can be appreciated that, in all cases, the required number of features is lower than or equal to seven and that the mean cross-validation accuracy is above 85%, for all the three axes of the accelerometer. The best cross-validation accuracies and the number of features needed to achieve these are depicted in Figure 7.

Table 1. Feature selection results for each of the three axes acquired by the triaxial accelerometer. The first row (number of features) shows the optimal number required to achieve the best cross-validation accuracy. The second row (best feature subset) shows all of the concrete feature subsets, giving the highest cross-validation accuracy as a list of numbers the legend of which corresponds to the list provided in Section 3.3. The subset employed for the subsequent classifier performance evaluation stage appears in bold. Each column corresponds to each of the rotating component classification problem under consideration.

		Classification Problem				
		Engine Speed	Threshing Cylinder Operation	Threshing Cylinder Balance	Straw Chopper Operation	Straw Chopper Balance
Transverse X axis of the accelerometer	Number of features	1	2	5	2	1
	Best feature subset(s)	{9}	{10,11}	{4,6,7,9,11}	{2,8} ;{2,5}	5
	Cross-validation accuracy	100%	97.87%	68.29%	80.85%	80%
	Mean CVA	85.40%				
Longitudinal Y axis of the accelerometer	Number of features	3	1	7	2	5
	Best feature subset(s)	{6,7,10} ; {5,7,9}; {5,6,10}; {1,6,10}	{5}	{1,2,7,8,9,11,12} ; {1,2, 4,7,8,11,12}; {1,2,4,6,7,11,12}; {1,2,3,5,7,8,11}	{4,11}	{1,3,5,7,12}
	Cross-validation accuracy	100%	97.87%	87.49%	91.49%	90%
	Mean CVA	93.37%				
Vertical Z axis of the accelerometer	Number of features	1	2	6	6	4
	Best feature subset(s)	{9}	{2,11} ;{2,3}	{2,3,5,6,8,11}	{1,4,5,7,8,10}	{1,2,7,10}
	Cross-validation accuracy	100%	100%	65.85%	82.98%	100%
	Mean CVA	89.77%				

Figure 7. Number of features and cross-validation accuracy for each of the working conditions under consideration—(ES) engine speed, (TO) threshing cylinder operation, (TB) threshing cylinder balance, (SCO) straw chopper operation, and (SCB) straw chopper balance—using the accelerometer channel corresponding to (a) the transverse X axis; (b) the longitudinal Y axis; and (c) the vertical Z axis.



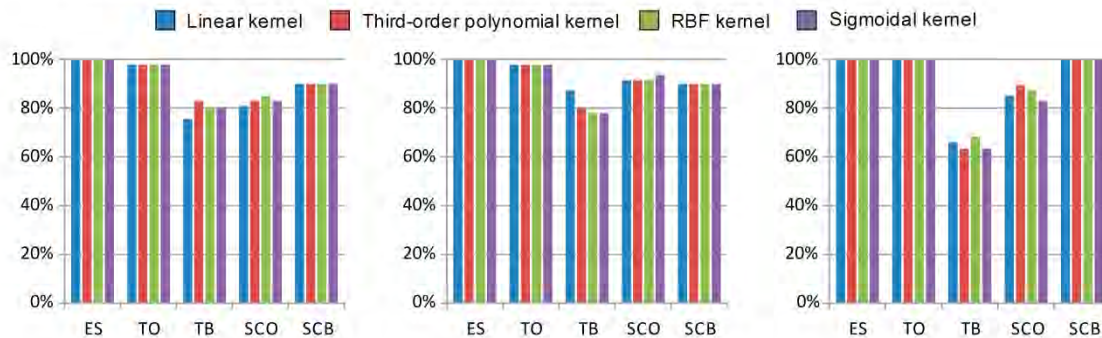
4.2. SVM Classifier Performance Evaluation

The results of the linear and nonlinear SVM classifier optimization, showing the best cross-validation accuracies and the related optimal parameters, are shown in Table 2. The previously selected features, highlighted in bold in Table 1, were used as input to the SVM classifier. Note that the nonlinear kernels did not outperform the linear kernel in most cases. Even in those cases where the accuracy was improved, only slight differences never over 10% were observed. It therefore appears that the use of linear SVM classification is sufficient to solve the problem. A comparison of kernel cross-validation accuracy is also provided in Figure 8.

Table 2. Performance results for each of the three axes acquired by the triaxial accelerometer, comparing the different SVM kernels, and showing both the optimized parameters (C, γ, c_0) and the best cross-validation accuracy (CVA). The best result for each classification problem appears in bold.

		Classification Problem					
		Engine Speed	Threshing Cylinder Operation	Threshing Cylinder Balance	Straw Chopper Operation	Straw Chopper Balance	
Transverse X axis of the accelerometer	Linear kernel	CVA	100%	97.87%	75.61%	80.85%	90.00%
		C	1	1	6	1	1.2
	Third-order polynomial kernel	CVA	100%	97.87%	82.93%	82.98%	90.00%
		C	0.03	32768	8192	2048	0.03
		γ	8	0.125	0.125	32	8
		c_0	0.03	0.03	0.5	0.5	0.03
	RBF kernel	CVA	100%	97.87%	80.49%	85.10%	90.00%
		C	0.125	512	32	32	0.5
		γ	2	0.125	2	8	2
	Sigmoidal kernel	CVA	100%	97.87%	80.49%	82.98%	90.00%
		C	2	2048	2048	8	2
		γ	0.5	0.125	0.125	8	2
		c_0	0.03	0.03	0.03	0.5	0.03
	Longitudinal Y axis of the accelerometer	Linear kernel	CVA	100%	97.87%	87.49%	91.49%
C			1	1	1	1	1
Third-order polynomial kernel		CVA	100%	97.87%	80.49%	91.49%	90.00%
		C	8192	0.03	8192	0.03	2048
		γ	0.125	8	0.002	8	0.125
		c_0	0.03	0.03	8	0.03	0.03
RBF kernel		CVA	100%	97.87%	78.05%	91.49%	90.00%
		C	0.5	0.5	2	2	2
		γ	8	8	0.5	2	2
Sigmoidal kernel		CVA	100%	97.87%	78.05%	93.62%	90.00%
		C	2	32	512	8192	8
		γ	0.5	0.125	0.008	0.125	0.5
		c_0	0.03	0.03	0.03	0.125	0.03
Vertical Z axis of the accelerometer		Linear kernel	CVA	100%	100%	65.85%	85.10%
	C		1	1	1	430	1
	Third-order polynomial kernel	CVA	100%	100%	63.41%	89.36%	100%
		C	8192	512	2048	8192	0.03
		γ	0.125	0.5	0.125	0.03	8
		c_0	0.03	0.03	0.5	2	0.03
	RBF kernel	CVA	100%	100%	68.29%	87.23%	100%
		C	0.125	32	2	8192	2
		γ	2	0.5	32	0.03	0.5
	Sigmoidal kernel	CVA	100%	100%	63.41%	82.97%	100%
		C	2	128	512	32	8
		γ	0.5	0.125	0.5	0.125	0.5
		c_0	0.03	0.03	0.125	0.03	0.03

Figure 8. Cross-validation accuracy for each kernel under the following working conditions—(*ES*) engine speed, (*TO*) threshing cylinder operation, (*TB*) threshing cylinder balance, (*SCO*) straw chopper operation, and (*SCB*) straw chopper balance—using the accelerometer channel corresponding to (a) the transverse *X* axis; (b) the longitudinal *Y* axis; and (c) the vertical *Z* axis.



5. Discussion

This article investigates a method of estimating the status of various rotating components in agro-industrial machinery by processing vibration signals acquired from a single point of the machine structure. It offers three major findings.

The first finding of this article is that it is possible to accurately estimate the status of some rotating components in agro-industrial machinery by processing the vibration signal acquired from a single point on the machine. Moreover, the accelerometer sensor does not need to be placed very close to the rotating components, which makes the acquisition stage simple and non-intrusive. The results presented above reveal the potential of this method to estimate the status of distant components by processing vibration signals from a unique sensor located at a fixed position, midway along the harvester chassis (Figure 5), because a mean cross-validation accuracy higher than 85% was obtained. Previous work in the scientific literature has only analyzed isolated mechanical components, using one accelerometer for each isolated component [19,21,56]. It is worth noting that, to the best of our knowledge, no previous articles have approached the problem of estimating the status of various mechanical components from a unique vibration signal.

The second finding of this article is that the vibration signal can be acquired with a uniaxial accelerometer, the orientation of which has no significant effect on classification accuracy. The comparison of the results of cross-validation accuracy along the three accelerometer axes (Table 2) supports this conclusion. The higher differences observable in Table 2 for the threshing cylinder balance status shows differences of around 20%. However, almost no differences in accuracy were appreciated for the rest of the states, which were lower than 10% in all cases. Although vibrations are usually generated in a specific direction, the results obtained here suggest that the machine structure spreads them along all of the axes, making the use of an arbitrary axis for their detection possible.

The third finding of this article is that, when using an SVM classifier, an 85% mean cross-validation accuracy can be reached, which only requires a maximum of seven features as its input, with no

significant noticeable improvements from using nonlinear rather than linear kernels. Reviewing the results, a mean cross-validation accuracy greater than 85% was achieved, irrespective of the selected accelerometer axis. Analyzing the individual cross-validation accuracy obtained for each rotating component, the suitability of the SVM classifier for estimating each separate machinery status is evident. On the one hand, the rotating component status with the best cross-validation accuracy was the engine speed, with a cross-validation accuracy of 100% in all cases (Table 2). On the other hand, the worst cross-validation accuracy was obtained for threshing cylinder balance status, for which the cross-validation accuracy was between 63.41% and 87.49% (Table 2). A visual analysis of the vibration signal spectrum, revealed differences when the engine speed varied between high and low speed, while there were no visible changes in the signal spectrum when the threshing cylinder was either balanced or unbalanced. These results show that the proposed SVM classifier is able to classify the status of rotating machinery to a high degree of accuracy when the difference between the spectrum signals is noticeable, such as in the case of the engine speed status. They also show that it can obtain an acceptable cross-validation accuracy for rotating components when there is no visible difference between the spectrum signals, such as the threshing cylinder balance status. Comparing the fault detection accuracy in the present article against the results of Samanta *et al.* [56], who proposed an ANN-based classifier for the fault diagnostics of roller bearings based on data from several vibration signals and extracting only five time-domain features, this study has reported poorer results. Nevertheless, these differences can be justified by taking into account that in Samanta's article five vibration signals from different locations of a unique component were processed and because they were clean, as they came from the isolated mechanical component under analysis. Nevertheless, only one accelerometer sensor is employed in the present article to detect five states of three different rotating components and, furthermore, the vibration signal that is processed contains the superposed signals coming from the three components under analysis as well as from the other components of the machine. As can easily be understood, the present article approaches a much harder problem.

The major strength of the system proposed in this article is the simplicity of the data acquisition stage, employing only one sensor located at a single point on the machine for measuring the vibration signals. It is worth highlighting an article from Sugumaran *et al.* [21], who proposed an SVM-based classifier for the fault diagnostics of a unique roller bearing employing only one vibration signal. Our study, even though similar to Sugumaran's, is wider in the sense of trying to assess several machinery rotating components at once instead of just one. Furthermore, the present article contemplates the detection of further machine states and not only fault diagnostics.

Another strength of this article is that the proposed estimation method only needs seven features, at most, as the classifier input, yielding a simple SVM classifier with a low associated computational load. Moreover, the results showed no great differences in relation to the SVM kernel that was employed, which highlights that a simpler linear SVM classifier is sufficient to achieve good classification accuracy.

Nevertheless, there is a limitation to this work, which should be taken into account before implementing the proposed estimation method. This limitation is related to the data acquisition process performed in this article to validate the proposed SVM-based system. The vibration signals were acquired with the harvester wheels stopped to facilitate the acquisition procedure. If the proposed estimation method were to be used when the monitored machine is in motion, low-frequency

interference signals could appear. However, these signals are not expected to cause problems, because the frequencies of interest in the rotating components of these machines will almost certainly be much higher than the interference frequencies.

The main application fields of the proposed SVM-based system are machinery monitoring and predictive maintenance. In relation to machinery monitoring, this system could be used for detecting the operating status of particular mechanical components, simplifying the wiring and reducing the number of sensors that are required. In relation to predictive maintenance, the results suggest that further progress may lead to fast and low-cost machinery inspections, thereby avoiding many mechanical faults and replacing expensive, time-consuming inspections that are frequently required nowadays.

A mixture of both conventional vibration signal analysis features, such as frequency-domain [4,6,19,21,27,34] and time-domain [54–56] based features, and other unconventional features, such as nonlinear features [33,37,39], has been used in this article. The good classification accuracy levels, obtained for example with the *Central Tendency Measurement* feature when estimating the engine speed status (Table 1), highlights the usefulness of these unconventional features in the analysis of vibration signals for predictive maintenance. Nevertheless, regarding the straw chopper unbalance detection, the nonlinear features seem to be of little use. A future line for further research is opened by employing other unconventional features in vibration analysis for predictive maintenance.

Furthermore, this article opens a new future line of research by extending the system that is proposed in this paper to the use of more than one accelerometer located at different points on the machine. It is expected that the processing of all those signals together could enable the estimation of an even higher number of machine states and could also improve the accuracy of the estimation.

6. Conclusions

The results obtained in this study have provided evidence that (i) accurate estimation of the status of various rotating components in agro-industrial machinery is possible by processing the vibration signal acquired from a single point on the machine structure; (ii) the vibration signal can be acquired with a uniaxial accelerometer, the orientation of which does not significantly affect the classification accuracy; and, (iii) when using an SVM classifier, an 85% mean cross-validation accuracy can be reached, which only requires a maximum of seven features as its input, and no significant improvements are noted between the use of either nonlinear or linear kernels. Follow up research may lead to a simplification of the wiring and a reduction in the number of sensors required in machinery monitoring, as well as to fast and low cost machinery inspections in predictive maintenance.

Acknowledgments

Ruben Ruiz-Gonzalez was financed during this article's research by a collaboration grant from the *Ministry of Education, Culture and Sport* of Spain (BOE-A-2013-7736).

Víctor Martínez-Martínez's work was made possible thanks to a *Formación de Personal Investigador* program grant, financed by the *Universidad de Valladolid* (Spain) and co-financed by *Banco Santander*.

Author Contributions

The work presented here was done in four stages. The first stage consisted in the work proposal and experiments design, and this stage was done collaboratively by the four authors. The second stage consisted in the realization of the experiments and the related data acquisition. This work was done in Aguilar de Bureba (Burgos, Spain) by Francisco Javier Gomez-Gil, Jaime Gomez-Gil, and Ruben Ruiz-Gonzalez. The third stage consisted in the data processing, and it was done by Ruben Ruiz-Gonzalez under the supervision of Jaime Gomez-Gil, Víctor Martínez-Martínez and Francisco Javier Gomez-Gil. The fourth stage was the article writing, which was done collaboratively by the four authors.

Conflicts of Interest

The authors declare no conflict of interest.

References

1. Martin, K.F. A review by discussion of condition monitoring and fault diagnosis in machine tools. *Int. J. Mach. Tools Manuf.* **1994**, *34*, 527–551.
2. Jardine, A.K.S.; Lin, D.; Banjevic, D. A review on machinery diagnostics and prognostics implementing condition-based maintenance. *Mech. Syst. Signal Proc.* **2006**, *20*, 1483–1510.
3. Other predictive maintenance techniques. In *Practical Machinery Vibration Analysis and Predictive Maintenance*; Girdhar, P., Scheffer, C., Eds.; Newnes: Oxford, UK, 2004; pp. 221–234.
4. Scheffer, C.; Girdhar, P. *Practical Machinery Vibration Analysis and Predictive Maintenance*; Newnes: Oxford, UK, 2004.
5. Wang, W.Q.; Ismail, F.; Farid Golnaraghi, M. Assessment of gear damage monitoring techniques using vibration measurements. *Mech. Syst. Signal Proc.* **2001**, *15*, 905–922.
6. Peng, Z.K.; Chu, F.L. Application of the wavelet transform in machine condition monitoring and fault diagnostics: A review with bibliography. *Mech. Syst. Signal Proc.* **2004**, *18*, 199–221.
7. Li, Z.; Yan, X.; Tian, Z.; Yuan, C.; Peng, Z.; Li, L. Blind vibration component separation and nonlinear feature extraction applied to the nonstationary vibration signals for the gearbox multi-fault diagnosis. *Measurement* **2013**, *46*, 259–271.
8. Albarbar, A.; Gu, F.; Ball, A.D. Diesel engine fuel injection monitoring using acoustic measurements and independent component analysis. *Measurement* **2010**, *43*, 1376–1386.
9. Taghizadeh-Alisaraei, A.; Ghobadian, B.; Tavakoli-Hashjin, T.; Mohtasebi, S.S. Vibration analysis of a diesel engine using biodiesel and petrodiesel fuel blends. *Fuel* **2012**, *102*, 414–422.
10. Vulli, S.; Dunne, J.F.; Potenza, R.; Richardson, D.; King, P. Time-frequency analysis of single-point engine-block vibration measurements for multiple excitation-event identification. *J. Sound Vibr.* **2009**, *321*, 1129–1143.
11. Wang, X.; Makis, V.; Yang, M. A wavelet approach to fault diagnosis of a gearbox under varying load conditions. *J. Sound Vibr.* **2010**, *329*, 1570–1585.

12. Bin, G.F.; Gao, J.J.; Li, X.J.; Dhillon, B.S. Early fault diagnosis of rotating machinery based on wavelet packets—Empirical mode decomposition feature extraction and neural network. *Mech. Syst. Signal Proc.* **2012**, *27*, 696–711.
13. Chen, F.; Tang, B.; Chen, R. A novel fault diagnosis model for gearbox based on wavelet support vector machine with immune genetic algorithm. *Measurement* **2013**, *46*, 220–232.
14. Rodriguez-Donate, C.; Romero-Troncoso, R.; Cabal-Yepez, E.; Garcia-Perez, A.; Osornio-Rios, R. Wavelet-based general methodology for multiple fault detection on induction motors at the startup vibration transient. *J. Vib. Control* **2011**, *17*, 1299–1309.
15. Jayaswal, P.; Verma, S.; Wadhvani, A. Development of EBP-Artificial neural network expert system for rolling element bearing fault diagnosis. *J. Vib. Control* **2011**, *17*, 1131–1148.
16. McFadden, P.D.; Cook, J.G.; Forster, L.M. Decomposition of gear vibration signals by the Generalised S Transform. *Mech. Syst. Signal Proc.* **1999**, *13*, 691–707.
17. Wang, Y.S.; Ma, Q.H.; Zhu, Q.; Liu, X.T.; Zhao, L.H. An intelligent approach for engine fault diagnosis based on Hilbert–Huang transform and support vector machine. *Appl. Acoust.* **2014**, *75*, 1–9.
18. Lei, Y.; Lin, J.; He, Z.; Zuo, M.J. A review on empirical mode decomposition in fault diagnosis of rotating machinery. *Mech. Syst. Signal Proc.* **2013**, *35*, 108–126.
19. Cheng, G.; Cheng, Y.-L.; Shen, L.-H.; Qiu, J.-B.; Zhang, S. Gear fault identification based on Hilbert–Huang transform and SOM neural network. *Measurement* **2013**, *46*, 1137–1146.
20. Li, Y.; Tse, P.W.; Yang, X.; Yang, J. EMD-based fault diagnosis for abnormal clearance between contacting components in a diesel engine. *Mech. Syst. Signal Proc.* **2010**, *24*, 193–210.
21. Sugumaran, V.; Ramachandran, K.I. Effect of number of features on classification of roller bearing faults using SVM and PSVM. *Expert Syst. Appl.* **2011**, *38*, 4088–4096.
22. Vapnik, V. N. *Statistical Learning Theory*; Wiley: New York, NY, USA, 1998; p. 736.
23. Moguerza, J.M.; Muñoz, A. Support vector machines with applications. *Statist. Sci.* **2006**, *21*, 322–336.
24. Joachims, T. *Learning to Classify Text Using Support Vector Machines: Methods, Theory and Algorithms*; Kluwer Academic Publishers: New York, NY, USA, 2002; p. 205.
25. Wu, C.-H.; Ho, J.-M.; Lee, D.T. Travel-time prediction with support vector regression. *IEEE Trans. Intell. Transp. Syst.* **2004**, *5*, 276–281.
26. Su, H.; Shi, T.; Chen, F.; Huang, S. New method of fault diagnosis of rotating machinery based on distance of information entropy. *Front. Mech. Eng.* **2011**, *6*, 249–253.
27. Dai, J.; Chen, C.L.P.; Xu, X.-Y.; Huang, Y.; Hu, P.; Hu, C.-P.; Wu, T. Machinery vibration signals analysis and monitoring for fault diagnosis and process control. In *Advanced Intelligent Computing Theories and Applications. With Aspects of Theoretical and Methodological Issues*; Huang, D.-S., Wunsch, D., II, Levine, D., Jo, K.-H., Eds.; Springer: Berlin, Germany, 2008; Volume 5226, pp. 696–703.
28. Widodo, A.; Yang, B.-S. Support vector machine in machine condition monitoring and fault diagnosis. *Mech. Syst. Signal Proc.* **2007**, *21*, 2560–2574.
29. Jain, A.K.; Duin, R.P.W.; Mao, J. Statistical pattern recognition: A review. *IEEE Trans. Pattern Anal. Mach. Intell.* **2000**, *22*, 4–37.

30. Kotsiantis, S.B. Supervised machine learning: A review of classification techniques. *Informatica* **2007**, *31*, 249–268.
31. Doğanaksoy, A.; Göloğlu, F. On Lempel-Ziv Complexity of Sequences. In *Sequences and Their Applications—SETA 2006*; Gong, G., Hellesteth, T., Song, H.-Y., Yang, K., Eds.; Springer: Berlin, Germany, 2006; Volume 4086, pp. 180–189.
32. Vanluchene, A.L.; Vereecke, H.; Thas, O.; Mortier, E.P.; Shafer, S.L.; Struys, M.M. Spectral entropy as an electroencephalographic measure of anesthetic drug effect: A comparison with bispectral index and processed midlatency auditory evoked response. *Anesthesiology* **2004**, *1*, 34–42.
33. Hornero, R.; Escudero, J.; Fernandez, A.; Poza, J.; Gomez, C. Spectral and nonlinear analyses of MEG background activity in patients with Alzheimer's disease. *IEEE Trans. Biomed. Eng.* **2008**, *55*, 1658–1665.
34. Gao, G.; Zhu, Y.; Duan, G.; Zhang, Y. Intelligent fault identification based on wavelet packet energy analysis and SVM. In Proceedings of the 9th International Conference on Control, Automation, Robotics and Vision (ICARCV'06), Singapore, 5–8 December 2006; pp. 1–5.
35. Grassberger, P.; Procaccia, I. Measuring the strangeness of strange attractors. *Phys. D* **1983**, *9*, 189–208.
36. Li, M.; Vitányi, P. *An Introduction to Kolmogorov Complexity and Its Applications*, 3rd ed.; Springer: New York, NY, USA, 2008; p. 792.
37. Aboy, M.; Hornero, R.; Abásolo, D.; Álvarez, D. Interpretation of the Lempel-Ziv complexity measure in the context of biomedical signal analysis. *IEEE Trans. Biomed. Eng.* **2006**, *53*, 2282–2288.
38. Pincus, S.M. Approximate entropy as a measure of system complexity. *Proc. Natl. Acad. Sci. USA* **1991**, *88*, 2297–2301.
39. Richman, J.S.; Moorman, J.R. Physiological time-series analysis using approximate entropy and sample entropy. *Am. J. Physiol. Heart Circ. Physiol.* **2000**, *278*, H2039–H2049.
40. Aggarwal, N.; Agrawal, R.K. First and Second order statistics features for classification of magnetic resonance brain images. *J. Signal Inf. Proc.* **2012**, *3*, 146–153.
41. Zhou, B.-H.; Liu, P.; Liu, N.B.; Wu, X.H.; Lu, R.; Ni, X.M. Median frequency of surface EMG signal of antagonist muscles during repeated contractions. In Proceeding of the 1992 14th Annual International Conference of the IEEE Engineering in Medicine and Biology Society, Paris, France, 29 October–1 November 1992; Volume 4, pp. 1626–1627.
42. Wang, X.; Paliwal, K.K. Feature extraction and dimensionality reduction algorithms and their applications in vowel recognition. *Pattern Recognit.* **2003**, *36*, 2429–2439.
43. Cortes, C.; Vapnik, V. Support-Vector networks. *Mach. Learn.* **1995**, *20*, 273–297.
44. Haykin, S. *Neural Networks: A Comprehensive Foundation*, 2nd ed.; Prentice Hall PTR: New Jersey, NJ, USA, 1998; p. 842.
45. Ren, J. ANN vs. SVM: Which one performs better in classification of MCCs in mammogram imaging. *Knowl. Based Syst.* **2012**, *26*, 144–153.
46. Hsu, C.-W.; Lin, C.-J. A comparison of methods for multiclass support vector machines. *IEEE Trans. Neural Netw.* **2002**, *13*, 415–425.

47. Ferris, M.C.; Munson, T.S. Interior-point methods for massive support vector machines. *SIAM J. Optim.* **2006**, *13*, 783–804.
48. Platt, J.C. *Sequential Minimal Optimization: A Fast Algorithm for Training Support Vector Machines*; Microsoft Research Technical Report MSR-TR-98-14, 21 April 1998.
49. Platt, J.C. Fast training of support vector machines using sequential minimal optimization. In *Advances in Kernel Methods: Support Vector Learning*, 1st ed.; Schölkopf, B., Burges, C.J.C., Smola, A.J., Eds.; MIT Press: Cambridge, UK, 1998.
50. Shilton, A.; Palaniswami, M.; Ralph, D.; Tsoi, A.C. Incremental training of support vector machines. *IEEE Trans. Neural Netw.* **2005**, *16*, 114–131.
51. Campbell, C.; Cristianini, N. *Simple Learning Algorithms for Training Support Vector Machines*; University of Bristol: Bristol, UK, 1998.
52. Campbell, C.; Ying, Y. *Learning with Support Vector Machines*, 1st ed.; Morgan & Claypool Publishers: San Rafael, CA, USA, 2011.
53. Steinwart, I.; Christmann, A. *Support Vector Machines*, 1st ed.; Springer Publishing Company, Inc.: New York, NY, USA, 2008.
54. Norton, M.P.; Karczub, D.G. *Fundamentals of Noise and Vibration Analysis for Engineers*; Cambridge University Press: Cambridge, UK, 2003.
55. Tandon, N. A comparison of some vibration parameters for the condition monitoring of rolling element bearings. *Measurement* **1994**, *12*, 285–289.
56. Samanta, B.; Al-Balushi, K.R. Artificial Neural Network based fault diagnostics of rolling element bearings using time-domain features. *Mech. Syst. Signal Proc.* **2003**, *17*, 317–328.
57. Chang, C.-C.; Lin, C.-J. LIBSVM: A library for support vector machines. *ACM Trans. Intell. Syst. Technol.* **2011**, *2*, 27:1–27:27.
58. Chang, C.-C.; Lin, C.-J. LIBSVM—A Library for Support Vector Machines. Available online: <http://www.csie.ntu.edu.tw/~cjlin/libsvm> (accessed on 3 August 2014).
59. Hsu, C.-W.; Chang, C.-C.; Lin, C.-J. *A Practical Guide to Support Vector Classification*; Department of Computer Science and Information Engineering, National Taiwan University: Taipei, Taiwan, 2010.

© 2014 by the authors; licensee MDPI, Basel, Switzerland. This article is an open access article distributed under the terms and conditions of the Creative Commons Attribution license (<http://creativecommons.org/licenses/by/4.0/>).

Article 2: Vehicle tracking monitoring

The second article tackles the **vehicle tracking monitoring** problem, previously described in chapter —Introduction to the compendium”. The main bibliographic data about this article is shown below:

- Title: A data fusion system of GNSS data and on-vehicle sensors data for improving car positioning precision in urban environments.
- Authors: Carlos Melendez-Pastor; Ruben Ruiz-Gonzalez; Jaime Gomez-Gil.
- Journal: Expert Systems with Applications.
- Editor: Elsevier.
- Impact factor: 3.768 (2017).
- Journal Ranking:
 - Q1 on *Operations Research & Management Science* (8/84).
 - Q1 on *Engineering, Electrical & Electronic* (42/260).
 - Q1 on *Computer Science, Artificial Intelligence* (20/132).
- Date of publication: September, 2017.
- ISSN: 0957-4174.
- Volume: 80.
- Pages: 28-38.
- DOI: 10.1016/j.eswa.2017.03.018.
- URL: <https://www.sciencedirect.com/science/article/pii/S0957417417301641>.
- Number of cites: 13.

The article presented below is a version of the original article published in the previously mentioned journal. This version of the article has been authorized by the journal editor to be included in this PhD thesis as a compendium of publications.



Contents lists available at ScienceDirect

Expert Systems With Applications

journal homepage: www.elsevier.com/locate/eswa

A data fusion system of GNSS data and on-vehicle sensors data for improving car positioning precision in urban environments



Carlos Melendez-Pastor¹, Ruben Ruiz-Gonzalez^{1,*}, Jaime Gomez-Gil¹

Department of Signal Theory, Communications and Telematics Engineering, University of Valladolid, Valladolid 47011, Spain

ARTICLE INFO

Article history:

Received 26 July 2016

Revised 6 March 2017

Accepted 7 March 2017

Available online 8 March 2017

Keywords:

Data fusion

Extended Kalman filter (EKF)

Global navigation satellite system (GNSS)

On-vehicle sensors

On-board diagnostics (OBD)

Ackerman steering geometry

ABSTRACT

Accurate car positioning on the Earth's surface is a requirement for many state-of-the-art automotive applications, but current low-cost Global Navigation Satellite System (GNSS) receivers can suffer from poor precision and transient unavailability in urban areas. In this article, a real-time data fusion system of absolute and relative positioning data is proposed with the aim of increasing car positioning precision. To achieve this goal, a system based on the Extended Kalman Filter (EKF) was employed to fuse absolute positioning data coming from a low-cost GNSS receiver with data coming from four wheel speed sensors, a lateral acceleration sensor, and a steering wheel angle sensor. The bicycle kinematic model and the Ackerman steering geometry were employed to particularize the EKF. The proposed system was evaluated through experimental tests. The results showed precision improvements of up to 50% in terms of the Root Mean Square Error (RMSE), 50% in terms of the 95th-percentile of the distance error distribution, and 75% in terms of the maximum distance error, with respect to using a stand-alone, low-cost GNSS receiver. These results suggest that the proposed data fusion system for car vehicles can significantly reduce the positioning error with respect to the positioning error of a low-cost GNSS receiver. The best precision improvements of the system are expected to be achieved in urban areas, where tall buildings hinder the effectiveness of GNSS systems. The main contribution of this work is the proposal of a novel system that enables accurate car positioning during short GNSS signal outages. This advance could be integrated in larger expert and intelligent systems such as autonomous cars, helping to make self-driving easier and safer.

© 2017 Elsevier Ltd. All rights reserved.

1. Introduction

Positioning technologies for locating a vehicle on the Earth's surface are recurrently employed by applications such as Advanced Driver Assistance System (ADAS) (Pérez et al., 2015) and vehicle navigation systems (Mintsis, Basbas, Papaioannou, Taxiltaris, & Tziavos, 2004). Vehicle positioning can rely exclusively on Global Navigation Satellite Systems (GNSSs) as the source of information to provide position and velocity. This absolute positioning technology can be accurate and highly available in environments with good satellite visibility. However, GNSS positioning precision can be degraded in urban environments, such as streets surrounded by high buildings, and the positioning can be canceled in environments such as tunnels (Kaplan & Hegarty, 2005; French, 1996).

Security systems in modern vehicles, such as Anti-lock Braking System (ABS), Electronic Stability Control (ESC), Traction Control System (TCS), and Electronic Brakeforce Distribution (EBD), use data from sensors located in different parts of the vehicle. Wheel speeds, steering wheel angle, lateral and longitudinal accelerations, vehicle rotation angular speed, and vehicle rotation angular acceleration are parameters continuously acquired and monitored in modern cars (Robert Bosch GmbH, 2007). The processing of these parameters coming from on-vehicle sensors enables relative positioning (Lin, 1991; Titterton & Weston, 2004).

The Extended Kalman Filter (EKF) (Sorenson, 1985; Jazwinski, 2007) allows the statistically optimal data fusion of absolute positioning data coming from GNSSs with data for relative positioning coming from on-vehicle sensors. Making use of the EKF, the positioning precision can be thus improved.

Among other applications, the Kalman filter has been widely used in the literature to (i) fuse data from Global Positioning System (GPS) and Inertial Navigation System (INS) (Tin Leung, Whidborne, Purdy, & Dunoyer, 2011); (ii) fuse data from GPS, INS, and

* Corresponding author.

E-mail addresses: cmelpas@ribera.tel.uva.es (C. Melendez-Pastor), rriugon@ribera.tel.uva.es (R. Ruiz-Gonzalez), jgomez@tel.uva.es (J. Gomez-Gil).

¹ These authors contributed equally to this work.

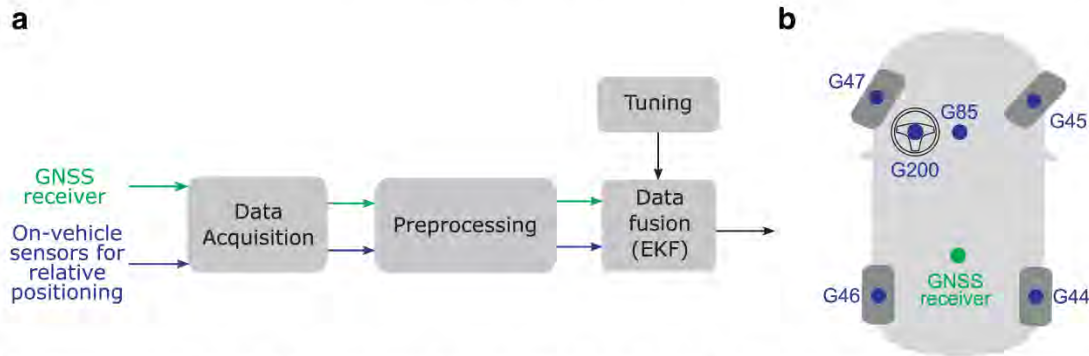


Fig. 1. (a) Overview of the building blocks in the proposed system. (b) Location of the sensors employed in the proposed system. In green, the absolute positioning sensor: GNSS receiver. In blue, the on-vehicle sensors for relative positioning: wheel speed sensors (G44–G47), lateral acceleration sensor (G85), and steering wheel angle sensor (G200). (For interpretation of the references to color in this figure legend, the reader is referred to the web version of this article.)

Wheel Speed Sensors (WSS) (Leung, Whidborne, Purdy, & Barber, 2011); (iii) fuse data from GPS and positioning data obtained by artificial vision (Schleicher, Bergasa, Ocaña, Barea, & López, 2010); and (iv) smooth the path followed by vehicles (Gomez-Gil, Ruiz-Gonzalez, Alonso-Garcia, & Gomez-Gil, 2013). A line of research for the data fusion of low-cost GPS and on-vehicle sensors in cars was initiated in 1999 by Abbott and Powell (Abbott & Powell, 1999). Since then, more articles have been published in this line of research (Bonnifait, Bouron, Crubille, & Meizel, 2001; El Najjar & Bonnifait, 2005; Gning & Bonnifait, 2005; Song, Li, Tang, Zhang, & Li, 2014). The present article makes a new contribution to this same line of research by proposing an alternative approach for accomplishing the data fusion, as well as by proposing a different model for the car system's state.

This article proposes and experimentally evaluates an EKF-based data fusion system for improving car positioning precision. This system combines data from a low-cost GNSS receiver with data coming from six on-vehicle sensors: four wheel speed sensors, a lateral acceleration sensor, and a steering wheel angle sensor. As compared to the aforementioned articles in the related literature, the proposed system makes use of a different and modified model for the car system's state, not found in any previous related article, so far as the authors are aware.

2. Description of the proposed system

2.1. Overview

The proposed data fusion system, whose main building blocks (Fig. 1a) could be deployed in a microcontroller-based system, takes as input GNSS data, along with data for relative positioning coming from other on-vehicle sensors (Fig. 1b). As far as this article is concerned, just the four wheel speed sensors, a lateral acceleration sensor, and a steering wheel angle sensor (Fig. 1b) were employed for relative positioning, along with a GNSS receiver for absolute positioning. Nevertheless, this does not preclude the incorporation of other relative positioning sensors, e.g. longitudinal accelerometers, which could be readily considered with few straightforward changes in the system architecture and its processing scheme.

The data supplied by the aforementioned sensors, following the scheme depicted in Fig. 1a, is then preprocessed and, thereafter, combined via the Extended Kalman Filter. By taking into account all the redundant data, this system provides a more precise estimation of the actual state of the vehicle.

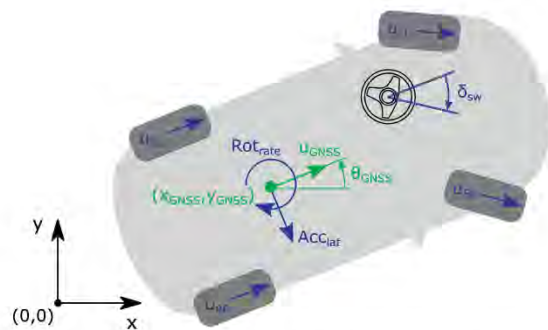


Fig. 2. Preprocessed measured variables obtained by the system, to be later employed in the data fusion module. The schematic diagram represents, in blue, the measurements obtained from the on-vehicle sensors for relative positioning and, in green, the measurements provided by the GNSS receiver. The meaning of all the represented variables is explained in Section 2.2.3. (For interpretation of the references to color in this figure legend, the reader is referred to the web version of this article.)

2.2. System building blocks

In this subsection, further details about the functioning of all the building blocks of the proposed system (Fig. 1a) are provided.

2.2.1. Data acquisition

The data acquisition block addresses the extraction of the raw data supplied by all the sensors from the system. Typically, RMC NMEA 0183 (National Marine Electronics Association 0183) sentences are acquired at a certain sampling rate from the GNSS receiver, and the raw data from the on-vehicle sensors for relative positioning is also obtained. This raw data is fed into the subsequent preprocessing block.

2.2.2. Preprocessing

The raw data, coming from the aforementioned sensors, must be preprocessed in order to obtain meaningful and comparable data for the subsequent data fusion step. This preprocessing block requires the performance of several actions, which can be conceptually encompassed in the following two steps: (1) The conversion of the raw data and electric signals provided by the sensors into the meaningful variables depicted in Fig. 2. This step includes the conversion from GNSS geodetic coordinates to the Universal Trans-

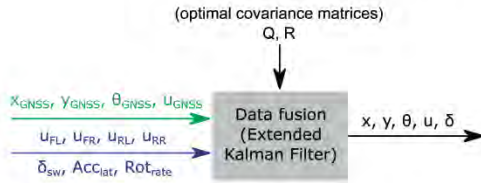


Fig. 3. Input (measured) variables for EKF-based data fusion and output (filtered) system state variables. In green, the measurements provided by the GNSS receiver. In blue, the measurements provided by the on-vehicle sensors. In black, the output system state variables. The optimal covariance matrices (\mathbf{Q} and \mathbf{R}) are employed to weight the reliability on each individual measurement. (For interpretation of the references to color in this figure legend, the reader is referred to the web version of this article.)

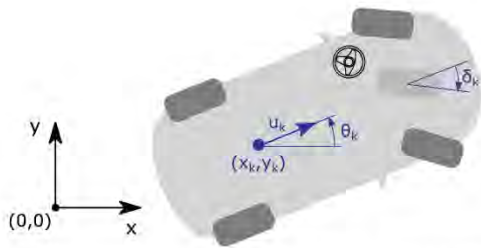


Fig. 4. Car-system state variables, where all the variables needed to completely define the kinematic state of the car system are depicted.

verse Mercator (UTM) planar projection as well as other basic conversions, such as converting every involved variable into SI units. (2) The synchronization, resampling, and interpolation of the acquired data so that all the digital samples from each sensor correspond to the same temporal instant.

The output data from this preprocessing block is the set of measured variables represented in Fig. 2, which is fed into the subsequent data fusion block.

2.2.3. Data fusion

The output variables coming from the preprocessing block (Fig. 2) are fed as measurements into the Extended Kalman Filter (Fig. 3), which is responsible for performing the data fusion of all these measurements in order to achieve, as its output, an optimal estimation of the system state.

In this article, the Extended Kalman Filter was particularized for the car vehicle system (Fig. 4) by introducing the Ackerman steering geometry into the bicycle kinematic model for describing car motion (Jazar, 2014). For completely specifying the car-system state, with regard to its positioning, the bicycle model is here assumed as an approximation. In this scenario, the five variables depicted in Fig. 4 are enough to describe the system's kinematic state at a discrete instant k . Thus, the positioning-related state of the car system can be fully determined by the set of five variables shown in Eq. (1):

$$\mathbf{x}_k = (x_k, y_k, \theta_k, u_k, \delta_k)^T \quad (1)$$

where x_k denotes the UTM position in the X axis or Easting position; y_k denotes the UTM position in the Y axis or Northing position; θ_k denotes the vehicle heading direction with respect to the positive X axis; u_k denotes the speed of the vehicle; and δ_k de-

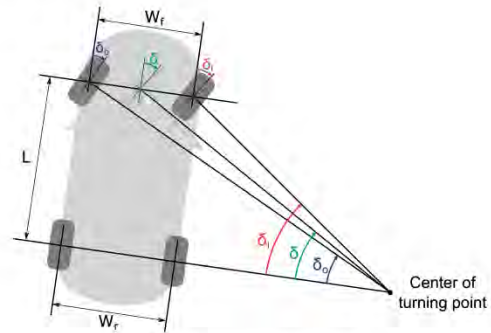


Fig. 5. Ackerman steering model.

notes the angle formed by the virtual front wheel and the vehicle heading angle.

In this article, the GNSS receiver and the on-vehicle sensors for relative positioning (Fig. 2) provide the measured variables shown in Eq. (2):

$$\bar{\mathbf{z}}_k = (x_{GNSS}, y_{GNSS}, \theta_{GNSS}, u_{GNSS}, u_{FL}, u_{FR}, u_{RL}, u_{RR}, \delta_{sw}, Acc_{lat}, Rot_{rate})^T \quad (2)$$

where x_{GNSS} denotes the UTM easting position in the X axis supplied by the GNSS receiver; y_{GNSS} denotes the UTM northing position in the Y axis supplied by the GNSS receiver; θ_{GNSS} denotes the heading direction supplied by the GNSS receiver; u_{GNSS} denotes the speed of the vehicle supplied by the GNSS receiver; u_{FL} denotes the front-left wheel speed; u_{FR} denotes the front-right wheel speed; u_{RL} denotes the rear-left wheel speed; u_{RR} denotes the rear-right wheel speed; δ_{sw} denotes the turning angle of the steering wheel with respect to the equilibrium; Acc_{lat} denotes the lateral or centripetal acceleration; and Rot_{rate} denotes the rotation rate of the vehicle, i.e. the rate of change of the heading angle.

The relationships between the system state variables (\mathbf{x}_k) and the measurement variables (\mathbf{z}_k) were deduced by applying the Ackermann steering geometry (Fig. 5) as a good approximation for the car vehicle. A detailed derivation of these relationships can be found in Appendix A.

Considering these state (\mathbf{x}_k) and measurement (\mathbf{z}_k) vectors, the concrete particularization of the Extended Kalman Filter yielded the following functions \mathbf{f} and \mathbf{h} for the state prediction and measurement update, respectively, as shown in Eqs. (3) and (4):

$$\mathbf{x}_k = \begin{pmatrix} x_k \\ y_k \\ \theta_k \\ u_k \\ \delta_k \end{pmatrix} = \mathbf{f}(\mathbf{x}_{k-1}) + \mathbf{w}_{k-1} = \begin{pmatrix} x_{k-1} + \Delta t \cdot u_{k-1} \cdot \cos(\theta_{k-1}) \\ y_{k-1} + \Delta t \cdot u_{k-1} \cdot \sin(\theta_{k-1}) \\ \theta_{k-1} + \Delta t \cdot \frac{u_{k-1}}{L} \cdot \tan(\delta_{k-1}) \\ u_{k-1} \\ \delta_{k-1} \end{pmatrix} + \mathbf{w}_{k-1} \quad (3)$$

$$\begin{aligned} \mathbf{z}_k &= (X_{GNSS}, Y_{GNSS}, \theta_{GNSS}, u_{GNSS}, u_{FL}, u_{FR}, u_{RL}, u_{RR}, \delta_{SW}, Acc_{lat}, Rot_{rate})^T \\ &= \mathbf{h}(\mathbf{x}_k) + \mathbf{v}_k \\ &= \begin{pmatrix} x_k, y_k, \theta_k, u_k, \sqrt{(\tan(\delta_k) \cdot L)^2 + \left(L + \tan(\delta_k) \cdot \frac{W_f}{2}\right)^2} \\ \sqrt{(\tan(\delta_k) \cdot L)^2 + \left(L - \tan(\delta_k) \cdot \frac{W_f}{2}\right)^2} \\ \left(1 + \frac{W_f \cdot \tan(\delta_k)}{2L}\right) \cdot u_k \\ \left(1 - \frac{W_f \cdot \tan(\delta_k)}{2L}\right) \cdot u_k, \delta_k \cdot S_{ratio}, \\ \frac{u_k^2}{L} \cdot \tan(\delta_k), \frac{u_k}{L} \cdot \tan(\delta_k) \end{pmatrix} + \mathbf{v}_k \end{aligned} \quad (4)$$

where $\mathbf{w}_k \sim N(0, \mathbf{Q})$ is the process noise, following a Gaussian distribution with zero vector mean and covariance matrix \mathbf{Q} ; $\mathbf{v}_k \sim N(0, \mathbf{R})$ is the measurement noise, following a Gaussian distribution with zero vector mean and covariance matrix \mathbf{R} ; L is the distance between the front and rear vehicle axles; W_f is the distance between wheels on the front axle; S_{ratio} is the steering ratio, i.e. the quotient factor that relates the angle to which the steering wheel is turned and the angle to which the virtual central front wheel turns as a consequence; and Δt is the time elapsed between two consecutive samples, i.e. $\Delta t = t_k - t_{k-1}$ if t_k denotes the time when the k th sample is obtained.

The EKF implementation requires the calculation of two additional matrices for its underlying operation: \mathbf{F}_k , the state transition matrix, and \mathbf{H}_k , the observation matrix. In complex cases, they must be computed numerically, on the fly, at each discrete instant, but as far as this model is concerned, analytical derivations can be straightforwardly obtained for both \mathbf{F}_k and \mathbf{H}_k by computing the Jacobian matrix of the aforementioned \mathbf{f} and \mathbf{h} functions, respectively. The results from such calculations are provided in Eqs. (5) and (6), respectively:

$$\mathbf{F}_k = \left. \frac{\partial \mathbf{f}}{\partial \mathbf{x}_k} \right|_{\hat{\mathbf{x}}_{k|k}} = \begin{pmatrix} 1 & 0 & -\Delta t \cdot \hat{u}_{k|k} \cdot \sin(\hat{\theta}_{k|k}) & \Delta t \cdot \cos(\hat{\theta}_{k|k}) & 0 & 0 & 0 & 0 & 0 & 0 & 0 \\ 0 & 1 & \Delta t \cdot \hat{u}_{k|k} \cdot \cos(\hat{\theta}_{k|k}) & \Delta t \cdot \sin(\hat{\theta}_{k|k}) & 0 & 0 & 0 & 0 & 0 & 0 & 0 \\ 0 & 0 & 1 & \frac{\Delta t}{L} \cdot \tan(\hat{\delta}_{k|k}) & \Delta t \cdot \frac{\hat{u}_{k|k}}{L} \cdot (1 + \tan^2(\hat{\delta}_{k|k})) & 0 & 0 & 0 & 0 & 0 & 0 \\ 0 & 0 & 0 & 1 & 0 & 0 & 0 & 0 & 0 & 0 & 0 \\ 0 & 0 & 0 & 0 & 1 & 0 & 0 & 0 & 0 & 0 & 0 \\ 0 & 0 & 0 & 0 & 0 & 1 & 0 & 0 & 0 & 0 & 0 \end{pmatrix} \quad (5)$$

$$\mathbf{H}_k = \left. \frac{\partial \mathbf{h}}{\partial \mathbf{x}_k} \right|_{\hat{\mathbf{x}}_{k|k-1}} = \begin{pmatrix} 1 & 0 & 0 & 0 & 0 & 0 & 0 & 0 & 0 & 0 & 0 \\ 0 & 1 & 0 & 0 & 0 & 0 & 0 & 0 & 0 & 0 & 0 \\ 0 & 0 & 1 & 0 & 0 & 0 & 0 & 0 & 0 & 0 & 0 \\ 0 & 0 & 0 & 1 & 0 & 0 & 0 & 0 & 0 & 0 & 0 \\ 0 & 0 & 0 & 0 & H_{k,5,4} & 0 & 0 & 0 & 0 & 0 & 0 \\ 0 & 0 & 0 & 0 & H_{k,6,4} & 0 & 0 & 0 & 0 & 0 & 0 \\ 0 & 0 & 0 & 0 & 0 & H_{k,5,5} & 0 & 0 & 0 & 0 & 0 \\ 0 & 0 & 0 & 0 & 0 & 0 & H_{k,6,5} & 0 & 0 & 0 & 0 \\ 0 & 0 & 0 & 0 & \left(1 + \frac{W_f \cdot \tan(\hat{\delta}_{k|k-1})}{2L}\right) & \frac{W_f \cdot (1 + \tan^2(\hat{\delta}_{k|k-1}))}{2L} & 0 & 0 & 0 & 0 & \hat{u}_{k|k-1} \\ 0 & 0 & 0 & 0 & \left(1 - \frac{W_f \cdot \tan(\hat{\delta}_{k|k-1})}{2L}\right) & -\frac{W_f \cdot (1 + \tan^2(\hat{\delta}_{k|k-1}))}{2L} & 0 & 0 & 0 & 0 & -\hat{u}_{k|k-1} \\ 0 & 0 & 0 & 0 & 0 & 0 & 0 & 0 & 0 & 0 & S_{ratio} \\ 0 & 0 & 0 & 0 & \frac{2 \cdot \hat{u}_{k|k-1}}{L} \cdot \tan(\hat{\delta}_{k|k-1}) & \frac{\hat{u}_{k|k-1}}{L} \cdot (1 + \tan^2(\hat{\delta}_{k|k-1})) & 0 & 0 & 0 & 0 & 0 \\ 0 & 0 & 0 & 0 & \frac{\tan(\hat{\delta}_{k|k-1})}{L} & \frac{\hat{u}_{k|k-1}}{L} \cdot (1 + \tan^2(\hat{\delta}_{k|k-1})) & 0 & 0 & 0 & 0 & 0 \end{pmatrix} \quad (6)$$

where:

$$\begin{aligned} H_{k,5,4} &= \frac{\sqrt{\left(L \cdot \tan(\hat{\delta}_{k|k-1})\right)^2 + \left(L + \frac{W_f}{2} \cdot \tan(\hat{\delta}_{k|k-1})\right)^2}}{L}, \\ H_{k,5,5} &= \frac{\left(1 + \tan^2(\hat{\delta}_{k|k-1})\right) \cdot \left(\left(L^2 + \frac{W_f^2}{4}\right) \cdot \tan(\hat{\delta}_{k|k-1}) + \frac{L \cdot W_f}{2}\right) \cdot \hat{u}_{k|k-1}}{L \sqrt{\left(L \cdot \tan(\hat{\delta}_{k|k-1})\right)^2 + \left(L + \frac{W_f}{2} \cdot \tan(\hat{\delta}_{k|k-1})\right)^2}}, \\ H_{k,6,4} &= \frac{\sqrt{\left(L \cdot \tan(\hat{\delta}_{k|k-1})\right)^2 + \left(L - \frac{W_f}{2} \cdot \tan(\hat{\delta}_{k|k-1})\right)^2}}{L}, \\ H_{k,6,5} &= \frac{\left(1 + \tan^2(\hat{\delta}_{k|k-1})\right) \cdot \left(\left(L^2 + \frac{W_f^2}{4}\right) \cdot \tan(\hat{\delta}_{k|k-1}) - \frac{L \cdot W_f}{2}\right) \cdot \hat{u}_{k|k-1}}{L \sqrt{\left(L \cdot \tan(\hat{\delta}_{k|k-1})\right)^2 + \left(L - \frac{W_f}{2} \cdot \tan(\hat{\delta}_{k|k-1})\right)^2}}. \end{aligned}$$

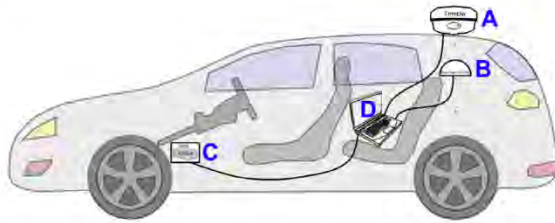


Fig. 6. Car schematic outlining the materials setup throughout the experimental tests: (A) a Trimble R4 accurate high-end GPS receiver with RTK corrections, (B) an EverMore SA-320 low-cost GPS receiver, (C) an OBD-II VAG-COM 10.6 adapter, and (D) an Asus K72Jk laptop computer.

2.2.4. Tuning

The tuning block is responsible for feeding the optimal noise covariance matrices (\mathbf{Q} and \mathbf{R}) to the data fusion module so that it can achieve the best possible results. So far, the proposed system works with static matrices, which are tuned in advance and fixed for every instant of time.

3. Experimental section for system performance evaluation

The real-time system proposed in Section 2 was assessed in post-processing using the setup represented in Fig. 6 and following the scheme depicted in Fig. 7.

3.1. Materials

The materials employed in the experimental tests of this article were: a low-cost GPS receiver, an accurate high-end GPS receiver, a laptop computer, and a car vehicle with embedded relative positioning sensors available through an OBD-II adapter. Fig. 6 shows, schematically, the experimental setup for the tests.

The low-cost GPS receiver was an EverMore SA-320 with a SiRF-starIII chipset, and it was employed to acquire the GPS positions at a 5 Hz sampling rate. The accurate high-end GPS receiver, which acquired GPS positions at a sampling rate of 1 Hz, was a Trimble R4 configured to use RTK (Real Time Kinematic) corrections, and it was employed as a ground truth reference so as to assess the precision of the deployed system. The employed RTK corrections were supplied by the Agro-Food Technological Institute of Castilla y León (ITACyL) ("Network of GNSS stations of Castilla y León", 2016). The laptop employed in the tests was an Asus K72Jk, and it was used to acquire and store the data from all the connected sensors. Furthermore, the laptop was also used for the subsequent post-processing stages. The car vehicle was a Seat León MK2, and it was employed, together with all the sensors on board the car, to perform the tests along real urban area roads in Valladolid, Spain.

The car sensors employed during the tests, as well as the measurements obtained from each of them, were the same as depicted in Fig. 1b: (i) the G85 sensor, measuring the steering wheel angle (δ_{sw}); (ii) the G200 sensor, measuring both the lateral acceleration (Acc_{lat}) as a direct measurement and the vehicle's rotation rate or angular speed (Rot_{rate}) as an indirect measurement; (iii) the G47 sensor, measuring the speed of the front left wheel (u_{FL}); (iv) the G45 sensor, measuring the speed of the front right wheel (u_{FR}); (v) the G46 sensor, measuring the speed of the rear left wheel (u_{RL}); and (vi) the G44 sensor, measuring the speed of the rear right wheel (u_{RR}).

3.2. Methods

The stages involved in this article are summarized as: (i) data acquisition stage, (ii) preprocessing stage, (iii) filter tuning stage,

(iv) data fusion particularization via Extended Kalman Filter, and (v) positioning error evaluation. An overview of this whole process is illustrated in Fig. 7.

3.2.1. Data acquisition stage

First, the data acquisition stage was performed. In this stage, a typical urban path was followed by the vehicle equipped with the aforementioned on-board sensors. RMC NMEA 0183 sentences were acquired from both GPS receivers at a sampling rate of 1 Hz and 5 Hz for the high-end and low-cost one, respectively. The accurate GPS receiver employed RTK corrections which were provided by the Agro-Food Technological Institute of Castilla y León (ITACyL). For its part, the low-cost GPS receiver did not employ any kind of correction for positioning improvement. During all the recordings, the presence of no outages was ensured in order to keep an accurate reference from the high-end GNSS receiver. Simultaneously, data was obtained from the several relative positioning sensors of the car through the OBD-II standard by using a VAG-COM 10.6 connector. The real experimental setup for the tests is shown in Fig. 6, and the measurements taken from both sources are depicted in Fig. 2.

It is worth mentioning, at this stage, that the heading angle for the EverMore SA-320 low-cost GPS receiver was obtained in this case from the sixth field (*Track angle in degrees with respect to the True North*) as provided in the RMC NMEA 0183 sentences. Since no built-in compass was available inside the receiver, this value was internally computed from consecutive positions along the followed trajectory.

3.2.2. Preprocessing stage

Second, the preprocessing stage took place. It consisted of the following sub-stages: (i) data conversion from geodetic to UTM coordinates and conversion to SI units, (ii) resampling stage, (iii) synchronization stage, (iv) positioning offset elimination. In order to obtain the positions projected onto a 2D map, WGS84 to UTM conversion was first applied together with units' conversion into SI. After that, the sequence of data was interpolated using piecewise cubic interpolation and resampled, since the data from the diverse sensors was sampled at different rates and even at non-uniform instants of time. In order to keep a high enough temporal resolution, one with the error bounded under 20 ms, a 50 Hz sampling rate was chosen. This way, a new sequence with more samples per second was obtained, making the subsequent synchronization stage easier too. After this processing, the sequences coming from different sensors were synchronized, since the clocks of the different subsystems differed slightly. Last, since the absolute positioning error was left out of the evaluation, the positioning data coming from the Trimble R4 was spatially aligned with the data from the low-cost GPS receiver so as to focus solely on the relative positioning precision of the deployed system.

3.2.3. Filter tuning stage

Third, after having particularized the filter properly, the tuning stage took place. This stage undertook the computation of optimal \mathbf{Q} and \mathbf{R} noise covariance matrices for the EKF. The optimality criterion employed in this article was the reduction of the error throughout a sample training trajectory. In order to tune the covariance matrices, a hand-tuning approach was employed instead of other feasible alternative tuning techniques (Abbeel, Coates, Montemerlo, Ng, & Thrun, 2005), assuming non-correlation among noise components. This approach was selected since neither reliable nor accurate ground truth reference for the whole system state was available.

3.2.4. Data fusion particularization via extended Kalman filter

Fourth, the Extended Kalman Filter particularization derived in Section 2.2.3 was applied to the preprocessed data. This data fu-

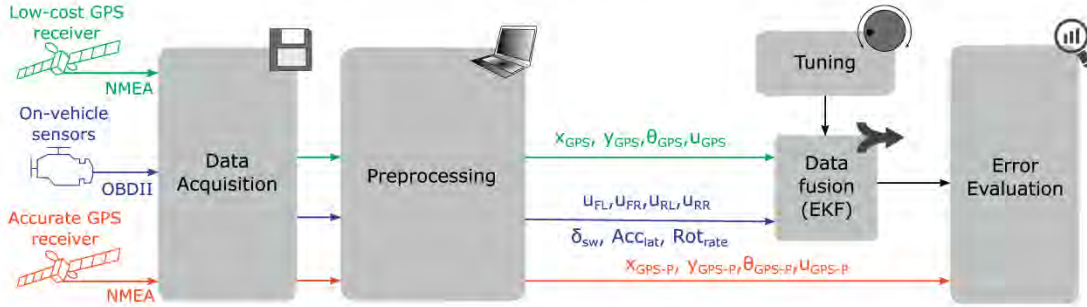


Fig. 7. Block diagram summarizing the stages undertaken in the experimental tests for assessing the performance of the proposed system.

sion stage took as input the preprocessed measured variables from the previous stage and produced an optimal estimation of the state variables using the tuned covariance matrices.

3.2.5. Positioning error evaluation

Finally, in order to assess the improvements offered by the system developed here, positioning distance error with respect to the real path was computed for each point along the trajectory. A histogram of this error distribution was obtained before and after fusing the data, from which the Root Mean Square Error (RMSE) value, the 95th-percentile of the error distribution, and the maximum error value were calculated as statistical parameters.

4. Results

After having performed all the aforementioned stages (Section 3.2), the following results were obtained.

4.1. Tuning of Q and R covariance matrices

The optimal covariance matrices, obtained in the experimental tests following the hand-tuning process explained in Section 3.2.3, are shown in Eq. (7).

$$\begin{aligned}
 \mathbf{Q} &= \text{diag}\left(10^{-8} \text{ m}^2, 10^{-8} \text{ m}^2, 10^{-12} \text{ rad}^2, 10 \frac{\text{m}^2}{\text{s}^2}, 50 \text{ rad}^2\right) \\
 \mathbf{R} &= \text{diag}\left(1.15 \text{ m}^2, 1.75 \text{ m}^2, 0.1 \text{ rad}^2, \right. \\
 &\quad 0.0125 \frac{\text{m}^2}{\text{s}^2}, 0.45 \frac{\text{m}^2}{\text{s}^2}, 0.45 \frac{\text{m}^2}{\text{s}^2}, 0.45 \frac{\text{m}^2}{\text{s}^2}, \\
 &\quad \left. 0.45 \frac{\text{m}^2}{\text{s}^2}, 10^{-8} \text{ rad}^2, 0.01 \frac{\text{m}^2}{\text{s}^4}, 10^{-5} \frac{\text{rad}^2}{\text{s}^2}\right) \quad (7)
 \end{aligned}$$

It is worth remarking that the units of measurement for each component in Eq. (7) are those of the corresponding variable squared. Since the optimal matrices are diagonal, i.e. noise non-correlation between variables was assumed here, all non-zero elements in the covariance matrices simply represent variances.

The optimal covariance matrix \mathbf{Q} , shown in Eq. (7), evinces a high confidence in the prediction for both X and Y positions as well as for the heading angle. This seems to be reasonable, since no sudden changes in heading are expected to happen at the relatively high 50 Hz sampling rate. Therefore, in this case, the prediction given by the bicycle kinematic model is a very precise approximation. On the other hand, as shown by the high values of those components in matrix \mathbf{Q} , assuming constant speed and constant steering angle does not lead to reliable hypotheses, since accelerations and turnings are likely to occur in a normal trajectory described by the car. Meanwhile, regarding the uncertainties for each measurement provided in the optimal covariance matrix \mathbf{R} , it is

worth highlighting the high accuracy of the steering wheel angle, lateral acceleration, and rotation rate measurements obtained from the on-vehicle sensors. On the other hand, the speedometer-based measurements are less accurate than expected since the Electronic Control Unit (ECU) in the car provided speeds with a resolution of 1 km/h. Moreover, an increment in uncertainty for those measurements arose due to the imperfect matching between the expected Ackermann steering geometry and the actual one from the real car. It is also worth highlighting that the estimated variances for the GNSS-supplied X and Y positions are lower than expected due to three reasons: (i) the absolute positioning error being left out of consideration in this study, by artificially removing it beforehand in order to perform just the assessment in terms of relative positioning improvements, (ii) the non-Gaussianity of the actual positioning error distribution while assuming additive Gaussian noise for the EKF, and (iii) the EKF tuning process underestimating the GNSS positioning noise variances, since it is the only source of absolute positioning, and thus avoiding the inherent drifting apart due to an overconfidence in the remaining inertial sensors. Furthermore, the discrepancy between variances for the X and Y positions is explained by considering the function of the UTM projection as well as the particular geometric configuration of the GPS satellite constellation, i.e. Geometric Dilution Of Precision (GDOP), when the experiments were recorded.

4.2. Visual positioning improvements

The resulting trajectory after filtering, making use of the aforementioned matrices (Section 4.1), is shown in Fig. 8. A greater, qualitatively significant, similarity can be appreciated between the trajectories after applying the data fusion (blue) as compared to the one just based on the low-cost GNSS data (red) with respect to the ground truth reference (green).

4.3. Positioning error reduction quantification

Fig. 9 presents the distance error histogram with respect to real reference positions, before and after using the here-proposed system. It is observed that, before applying the proposed data fusion system, there are distance errors of up to 80 m (Fig. 9a) whereas, after applying it, the distance errors do not go any higher than 21 m (Fig. 9b).

The RMS value, the 95th-percentile, and the maximum were computed, on the basis of the statistical distribution of the distance errors shown in Fig. 9. These measurements can be employed to quantify the error improvement achieved by the proposed data fusion system. Table 1 shows these statistical parameters obtained from the distance error distribution, as well as the error reduction,

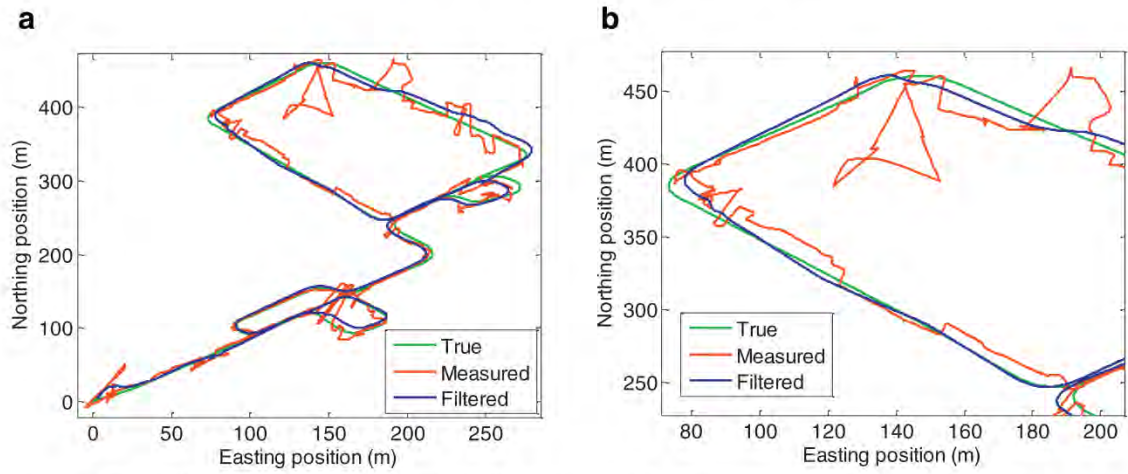


Fig. 8. (a) UTM projection of the 1.5-km-long test road path, and (b) a close-up of a region of interest (road intersection and turnarounds).

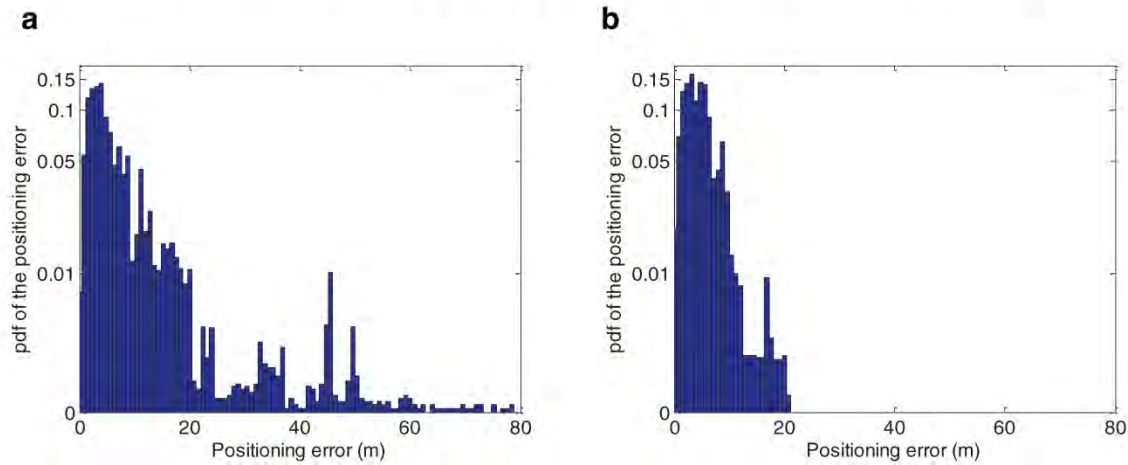


Fig. 9. Histogram of distance errors: (a) before applying the proposed data fusion system, and (b) after applying the proposed data fusion system. The histogram has been normalized so that it has a unitary area, representing an approximation to the probability density function (pdf) of the distance errors statistical random variable. Note that the Y-axis is not linear since μ -law companding algorithm, with a value of μ equal to 511, has been used in order to better show differences before and after applying the proposed data fusion system.

Table 1
Statistical parameters of the distribution of distance errors, before and after applying the proposed data fusion system, in the trajectory used for real tests shown in Fig. 8.

	Before	After	Error reduction
Distance Root-Mean Square Error (RMSE) (m)	11.6560	5.7427	50.73%
95th-percentile of distance error (m)	20.0	9.6	52%
Maximum distance error (m)	78.5859	20.4732	73.95%

computed as in Eq. (8):

$$\text{Error reduction (\%)} = \frac{\text{error_before} - \text{error_after}}{\text{error_before}} \times 100 \quad (8)$$

The maximum error was bounded below 21 m after applying the proposed method, as compared to the previous 80 m bound. Similarly, the RMSE and the 95th-percentile of distance error were reduced by roughly 50%. This result poses strong evidence of the quality of the data fusion system proposed by this study.

5. Discussion

The main finding of this study is that on-vehicle sensors data can be employed through the proposed data fusion system for improving the car positioning precision provided by a standalone low-cost GNSS receiver. The positioning precision improvement can reach up to 50% in terms of the RMSE, 50% in terms of the 95th-

percentile of the distance error distribution, and 75% in terms of the maximum distance error.

The aforementioned finding is supported by the results presented in Section 4, specifically by Figs. 8 and 9, and Table 1. Fig. 8 qualitatively shows the positioning precision improvements arising from the use of the proposed data fusion system. A significantly closer trajectory to the real one can be obtained after applying this system. Fig. 9 depicts the histogram of the errors before and after performing data fusion. As can be seen in these histograms (Fig. 9), the data fusion system achieves a shifting to the left in the errors distribution, having no errors greater than 21 m after performing data fusion (Fig. 9b); in contrast, the maximum errors reached 80 m when the low-cost GPS receiver was used on its own (Fig. 9a). Table 1 shows that, with respect to when the GPS receiver was used on its own, the positioning error reductions were 50.73%, 52%, and 73.95% in terms of the RMSE, the 95th-percentile of the distance error distribution, and the maximum distance error, respectively. These results provide evidence of the feasibility of employing the proposed data fusion system to improve car positioning precision when using low-cost GNSS receivers. Moreover, it is expected that the proposed system could be of great value in the event of short-term GNSS signal outages, which are prevalent in cities with tall buildings and skyscrapers.

The results of this article are in line with previous research regarding on-vehicle sensors and GNSS data fusion, despite the fact that most of the reviewed articles use different data fusion approaches. The article written by Bonnifait et al. (2001) proposes a multi-stage EKF-based system that first performs an odometry-based path reconstruction and then fuses its results with the GNSS-based path. In terms of positioning error reduction, significant local improvements are found in this article, although they do not seem to be consistent over time. El Najjar and Bonnifait's article (El Najjar & Bonnifait, 2005) proposes an EKF-based data fusion system of DGPS (Differential GPS) and ABS sensor measurements, which is complemented by a novel road-matching method based on the belief theory. By also using a map-matching technique, this data fusion approach is able to further reduce positioning errors, making this approach viable and useful when no GNSS data is available for long periods of time. In Gning and Bonnifait's article (Gning & Bonnifait, 2005), they propose a data fusion scheme based on Forward and Backward Propagation constraints for GNSS, two ABS rear wheel speed sensors, and gyroscope data. Their results show that EKF-based data fusion outperforms their novel proposed technique. The article written by Song et al. (2014) proposes a novel hybrid multi-sensor fusion strategy for positioning vehicles in tunnels based on Radio Frequency Identification (RFID) tags and on-vehicle sensors. Due to use of the short-range RFID technology, great improvements in positioning precision are achieved by this strategy. However, its huge associated cost of deployment, requiring the presence of RFID tags every 6 m, makes this approach currently unfeasible for widespread use in real life applications other than tunnels.

The system proposed in this article is a new contribution for two main reasons. The first reason is that the model employed to describe the state of car systems has not been previously used, so far as the authors are aware. Other articles (Bonnifait et al., 2001; El Najjar & Bonnifait, 2005; Gning & Bonnifait, 2005) have used both the angle rotated by the vehicle between consecutive samples, *i.e.* the change in the vehicle's heading direction, and the turning radius as intermediate variables, but the new proposed model avoids using any intermediate variable. This way, data fusion in this article is performed requiring less overall variables. It is expected that this reduction in the necessary number of variables will translate into a lower computational load associated with the EKF-based data fusion. The second reason is that the proposed system performs positioning data fusion as a single EKF-based stage

and is, thus, more flexible to the addition of new on-vehicle sensors as input or measured data. It is also expected that this reduction in the number of EKF-based stages will imply, once again, less computational load for the whole proposed system while not being detrimental in terms of precision.

One strength of the proposed system is its low implementation cost for most modern car vehicles. Two reasons can be highlighted for this claimed low-cost design: (i) today, most cars have all the necessary information to implement this system, with GNSS receivers on-board and many on-vehicle sensors available through the CAN bus of the vehicle; and (ii) modern car vehicles have an embedded on-board computer (Powertrain Control Module, PCM), so the software needed to combine all this information and estimate the position can be deployed in the embedded PCM. Taking these reasons into account, it will be possible to implement the proposed system for improving the car positioning precision without needing any additional hardware. Another strength of the proposed system is that, by its design, it can be adapted to incorporate more sensors, such as longitudinal accelerometers and wheel steering angle sensors, with greater ease.

The main weakness of this study lies in its not having contrasted the results with several low-cost GNSS receivers. Nevertheless, this weakness is not a significant issue since the low-cost GPS receiver employed in this article can be considered as an archetypical low-cost GPS receiver, which is representative of the main alternatives in the market. Moreover, the main performance benefits of the proposed system are expected to be reached during short-time GNSS signal outages, thus achieving significant precision improvements in those situations, even for high-end GNSS receivers. Although more precise techniques have been developed for enhancing the positioning provided by low-cost GNSS receivers, *e.g.* single-frequency Precise Point Positioning (PPP) (Chen & Gao, 2005), in the event of outages the proposed system would still be useful for improving vehicle's positioning. A second weakness is the fact that all experimental tests were performed in the same location (Valladolid, Spain). However, this weakness is also not a significant issue since it is expected that the behavior will be similar in other urban areas. Furthermore, the proposed system is expected to behave even better in urban environments with taller buildings than the ones present in Valladolid (Spain). A third weakness of this article is the way the real-time system was evaluated in post-processing. Nonetheless, this weakness is also not a significant issue. Other articles from the literature have also assessed real-time systems in post-processing in a similar fashion (Bonnifait et al., 2001; Gning & Bonnifait, 2005). Moreover, the alleged real-time capabilities of the proposed system have been checked, revealing that the real-time constraints can be guaranteed. In the conducted tests, it took less than 8 seconds to execute 260 seconds of data in a MATLAB® implementation running on an Asus K72Jk laptop. This fact reveals that, were this system to be deployed in a microprocessor-based device such as Raspberry Pi 3, it would be perfectly able to work in real-time, performing all the related processing in a bounded time before the subsequent data samples are available. Another weakness of the proposed data fusion system lies in the use of the not-perfectly-valid assumption, inherent to the Extended Kalman Filter, that the underlying noise is Gaussian. Other non-linear filtering techniques, such as the particle filter, could further improve the results of the proposed system by avoiding this assumption. Nevertheless, due to their associated higher computational load, they were discarded so as to meet the real-time constraints when executed in low-cost computing platforms.

Five main possible future lines, some of which the authors are already working in, have been detected for extending this article's work. A first future line of research could undertake the inclusion of map information into the model, by avoiding the fact that the

position lies within prohibited locations such as buildings or sidewalks, to further improve the car positioning precision. A second future line of research could consider the extension of the proposed system to be able to function even when no GNSS data is available for prolonged periods of time, also undertaking the precision and performance assessment of that future system during both short-term and long-term GNSS signal outages. A third future line of research could tackle the dynamic tuning of the covariance matrices involved in the EKF for data fusion, by characterizing the sensors accuracy and using the Dilution Of Precision (DOP) information from the GNSS constellation, to further improve the car positioning precision. A fourth future line of research could execute a fair performance comparison of the most remarkable state-of-the-art data fusion systems for improving car positioning precision, thus providing insightful advantages and disadvantages of each method, both theoretically and experimentally. A fifth future line of research could focus on integrating the proposed data fusion system into existing expert systems used in autonomous cars, probably including additional sensors for relative and absolute positioning, evaluating its suitability for self-driving in an experimental environment.

6. Conclusions

The main contribution of this work is the proposal of a novel system that enables keeping an accurate car positioning during GNSS signal outages while being simpler and more flexible to the incorporation of new sensors into it, as compared to other existing alternatives. The proposed data fusion system for car vehicles, which fuses data from a low-cost GNSS receiver with data from other on-vehicle sensors for relative positioning, can reduce the positioning error with respect to the positioning error of the low-cost GNSS receiver alone. This reduction can reach up to 50% in terms of the RMSE, 50% in terms of the 95th-percentile of the distance error distribution, and 75% in terms of the maximum distance error. The best precision improvements are achieved in urban areas, where tall buildings hinder the effectiveness of GNSS systems. Future work, tackling the dynamic tuning of the covariance matrices or incorporating additional sensors and map information into the model, among other possibilities, could further improve the performance of the here-proposed system, enabling a more accurate functioning even for prolonged periods of GNSS signal outages.

Acknowledgments

The work made in this article by Ruben Ruiz-Gonzalez was possible thanks to a "Formación de Personal Investigador" doctoral program grant, financed by the *Universidad de Valladolid* (Spain) and co-financed by *Banco Santander*.

The authors would like to express their sincere gratitude to Dr. Víctor Martínez-Martínez for his valuable, expert help and advice along all the stages of this study. The authors are also grateful for the helpful comments given by two anonymous reviewers on a previous draft of this manuscript. Furthermore, the authors want to acknowledge the valuable help provided with the language editing and proofreading of the article provided by the Writing Center of the University of Kentucky (USA), with a special mention to Jillian Winter and Leslie C. Davis.

Appendix A. Derivation of relationships between state and measured variables for a car vehicle

In this appendix, a formal derivation of the relationships between state and measured variables is provided.

Let us first introduce the notation and nomenclature employed throughout this appendix. Let us denote with subscripts FL, FR, RL, and RR, respectively, whenever we refer to the front left, front right, rear left, and rear right wheels. Let us continue with some definitions in Fig. A.1. L denotes the distance between the rear and front axles of the car vehicle; W_r denotes the length of the rear axle of the car; W_f denotes the length of the front axle of the car; R denotes the instantaneous turning radius of the central point in the rear axle; φ denotes the angle turned between two consecutive samples; δ denotes the equivalent angle turned by the virtual wheel used for the bicycle model; and d denotes the distance travelled between two consecutive samples by the central point of the rear axle of the car.

After having introduced the notation, and before starting with the derivations, a sign criterion for δ must be defined. In this article, δ is positive if clockwise and negative otherwise. Thus, in clockwise or right turns, δ is positive. In counter-clockwise or left turns, δ is negative.

Assuming the Ackerman steering geometry for the car vehicle, all four wheels turn with respect to the same turning point (Fig. A.1a). In turn, all the wheels move in such a way that they locally describe a circular trajectory, turning the same angle with respect to the turning point (Fig. A.1b).

Taking into account all the aforementioned considerations, we can now proceed to the derivations.

From basic trigonometry on rectangle triangles in Fig. A.1, it becomes obvious that:

$$R = \frac{L}{\tan \delta} \quad (\text{A.1})$$

Assuming, in Fig. A.1b, constant speed for the car vehicle between consecutive samples, the distance (d) travelled by the central point of the rear axle of the car vehicle (marked as a red point in Fig. A.1b) is:

$$d = u \cdot \Delta t = R \cdot \varphi \quad (\text{A.2})$$

where u denotes the car's speed, measured in the central point of the rear axle, and Δt is the time lapse between two consecutive samples.

Solving for u and $\frac{u}{R}$ in Eq. (A.2), we get:

$$u = \frac{R \cdot \varphi}{\Delta t} \rightarrow \frac{u}{R} = \frac{\varphi}{\Delta t} \quad (\text{A.3})$$

From Fig. A.1b, analogously to the case of the central point of the rear axle derived in Eq. (A.2), the distance travelled by each wheel between two consecutive samples is given by:

$$d_{FL} = u_{FL} \cdot \Delta t = R_{FL} \cdot \varphi \quad (\text{A.4})$$

$$d_{FR} = u_{FR} \cdot \Delta t = R_{FR} \cdot \varphi \quad (\text{A.5})$$

$$d_{RL} = u_{RL} \cdot \Delta t = R_{RL} \cdot \varphi \quad (\text{A.6})$$

$$d_{RR} = u_{RR} \cdot \Delta t = R_{RR} \cdot \varphi \quad (\text{A.7})$$

Rearranging Eqs. (A.4)–(A.7), solving for the wheel speeds, and also using Eqs. (A.1) and (A.3), the speed of each wheel is given by:

$$u_{FL} = \frac{R_{FL} \cdot \varphi}{\Delta t} = \frac{R_{FL}}{R} u = \frac{R_{FL} \cdot \tan(\delta)}{L} u \quad (\text{A.8})$$

$$u_{FR} = \frac{R_{FR} \cdot \varphi}{\Delta t} = \frac{R_{FR}}{R} u = \frac{R_{FR} \cdot \tan(\delta)}{L} u \quad (\text{A.9})$$

$$u_{RL} = \frac{R_{RL} \cdot \varphi}{\Delta t} = \frac{R_{RL}}{R} u = \frac{R_{RL} \cdot \tan(\delta)}{L} u \quad (\text{A.10})$$

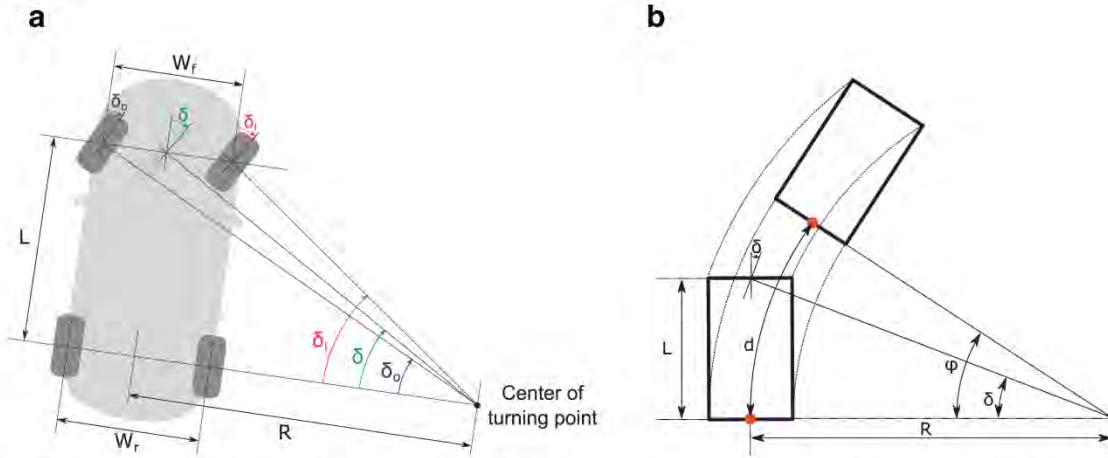


Fig. A.1. (a) Ackerman steering geometry, showing the relationship between the angle turned by each front wheel and the virtual central wheel used in the bicycle model. The “i” and “o” subscripts denote, respectively, the inner and outer front wheels with respect the center of turning point. For clockwise turns, the inner and outer wheels are, respectively, the front-right and front-left wheels, and vice versa for counter-clockwise turns. (b) Displacement between two consecutive samples, considering a time lapse short enough to assume a circular movement.

$$u_{RR} = \frac{R_{RR} \cdot \varphi}{\Delta t} = \frac{R_{RR}}{R} u = \frac{R_{RR} \cdot \tan(\delta)}{L} u \quad (A.11)$$

The turning radius for each wheel, i.e. the distance from each wheel to the center of turning point, can be computed from Fig. A.1 by using Pythagoras' theorem, as:

$$R_{FL} = \sqrt{L^2 + \left(R + \frac{W_f}{2}\right)^2} = \sqrt{L^2 + \left(\frac{L}{\tan \delta} + \frac{W_f}{2}\right)^2} \quad (A.12)$$

$$R_{FR} = \sqrt{L^2 + \left(R - \frac{W_f}{2}\right)^2} = \sqrt{L^2 + \left(\frac{L}{\tan \delta} - \frac{W_f}{2}\right)^2} \quad (A.13)$$

$$R_{RL} = R + \frac{W_r}{2} = \frac{L}{\tan \delta} + \frac{W_r}{2} \quad (A.14)$$

$$R_{RR} = R - \frac{W_r}{2} = \frac{L}{\tan \delta} - \frac{W_r}{2} \quad (A.15)$$

Introducing Eqs. (A.12)–(A.15) in Eqs. (A.8)–(A.11), we get:

$$u_{FL} = \frac{R_{FL} \cdot \tan(\delta)}{L} u = u \frac{\tan(\delta)}{L} \sqrt{L^2 + \left(\frac{L}{\tan \delta} + \frac{W_f}{2}\right)^2} \quad (A.16)$$

$$u_{FR} = \frac{R_{FR} \cdot \tan(\delta)}{L} u = u \frac{\tan(\delta)}{L} \sqrt{L^2 + \left(\frac{L}{\tan \delta} - \frac{W_f}{2}\right)^2} \quad (A.17)$$

$$u_{RL} = \frac{R_{RL} \cdot \tan(\delta)}{L} u = u \frac{\tan(\delta)}{L} \left(\frac{L}{\tan \delta} + \frac{W_r}{2}\right) \quad (A.18)$$

$$u_{RR} = \frac{R_{RR} \cdot \tan(\delta)}{L} u = u \frac{\tan(\delta)}{L} \left(\frac{L}{\tan \delta} - \frac{W_r}{2}\right) \quad (A.19)$$

Operating further in Eqs. (A.16)–(A.19), in order to avoid indeterminations caused by divisions by zero when $\delta = 0$, we finally get:

$$u_{FL} = \frac{\sqrt{(\tan(\delta) \cdot L)^2 + \left(L + \tan(\delta) \cdot \frac{W_f}{2}\right)^2}}{L} \cdot u \quad (A.20)$$

$$u_{FR} = \frac{\sqrt{(\tan(\delta) \cdot L)^2 + \left(L - \tan(\delta) \cdot \frac{W_f}{2}\right)^2}}{L} \cdot u \quad (A.21)$$

$$u_{RL} = \left(1 + \frac{W_r \cdot \tan(\delta)}{2L}\right) \cdot u \quad (A.22)$$

$$u_{RR} = \left(1 - \frac{W_r \cdot \tan(\delta)}{2L}\right) \cdot u \quad (A.23)$$

Focusing now on the lateral acceleration, assuming that the speed in the center of mass of the car and that the radius to the center of turning point are approximately the same as in the central point of the rear axle, it can be computed as:

$$Acc_{lat} = \frac{u^2}{R} = \frac{u^2}{L} \tan(\delta) \quad (A.24)$$

This previous approximation could be easily avoided and corrected for each particular car vehicle model by identifying the exact location of the center of mass for that specific car vehicle.

Additionally, the rotation rate of the car vehicle can be computed as the quotient of the angle turned by the car vehicle in the time lapse between two consecutive samples and this elapsed time. Thus, by using this definition along with Eqs. (A.1) and (A.3), we get:

$$Rot_{rate} = \frac{\varphi}{\Delta t} = \frac{u}{R} = \frac{u}{L} \cdot \tan(\delta) \quad (A.25)$$

The remaining relationship, between the steering wheel angle (δ_{sw}) and the turning angle of the virtual wheel (δ), is deduced by assuming a linear relationship between them. This assumption is usually correct in modern vehicles, so the quotient relationship between them is given by the steering ratio S_{ratio} . Thus, we have:

$$\delta_{sw} = S_{ratio} \cdot \delta \quad (A.26)$$

To conclude this appendix, it is worth noting that all the derivations made in this section, though just derived while turning clockwise, are valid for both clockwise and counter-clockwise turns. The criterion for the sign of δ captures the information of the turning direction, adapting all the equations and making them valid in both cases.

References

- Abbeel, P., Coates, A., Montemerlo, M., Ng, A. Y., & Thrun, S. (2005). Discriminative training of Kalman filters. In *Proceedings of Robotics: Science and Systems*. Cambridge, Massachusetts: MIT Press.
- Abbott, E., & Powell, D. (1999). Land-vehicle navigation using GPS. *Proceedings of the IEEE*, 87, 145–162.
- Bonnifait, P., Bouron, P., Crubille, P., & Meizel, D. (2001). Data fusion of four ABS sensors and GPS for an enhanced localization of car-like vehicles. In *Proceedings 2001 ICRA. IEEE International Conference on Robotics and Automation (Cat. No. 01CH37164): Vol. 2* (pp. 1597–1602).
- Chen, K., & Gao, Y. (2005). Real-time precise point positioning using single frequency data. In *Proceedings of the 18th International Technical Meeting of the Satellite Division of the Institute of Navigation, ION GNSS 2005: Vol. 2005* (pp. 1514–1523).
- El Najjar, M. E., & Bonnifait, P. (2005). A road-matching method for precise vehicle localization using belief theory and Kalman filtering. *Autonomous Robots*, 19, 173–191.
- French, G. T. (1996). *Understanding the GPS: An introduction to the global positioning system* (1st ed.). GeoResearch, Inc.
- Gning, A., & Bonnifait, P. (2005). Dynamic vehicle localization using constraints propagation techniques on intervals a comparison with Kalman filtering. In *Proceedings of the 2005 IEEE International Conference on Robotics and Automation* (pp. 4144–4149).
- Gomez-Gil, J., Ruiz-Gonzalez, R., Alonso-Garcia, S., & Gomez-Gil, F. (2013). A Kalman filter implementation for precision improvement in low-cost GPS positioning of tractors. *Sensors*, 13, 15307–15323.
- Jazar, R. N. (2014). Steering dynamics. *Vehicle dynamics: Theory and application* (pp. 387–495). New York, NY: Springer New York.
- Jazwinski, A. H. (2007). *Stochastic processes and filtering theory*. Dover Publications.
- Kaplan, E. D., & Hegarty, C. J. (2nd ed.). (2005). *Understanding GPS: Principles and applications*. Artech House.
- Leung, K. T., Whidborne, J. F., Purdy, D., & Barber, P. (2011). Road vehicle state estimation using low-cost GPS/INS. *Mechanical Systems and Signal Processing*, 25, 1988–2004.
- Lin, C.-F. (1991). *Modern navigation, guidance, and control processing: Vol. 2*. Englewood Cliffs: Prentice Hall.
- Mintsis, G., Basbas, S., Papaioannou, P., Taxiltaris, C., & Tziavos, I. N. (2004). Applications of GPS technology in the land transportation system. *European Journal of Operational Research*, 152, 399–409.
- Network of GNSS stations of Castilla y León. Available online accessed on 6 June 2016 <http://gnss.itacyl.es>.
- Pérez, J., Gonzalez, D., Milanés, V., Perallos, A., Hernandez-Jayo, U., & Onieva, E. (2015). Vehicle control in ADAS applications. *Intelligent transport systems* (pp. 206–219). John Wiley & Sons, Ltd.
- Robert Bosch GmbH (2007). *Bosch automotive electrics and automotive electronics* (5th ed.). Springer Fachmedien Wiesbaden.
- Schleicher, D., Bergasa, L. M., Ocaña, M., Barea, R., & López, E. (2010). Low-cost GPS sensor improvement using stereovision fusion. *Signal Processing*, 90, 3294–3300.
- Song, X., Li, X., Tang, W., Zhang, W., & Li, B. (2014). A hybrid positioning strategy for vehicles in a tunnel based on RFID and in-vehicle sensors. *Sensors*, 14, 23095–23118.
- Sorenson, H. W. (Ed.). (1985). *Kalman filtering: Theory and application*. IEEE Press.
- Tin Leung, K., Whidborne, J., F., Purdy, D., & Dunoyer, A. (2011). A review of ground vehicle dynamic state estimations utilising GPS/INS. *Vehicle System Dynamics*, 49, 29–58.
- Titterton, D., & Weston, J. L. (2004). *Strapdown inertial navigation technology: Vol. 17*. IET.

Article 3: Flow rate monitoring

The third article tackles the **flow rate monitoring** problem, previously described in chapter “Introduction to the compendium”. The main bibliographic data about this article is shown below:

- Title: An acoustic method for flow rate estimation in agricultural sprayer nozzles.
- Authors: Ruben Ruiz-Gonzalez; Timothy S. Stombaugh; Víctor Martínez-Martínez; Jaime Gomez-Gil.
- Journal: Computers and Electronics in Agriculture.
- Editor: Elsevier.
- Impact factor: 2.427 (2017).
- Journal Ranking:
 - Q1 on *Agriculture, Multidisciplinary* (7/57).
 - Q2 on *Computer Science, Interdisciplinary Applications* (39/105).
- Date of publication: September 2017.
- ISSN: 0168-1699.
- Volume: 141.
- Pages: 255-266.
- DOI: 10.1016/j.compag.2017.08.003.
- URL: <https://www.sciencedirect.com/science/article/pii/S0168169917306282>.
- Number of cites: 1.

The article presented below is a version of the original article published in the previously mentioned journal. This version of the article has been authorized by the journal editor to be included in this PhD thesis as a compendium of publications.



Contents lists available at ScienceDirect

Computers and Electronics in Agriculture

journal homepage: www.elsevier.com/locate/compag

Original papers

An acoustic method for flow rate estimation in agricultural sprayer nozzles

Ruben Ruiz-Gonzalez^{a,*}, Timothy S. Stombaugh^b, Víctor Martínez-Martínez^a, Jaime Gomez-Gil^a^a Department of Signal and Communications Theory and Telematics Engineering, University of Valladolid, Valladolid 47011, Spain^b Biosystems and Agricultural Engineering Department, University of Kentucky, Lexington, KY 40546, USA

ARTICLE INFO

Article history:

Received 23 May 2017

Received in revised form 1 August 2017

Accepted 4 August 2017

Available online 10 August 2017

Keywords:

Agricultural sprayer nozzle

Flowmeter

Acoustic signal

Microphone

Frequency analysis

Cost-effective solution

ABSTRACT

The cost of current flow rate measurement devices is quite high compared to the cost of low-end microphones. This circumstance, together with the fact that common agricultural sprayers have more than 50 nozzles, makes the use of current flow rate measurement devices cost-prohibitive. That considered, this article examines, by proposing one particular method, the feasibility of using microphones as flowmeters for nozzle tips in agricultural sprayers. The proposed method consists of the following stages: (i) acquisition of the digital acoustic data sequence, (ii) signal preprocessing, (iii) frequency domain transformation using Fast Fourier Transform (FFT) analysis, (iv) in-band power calculation, (v) power normalization, and (vi) regression or curve fitting. This method was assessed in an in-lab sprayer test bench employing 11 commercial nozzle tips at several operating flow rates within or close to those recommended by the manufacturers. The experimental results yielded, for all the tested nozzle tips, average absolute and relative Root Mean Square Error (RMSE) values always below 0.08 liters per minute (lpm) and 5%, respectively, while the overall mean absolute and relative RMSE values were lower than 0.05 lpm and 2.5%. Furthermore, for each tested nozzle tip, the Maximum Absolute Error (MAE) was always bounded below 0.3 lpm, being the absolute error lower than 0.15 lpm for 95% of the time. The accuracies when employing a high-end microphone instead of a low-end one presented no statistically significant differences. These results provide strong evidence of the feasibility of accurately estimating the nozzle tip flow rate in real time based on acoustic signals. Moreover, no significant improvements are to be expected by using a high-end microphone instead of a low-end one. However, there are still some issues that should be tackled in order to enable the application of this method in real agricultural settings.

© 2017 Elsevier B.V. All rights reserved.

1. Introduction

In the last few decades, agricultural sprayer technology has been continuously evolving toward the ability to accurately measure and control the flow rate of each individual nozzle on a spray boom (Hughes and Frost, 1985; Mulla, 2013). The recognition has been made that there can be significant variation between nozzles on a boom, and that the effects of vehicle turning maneuvers can be severely detrimental when trying to achieve a uniform chemical

application. By being able to control the flow rate of each individual nozzle, both a higher uniformity in turns and a more consistent application along straight paths can be achieved in the spread pattern of chemicals (pesticides, insecticides, fertilizers, and herbicides), which provides two distinct advantages. First, the reduction in the waste of chemicals would allow farmers to reduce the amount of chemicals used, thereby reducing production costs (Loghavi and Behzadi Mackvandi, 2008). Second, in some applications the amount of chemicals to be dispatched is absolutely critical: when incorrect amounts are sprayed, either the chemicals will lack effectiveness because of under-application, or soil and crops will lose quality and yield, or they can be polluted and even irreversibly damaged, because of the over-application of chemicals (Gopala Pillai et al., 1999; Loghavi and Behzadi Mackvandi, 2008; Michael et al., 1990; Nordmeyer et al., 1997).

To provide a finer resolution of control, solenoid-based electronic valves, controlled by Pulse-Width Modulation (PWM), have

Abbreviations: DAQ, Data Acquisition; DFT, Discrete Fourier Transform; FFT, Fast Fourier Transform; IIR, Infinite Impulse Response; lpm, liters per minute; PSD, Power Spectral Density; PWM, Pulse-Width Modulation; RMSE, Root Mean Square Error; USB, Universal Serial Bus.

* Corresponding author.

E-mail addresses: r.ruizon@ribera.tel.uva.es (R. Ruiz-Gonzalez), tim.stombaugh@uky.edu (T.S. Stombaugh), vmarmar@ribera.tel.uva.es (V. Martínez-Martínez), jgomez@tel.uva.es (J. Gomez-Gil).

<http://dx.doi.org/10.1016/j.compag.2017.08.003>

0168-1699/© 2017 Elsevier B.V. All rights reserved.

been employed in agriculture at the nozzle level (Gil et al., 2013; Hui et al., 2014). The practical implementations of nozzle-level PWM control have been limited to open-loop control, which implicitly relies on uniformity and consistency of all the components across the boom for control accuracy. Feedback control would be much more accurate, but it would require reliable, real-time flow measurements from each nozzle. There is no currently available flow metering technology that could provide suitable accuracy at reasonable cost and size for implementation at each nozzle. The goal of this study is to develop an acoustic-based flow measuring technology that would be appropriate for implementation at the individual nozzle level to facilitate feedback control.

Many published articles have addressed the sound generation of nozzles and orifices (Cann and Leehey; Sheen, 2011; Zhang et al., 2004). These studies have shown that the intensity and spectrum of the acoustic signal generated by nozzles and orifices change when the flow rate changes. Testud et al. (2009), Testud et al. (2007) investigated the sound generation by the presence of single-hole and multi-hole orifice plates along the pipe, showing that the characteristic whistling frequency of the emitted sound signal depends on the flow rate. Howe (2004) showed that inner cavities in the pipe generate a sound signal whose acoustic intensity depends on the flow speed as a cubic function and whose cavity resonant tone frequency also depends on the speed of the stream flow. Druault et al. (2011) also found a dependence of the acoustic signal spectrum on the flow rate due to the presence of a cavity along the pipe. Kobayashi et al. (2009) studied, for an ocarina musical instrument, the dependence of the acoustic signal on the flow rate due to the presence of a cavity along the pipe.

Guided by the aforementioned research, the present study relies on the working hypothesis that flow rate changes through the sprayer nozzle tip will predictably change its generated acoustic signal both in intensity and frequency distribution. This hypothesis has already been proven valid in previous studies for taps or faucets (Jacobs et al., 2015; Kakuta et al., 2012). So far as the authors are aware, despite all the research advances, no prior progress has been made towards providing a relationship between the generated acoustic signal and the flow rate for sprayer nozzles. Thus, the proposal of this new acoustic flow rate estimation method is intended to become a point of inception for further research to gain more insight about flow rate estimation through acoustic signal processing.

The main goal of this article is to provide evidence supporting the viability of accurately estimating the flow rate of individual sprayer nozzles based on the acoustic signal measured close to the nozzle tip. To this end, four specific objectives can be highlighted: (i) the proposal of a new real-time flow rate estimation method based on the acoustic signal acquired by a nearby microphone, (ii) the assessment of this method's performance, (iii) the comparison of performance employing low-end versus high-end microphones, and (iv) the analysis of the influence of the nozzle-to-microphone distance on flow rate estimation.

This article describes the aforementioned proposed flow rate estimation method and presents the Materials and Methods employed to undertake the research in this study (Section 2), presents the main results obtained from the assessment of this method (Section 3), and presents a discussion of this study's findings and conclusions (Sections 4 and 5).

2. Materials and methods

All tests in this study were performed in a well-adapted laboratory belonging to the Department of Biosystems and Agricultural Engineering at the University of Kentucky in Lexington, KY, USA.

2.1. Materials

The experimental setup used to conduct the experiments in this study consisted of the following elements, where the item numbers in the list match the labels employed in Fig. 1:

1. A laboratory sprayer test bench equipped with a water tank, a supply pump, hoses, pipes, a flowmeter, a flow controller, and one nozzle mounting adapter.
2. A 200-liter water tank and a supply pump, which was composed of a Dayton® 5K117BD industrial motor and an Oberdorfer™ 101BM07MC gear pump.
3. An OMEGA Engineering Inc. FMG202-NPT low-flow magnetic flowmeter, which was employed to measure flow rates during the recording experiments to provide ground truth reference for the evaluation of the proposed flow rate estimation method.
4. A LCR-5LPM-D-100PSIG5V liquid flow controller from Alicat Scientific, Inc., which was employed to control the flow rate at which water flowed through the nozzle tip. The accuracy specified by the manufacturer is 2% Full Scale (Technical Data for Alicat LC & LCR Liquid Flow Controllers). The fact of this error being given as relative to the full scale implies higher relative errors for low flow rates.
5. A Wilger Combo-Rate Modular Nozzle Body that was used to mount the nozzle tips.
6. A low-cost CUI CMC-5044PF-A electret microphone (CUI CMC-5044PF-A electret microphone datasheet), plus preprocessing electronics. A very simple electronic circuit (Fig. 2a), which was specified by the manufacturer, was used for impedance adaptation and high-pass filtering of the signal provided by the microphone.
7. A high-end Knowles BL-2199-000 microphone (Knowles BL-21994-000 microphone datasheet), plus preprocessing electronics, which was used to check the results provided by the aforementioned low-end microphone. A very simple electronic circuit (Fig. 2b) was used for powering this microphone and setting its proper operating point.
8. A NI USB-4431 National Instruments (NI) data acquisition (DAQ) module, which was used to digitize the signals provided by both analog microphone sensors.
9. A Dell Latitude E6400 laptop computer, which was employed to acquire and save the logged data coming from the data acquisition module. The connection between the laptop and the data acquisition system was made through a USB cable. The laptop was also employed to conduct the processing steps for the proposed flow rate estimation method, as explained in Section 2.2.

Eleven different agricultural nozzle tips were used in the experiments. These tips were chosen among the most commonly used tips from two mainstream manufacturers: TeeJet® (TeeJet® nozzle tips manufacturer webpage) and Wilger Industries Ltd (Wilger Industries Ltd. nozzle tips manufacturer webpage). Specifically, from TeeJet®, the following set of nozzle tips was used: AITT110-03, AIX110-03, TG-3, Turbo TIVP110-03, TwinJet 80-03, XRC80-04, and XRC80-06. From Wilger Industries Ltd, the following COMBO-JET® nozzle tips were used: ER80-03, MR80-04, MR80-06, and MR80-08. The selected set of nozzle tips is considered representative enough, covering most of the mainstream agricultural spraying applications, since they all present features differing in spray pattern (flat fan, twin flat, and cone spray), droplet size (fine, medium, and coarse), spray fan angle (80° and 110°), and flow rate operating range.

2.2. Methods

The main processing stages performed in this study can be conceptualized as follows (Fig. 3): (i) data acquisition (Section 2.2.1);

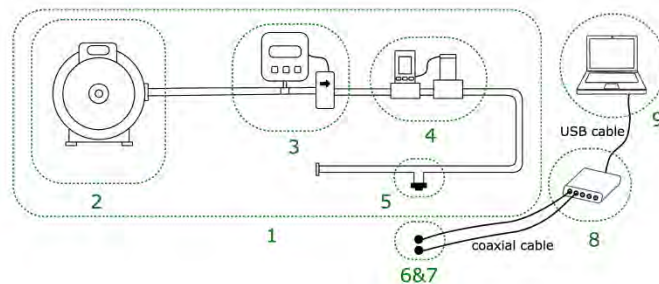


Fig. 1. Schematic of the setup employed for conducting the experimental tests. The elements in the schematic are: (1) sprayer test bench, (2) water tank and supply pump, (3) accurate reference flowmeter, (4) flow controller, (5) nozzle mounting adapter and nozzle tips, (6 & 7) low-end and high-end microphones, (8) data acquisition module, and (9) laptop computer.

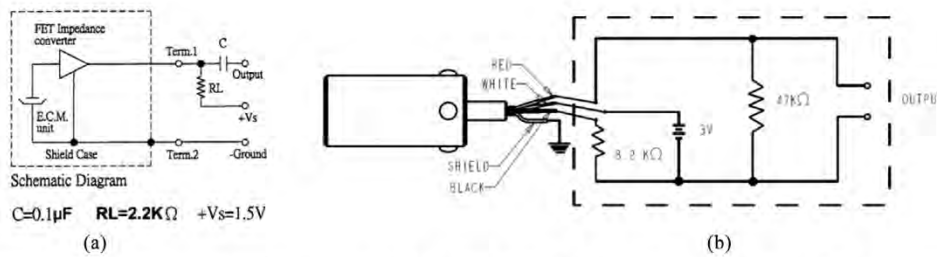


Fig. 2. Schematic of the preprocessing electronic circuits for the: (a) CUI CMC-5044PF-A microphone, and (b) Knowles BL-21994-000 microphone.

(ii) preprocessing (Section 2.2.2); (iii) Fast Fourier Transform (FFT) analysis (Section 2.2.3); (iv) in-band power calculation (Section 2.2.4); (v) power normalization (Section 2.2.5); (vi) regression or curve fitting (Section 2.2.6); and (vii) evaluation (Section 2.2.7). The first six stages correspond to actual stages of the proposed flow rate estimation method, while the last one was aimed at assessing the accuracy of this method. The whole processing, i.e. all stages except data acquisition, was performed and run in MATLAB® programming environment. Fig. 3 summarizes the main processing stages and contains an overview of the methods, which are explained in greater detail in the remainder of this subsection.

2.2.1. Data acquisition

Acoustic data were experimentally obtained from around the nozzle by using the aforementioned sprayer test bench. Both the low-end (CUI CMC-5044PF-A) and high-end (Knowles BL-21994-000) microphones were used to measure the acoustic signal simultaneously. The location of the microphones used for these recordings was as depicted in Fig. 4. After several trial and error tests, this location was considered the best for optimizing the overall method performance. Two analog input channels of the National Instruments

DAQ system, one for each microphone, were employed using the NI LabView software running on the aforementioned laptop.

The acquisition experiments involved setting up a constant flow rate of water through the nozzle. Water was selected because of economic and safety reasons, since it accurately represents the typically used mixture of water with fertilizers, herbicides, and pesticides. This mixture normally consists of around 99% of water, thus the alleged resemblance. Once the flow rate had been stabilized, 61-second-long recordings were simultaneously taken with both microphones using a sampling frequency of 100 kHz. Eleven different nozzle tips, previously mentioned in Section 2.1, were tested. For each nozzle tip, several flow rates were used, all within or close to the operating range recommended by the manufacturer in the respective product datasheet. For each nozzle tip at each tested flow rate, two recordings were taken: one for training purposes and the other for testing purposes. The training data were used to determine the parameters of the subsequent processing stages of the estimation method. The testing data were used to assess the performance of the method using these parameters.

A summary of the most important information related to the data acquisition stage is shown in Table 1.

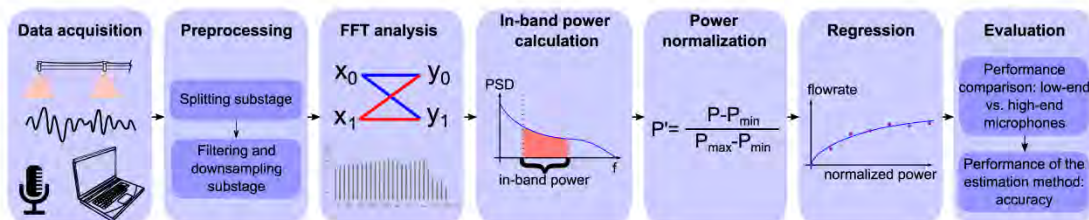


Fig. 3. Overall block diagram summarizing the main processing stages performed in this study.

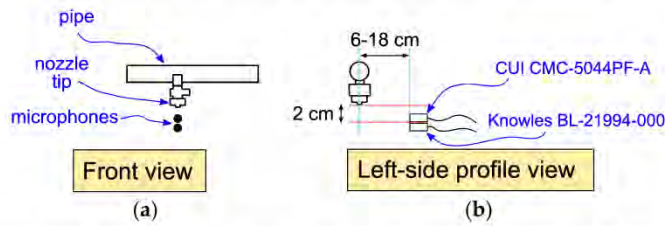


Fig. 4. Location of the microphones with respect to the nozzle tip: (a) front view, and (b) left-side profile view.

Table 1
Summary with the most relevant parameters for the data acquisition stage.

Parameter	Value
Liquid flowing through the nozzles:	Water
Number of acquisitions:	One per each nozzle tip and tested flow rate
Acquisition time/sample:	61 s
Sampling frequency:	100 kHz
Microphone's location:	
Vertical	2 cm
Horizontal	6–18 cm
Microphones models:	
Low-end microphone	CUI CMC-5044 PF-A
High-end microphone	Knowles BL-21994-000
Model of data acquisition module:	NI USB-4431

2.2.2. Preprocessing

The preprocessing stage consisted of two substages: (i) the splitting substage, and (ii) the filtering and downsampling substage. This stage was applied to each of the aforementioned 61-second-long acquired signals, i.e., for all the recordings.

In the splitting substage, the complete 61-second-long sequence was divided into 122 epochs of 0.5 s each. In order to achieve a real-time flow rate estimation, this time was empirically considered as the minimum epoch size able to prevent the loss of meaningful information from the acoustic signal. Thus, the subsequent stages are still able to accurately compute flow rates from this split signal.

In the filtering and downsampling substage, a digital IIR elliptic low-pass filter with a cutoff frequency of 4 kHz was applied to the split signal to avoid spectral aliasing in the subsequent downsampling stage. This cutoff frequency was chosen since all frequencies of interest for this method lie in a band below 2 kHz, as will be further detailed in Section 2.2.4. After the filtering, the signal was also downsampled by a factor of $M = 10$, to reduce its original length, thus avoiding unnecessary processing overload in terms of computational complexity. In this way, every 0.5 s the subsequent FFT analysis stage receives as input the preprocessed data from one of these 0.5-second-long epochs, consisting of $N = 5000$ samples. As a consequence, the whole flow rate estimation method is able to update the provided measurement every half a second, i.e. twice every second.

2.2.3. FFT analysis

In this stage the *Discrete Fourier Transform* (DFT) of each of the epochs was calculated using the *Fast Fourier Transform* (FFT) algorithm. Assuming that $x[n]$, with $n \in \mathbb{Z}$ and $n \in [0, N - 1]$, denotes the discrete-time signal associated with each epoch output from the previous stage, its DFT transform, $X[k]$, is computed using Eq. (1):

$$X[k] = \sum_{n=0}^{N-1} x[n] \cdot e^{-i2\pi kn/N}, \quad \text{for } k = 0, \dots, N-1 \quad (1)$$

where N denotes the length of the discrete signals $x[n]$ and $X[k]$.

After this step, the *Power Spectral Density* (PSD) was calculated using Eq. (2):

$$PSD[k] = 2 \cdot \frac{X[k] \cdot X^*[k]}{N \cdot f_s} \quad (2)$$

where $f_s = 10000$ Hz is the effective sampling frequency after the downsampling by a factor of ten, and the asterisk symbol denotes the complex conjugate of a complex number.

2.2.4. In-band power calculation

After having computed the PSD from the frequency spectrum via the FFT transform, the in-band power contained between 1450 and 1950 Hz was calculated by using the trapezoidal integration rule (Eq. (3)). This frequency band was chosen after being considered the most suitable for the subsequent flow rate estimation. The process that led to this choice consisted of performing an exhaustive search using bandwidths between 100 and 2000 Hz, sweeping for each tested bandwidth along all possible the frequency ranges from 0 to 50 kHz. This search looked for achieving high flow rate estimation accuracy and high robustness against noise at the same time. For this end, the frequency range with the smallest possible bandwidth, while presenting less than a 10% difference with respect to the best accuracy obtained among all tested ranges and bandwidths, was selected. This process was performed only using a representative nozzle (*Wilger COMBO-JET® MR80-04*). Therefore, the same frequency band was chosen for all tested nozzles in the experiments. This trial and error approach was constrained by the early observation of the frequency spectrum of the acoustic signal coming from the nozzle tip.

Therefore, the unnormalized in-band power, P , can be calculated as shown in Eq. (3):

$$P = \sum_{k=725}^{974} \frac{PSD[k] + PSD[k+1]}{2} \cdot 2 \text{ Hz} \quad (3)$$

In Eq. (3), $k = 725$ and $k = 974$ are, respectively, the indexes corresponding to the 1450 and 1948 Hz frequencies, since the employed frequential resolution was 2 Hz.

2.2.5. Power normalization

The output from the previous stage, namely the unnormalized in-band power, became the input to this stage. The normalization process consisted of applying a linear mapping so that the output of this stage, P_{norm} , i.e. the normalized in-band power, was a value bounded between 0 and 1. The zero and one values correspond, respectively, to the minimum and maximum tested flow rates of the particular nozzle tip assessed. Additionally, during the training phase in this stage, the values of P_{min} and P_{max} were obtained, once again individually for each assessed nozzle tip, as the mean in-band power of the 122 epochs for the minimum flow rate and for the maximum flow rate, respectively. The normalized power,

P_{norm} , was calculated from the unnormalized power, P , using the following linear mapping (Eq. (4)):

$$P_{norm} = \frac{P - P_{min}}{P_{max} - P_{min}} \quad (4)$$

2.2.6. Regression or curve fitting

After computing the normalized in-band power, for the training data for which the actual flow rate was known, the flow rate versus the normalized in-band power was plotted. Using a sixth root function, as shown in Eq. (5), the parameters k_1 and k_2 were adjusted for each assessed nozzle tip to better fit the empirical training data points by means of a transformed linear regression using the least squares approach. The fitted data curve was later used for flow rate estimation with the new testing data so that the output of this stage was an estimate of the volumetric flow rate measured in liters per minute (lpm).

The aforementioned sixth root function employed in this stage was:

$$x = (k_1 + k_2 \cdot P_{norm})^{1/6} \quad (5)$$

where x denotes the flow rate output, P_{norm} is the normalized in-band power coming from the previous stage, and k_1 and k_2 are constants determined during the curve fitting stage with the training data set.

For calibration purposes, for each microphone independently and whenever the nozzle tip or nozzle-to-microphone distance changes, all the stages described between Section 2.2.1 and Section 2.2.6 should be conducted again while the actual flow rate is measured simultaneously with an accurate flowmeter. In this way, a new different curve is fitted in order to be used for later estimation.

2.2.7. Evaluation

After having undertaken all the previous stages, the performance of the proposed method was assessed. For each nozzle tip, after having performed the corresponding training phase (Section 2.2.6), the method accuracy was evaluated for the testing data set. The evaluation stage consisted of using as input new acoustic signals and evaluating how accurate the method was in providing an estimate of the actual flow rate, which was measured concurrently with the accurate flowmeter. The absolute and relative *Root Mean Square Error* (RMSE), the maximum absolute error, and the 95% interpercentile range, as well as visual inspection, were used as performance metrics for evaluation.

The absolute and relative RMSE, the maximum absolute error, and the 95% interpercentile range values were calculated for all the aforementioned testing data experiments, i.e. one for each tested nozzle tip at several constant flow rates, as shown in Eqs. (6)–(9):

$$\text{AbsoluteRMSE} = \sqrt{\frac{1}{N} \sum_{i=1}^N (x_i - x_{GT})^2} \quad (6)$$

$$\text{RelativeRMSE} = \frac{\sqrt{\frac{1}{N} \sum_{i=1}^N (x_i - x_{GT})^2}}{x_{GT}} = \frac{\text{AbsoluteRMSE}}{x_{GT}} \quad (7)$$

$$\text{maximum absolute error} = \max_{1 \leq i \leq N} \{ |x_i - x_{GT}| \} \quad (8)$$

$$\text{95\% interpercentile range} = 97.5\text{th percentile} - 2.5\text{th percentile} \quad (9)$$

where x_i is the estimated flow rate value obtained by the proposed method at the i -th epoch, x_{GT} is the ground truth reference value provided by the accurate flowmeter, and $N = 122$ denotes the number of epochs for each experiment at a constant flow rate.

The assessment of the method, using the metrics previously introduced, consisted of three main evaluation experiments: (i) one for the accuracies of all tested nozzle tips, (ii) another for the influence of the quality of the measuring microphone, and (iii) a last one for the dependency on the location of the microphone.

In the first evaluation experiment, just the low-end microphone (CUI CMC-5044PF-A) was employed and it was located 6 cm from the nozzle tip (Fig. 4). In this experiment, all 11 nozzle tips were tested and compared for several flow rates lying within or close to their manufacturer recommended operating ranges.

In the second evaluation experiment, both the high-end (Knowles BL-21994-000) and low-end (CUI CMC-5044PF-A) microphones were used, once again placed 6 cm from the nozzle tip (Fig. 4). In order to report simpler results, three representative and commonly used nozzle tips were selected for comparison: TeeJet® XRC80-04, Wilger COMBO-JET® MR80-04, and TeeJet® AIX110-03. In addition to the aforementioned performance metrics, the correlation coefficients between the estimated flow rate discrete-time sequences for both the high-end and low-end microphones were computed. This value was used as a measurement of the coherence between the estimates provided by both microphones. Furthermore, for the same nozzle tip, a Welch's t -test between the absolute RMSE errors from both microphones was performed to detect the presence or absence of statistically significant differences by testing if both samples could come from the same probability distribution.

In the third evaluation experiment, once again just the low-end microphone (CUI CMC-5044PF-A) was employed, but several recordings were taken varying the nozzle-to-microphone separation distances to 6, 12, and 18 cm. In order to report simpler results, just one of the most commonly used nozzle tips was selected for comparison: Wilger COMBO-JET® MR80-04. The aforementioned performance metrics were computed for the recordings at these three separation distances in order to assess the influence of the distance on the method accuracy.

3. Results

For the sake of clarity, the main results of this study are presented in three separate subsections corresponding to each of the aforementioned evaluation experiments (Section 2.2.7). First, the estimation accuracy for all the tested nozzle tips was assessed. Second, the influence of the quality of the measuring microphone was evaluated. Last, the dependency on the location of the microphone was examined.

3.1. Accuracy results for different nozzle tips

In this subsection, the accuracy results obtained with the 11 aforementioned nozzle tips (Section 2.1) are reported while using the low-end microphone (CUI CMC-5044PF-A).

Fig. 5 depicts the flow rate discrete-time sequences estimated by the proposed method applied to four acquired, representative acoustic signals for each of the 122 0.5-second-long epochs. It can be seen that the proposed method makes real-time flow rate estimation possible, since the flow rate can be updated every 0.5 s, thus allowing for quick updates as the flow rate changes.

Table 2 reports the accuracies for all 11 tested nozzle tips. It can be seen that the average values for the absolute RMSE, the maximum absolute error, and the 95% interpercentile range of the error are always below 0.08, 0.32 and 0.31 liters per minute (lpm),

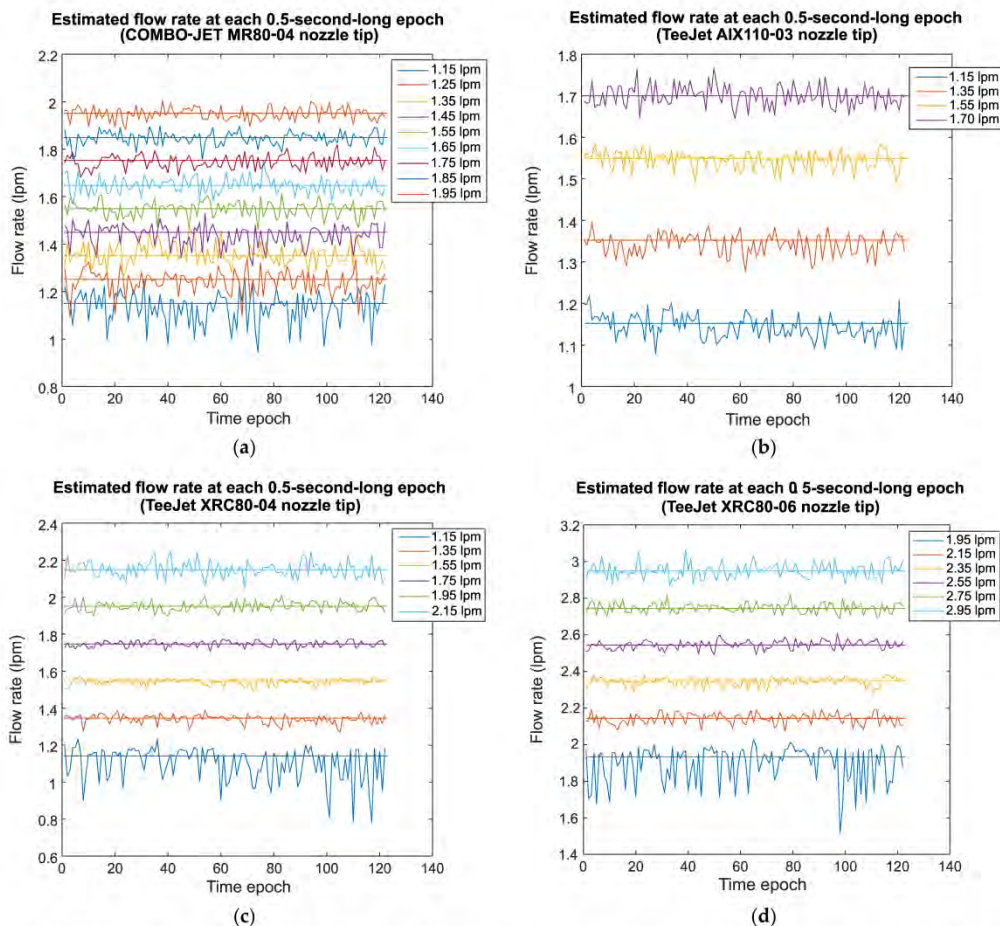


Fig. 5. Flow rate estimation results for each of the 122 0.5-second-long epochs while the flow rate was kept constant and the low-end microphone (CUI CMC-5044 PF-A) was 6 cm from the nozzle tip. (a) Wilger COMBO-JET[®] MR80-04 nozzle tip. (b) TeeJet[®] AIX110-03 nozzle tip. (c) TeeJet[®] XRC80-04 nozzle tip. (d) TeeJet[®] XRC80-06 nozzle tip.

respectively. Computing the relative RMSE, found by dividing the absolute RMSE by the actual flowrate, an average error always lower than 5% was obtained for every single nozzle. These facts provide strong evidence of the usefulness of the proposed flow rate estimation method, which led to high accuracies for all tested nozzle tips.

3.2. Accuracy comparison of high-end versus low-end microphones

In this subsection, a performance comparison between low-end and high-end microphones is tackled for the proposed flow rate estimation method. In order to simplify the comparison of the results from the two different microphones, only three representative nozzle tips were selected: TeeJet[®] XRC80-04, Wilger COMBO-JET[®] MR80-04, and TeeJet[®] AIX110-03. As previously noted, the same experiments were simultaneously recorded with both microphones for a more unbiased accuracy comparison between them.

Fig. 6 shows a comparison of the estimated flow rate discrete-time sequences for all 122 0.5-second-long epochs with both microphones for the TeeJet[®] XRC80-04 nozzle tip. A very high similarity is observed for the highest flow rates, while small discrepancies appear for the lowest flow rates. This plot is a proof of the high

coherence between the measurements provided by both microphones, which highlights the consistency of the proposed method with almost no dependence on the employed microphone.

Tables 3–5 show the results obtained while using the high-end microphone (Knowles BL-21994-000) together with those from the low-end one (CUI CMC-5044PF-A). A comparison between the performance for the TeeJet[®] XRC80-04 nozzle tip in Table 3 reveals that the high-end microphone does not outperform the low-end microphone. In fact, the accuracies were slightly worse for the high-end microphone. The same conclusion can be reached by comparing the results for the Wilger COMBO-JET[®] MR80-04 and TeeJet[®] AIX110-03 nozzle tips in Tables 4 and 5, respectively. This fact proves that highly accurate results can be achieved with a low-end microphone, with no significant improvements expected when using a high-end one. Another remarkable result is that moderate (0.40–0.59) to very strong (0.80–1.00) correlations are observed between the measurements provided by both microphones. This fact clearly highlights the existence of a significant coherence between the measurements provided by both devices. Moreover, performing the Welch’s *t*-test for the absolute RMSE errors obtained with both microphones in Tables 3–5; *p*-values of 0.7290, 0.0048, and 0.1363 were obtained, respectively. These

Table 2
Accuracy results of the proposed flow rate estimation method for the tested nozzle tips and flow rates using the low-end microphone (CUI CMC-5044PF-A).

Nozzle tip employed [operating flow rate range recommended by manufacturer]	Actual flow rate (lpm)	Absolute RMSE (lpm)	Relative RMSE (%)	Maximum absolute error (lpm)	95% interpercentile range (lpm)
Wilger COMBO-JET [®] MR80-04 [1.10–2.00 lpm]	1.15	0.0689	5.991	0.2065	0.2550
	1.25	0.0487	3.896	0.1570	0.2201
	1.35	0.0455	3.370	0.1291	0.1695
	1.45	0.0462	3.186	0.1407	0.1626
	1.55	0.0318	2.052	0.0887	0.1353
	1.65	0.0331	2.006	0.1028	0.1228
	1.75	0.0280	1.600	0.0688	0.1053
	1.85	0.0280	1.514	0.0925	0.1150
	1.95	0.0262	1.344	0.0667	0.1010
	Average	0.0396	2.773	0.1170	0.1541
Wilger COMBO-JET [®] MR80-06 [1.60–3.00 lpm]	1.92	0.0921	4.797	0.3008	0.2914
	2.12	0.0434	2.047	0.1267	0.1699
	2.31	0.0511	2.212	0.1188	0.1804
	2.49	0.0406	1.631	0.0935	0.1578
	2.68	0.0413	1.541	0.1128	0.1594
	2.87	0.0446	1.554	0.1043	0.1757
	Average	0.0439	2.297	0.1205	0.1618
Wilger COMBO-JET [®] MR80-08 [2.20–4.00 lpm]	2.57	0.1221	4.751	0.4658	0.4277
	2.77	0.0382	1.379	0.1207	0.1475
	2.96	0.0539	1.821	0.1493	0.2271
	3.16	0.0463	1.465	0.1297	0.1898
	3.34	0.0483	1.446	0.1095	0.1699
	3.53	0.0490	1.388	0.1474	0.2004
	3.72	0.0451	1.212	0.1111	0.1818
	3.92	0.0436	1.112	0.1233	0.1796
	4.12	0.0575	1.396	0.1704	0.2148
	Average	0.0560	1.775	0.1697	0.2154
Teejet [®] AIX110-03 [0.70–1.70 lpm]	1.15	0.0289	2.513	0.0726	0.1094
	1.35	0.0263	1.948	0.0733	0.0956
	1.55	0.0220	1.419	0.0602	0.0815
	1.70	0.0255	1.500	0.0658	0.0931
	Average	0.0257	1.845	0.0680	0.0949
Teejet [®] Turbo TTPV110-03 [0.70–1.70 lpm]	1.15	0.0239	2.078	0.0634	0.0980
	1.35	0.0316	2.340	0.0695	0.1232
	1.55	0.0349	2.252	0.0937	0.1418
	1.73	0.0545	3.150	0.1409	0.2231
	Average	0.0362	2.455	0.0919	0.1465
Teejet [®] ATTT110-03 [0.80–1.70 lpm]	1.55	0.1337	8.626	0.6491	0.5191
	1.75	0.0568	3.246	0.1639	0.2324
	1.95	0.0433	2.221	0.1195	0.1708
	Average	0.0779	4.697	0.3108	0.3074
Teejet [®] TG-3 [1.50–2.60 lpm]	1.55	0.0750	4.839	0.1830	0.3041
	1.75	0.0668	3.817	0.1664	0.2697
	1.95	0.0598	3.067	0.1675	0.2411
	2.15	0.0435	2.023	0.1320	0.1603
	2.35	0.0451	1.919	0.1397	0.1862
	Average	0.0580	3.133	0.1577	0.2323
Teejet [®] Twinjet 80-03 [1.00–1.40 lpm]	1.15	0.0267	2.322	0.0806	0.1010
	1.35	0.0277	2.052	0.0664	0.1033
	Average	0.0272	2.187	0.0735	0.1022
Wilger COMBO-JET [®] ER80-03 [0.80–1.50 lpm]	0.95	0.0651	6.853	0.2139	0.1990
	1.15	0.0162	1.409	0.0611	0.0586
	1.35	0.0232	1.719	0.0623	0.0912
	1.55	0.0621	4.006	0.2014	0.2357
	Average	0.0416	3.497	0.1347	0.1461
Teejet [®] XRC80-06 [1.40–2.75 lpm]	1.95	0.1168	5.990	0.4338	0.3296
	2.15	0.0306	1.423	0.0789	0.1089
	2.35	0.0252	1.072	0.0729	0.0969
	2.55	0.0236	0.925	0.0595	0.0851
	2.75	0.0269	0.978	0.0682	0.0978
	2.95	0.0405	1.373	0.1158	0.1557
	Average	0.0446	1.960	0.1427	0.1437
Teejet [®] XRC80-04 [0.90–1.85 lpm]	1.15	0.1065	9.261	0.3709	0.3372
	1.35	0.0254	1.881	0.0823	0.0924
	1.55	0.0189	1.219	0.0557	0.0638
	1.75	0.0163	0.931	0.0439	0.0595
	1.95	0.0257	1.318	0.0613	0.1019
	2.15	0.0423	1.967	0.1063	0.1644
	Average	0.0386	2.763	0.1228	0.1310

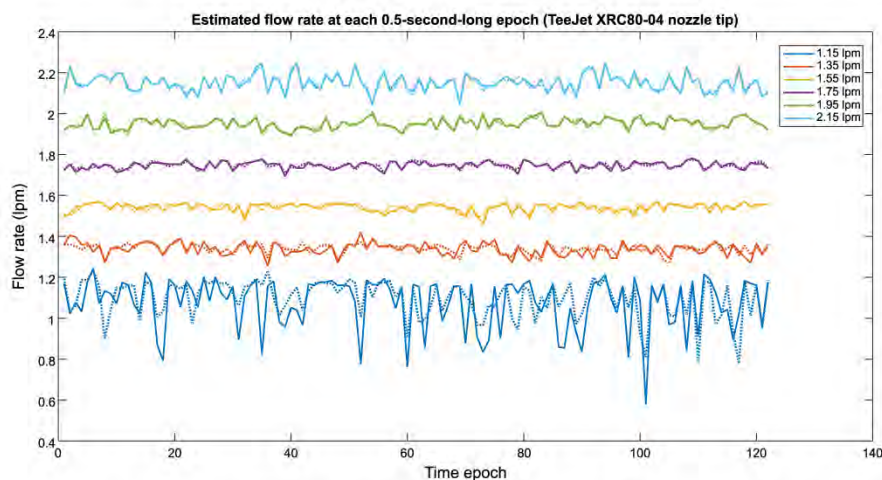


Fig. 6. Comparison of the flow rate estimation results for each of the 122 0.5-second-long epochs while the flow rate was kept constant and the microphones were 6 cm from the TeeJet® XRC80-04 nozzle tip. The solid and dotted lines represent the results for the high-end microphone (Knowles BL-21994-000) and the low-end microphone (CUI CMC-5044PF-A), respectively.

Table 3

Accuracy results of the proposed flow rate estimation method for the TeeJet® XRC80-04 nozzle tip. At the left side of the slash symbol (/), those results obtained employing the high-end microphone (Knowles BL-21994-000). At the right side of the slash symbol (/), those results obtained employing the low-end microphone (CUI CMC-5044PF-A).

Actual flow rate (lpm)	Absolute RMSE (lpm)	Maximum absolute error (lpm)	95% interpercentile range (lpm)	Correlation coefficient
1.15	0.1467/0.1065	0.5696/0.3709	0.4300/0.3372	0.6065
1.35	0.0334/0.0254	0.0958/0.0823	0.1214/0.0924	0.6574
1.55	0.0223/0.0189	0.0920/0.0557	0.0779/0.0638	0.8284
1.75	0.0182/0.0163	0.0568/0.0439	0.0698/0.0595	0.8880
1.95	0.0254/0.0257	0.0579/0.0613	0.0926/0.1019	0.9531
2.15	0.0415/0.0423	0.1077/0.1063	0.1633/0.1644	0.9700
Average	0.0479/0.0386	0.1633/0.1228	0.1592/0.1310	0.8172

Table 4

Accuracy results of the proposed flow rate estimation method for the Wilger COMBO-JET® MR80-04 nozzle tip. At the left side of the slash symbol (/), those results obtained employing the high-end microphone (Knowles BL-21994-000). At the right side of the slash symbol (/), those results obtained employing the low-end microphone (CUI CMC-5044PF-A).

Actual flow rate (lpm)	Absolute RMSE (lpm)	Maximum absolute error (lpm)	95% interpercentile range (lpm)	Correlation coefficient
1.15	0.1274/0.0689	0.2119/0.2065	0.3314/0.2550	0.4103
1.25	0.0786/0.0487	0.1821/0.1570	0.2429/0.2201	0.5084
1.35	0.0746/0.0455	0.1878/0.1291	0.2574/0.1695	0.4996
1.45	0.0842/0.0462	0.1941/0.1407	0.2522/0.1626	0.5489
1.55	0.0723/0.0318	0.1787/0.0887	0.2881/0.1353	0.6093
1.65	0.0645/0.0331	0.1799/0.1028	0.2373/0.1228	0.6910
1.75	0.0512/0.0280	0.1796/0.0688	0.2014/0.1053	0.6188
1.85	0.0442/0.0280	0.1308/0.0925	0.1796/0.1150	0.6114
1.95	0.0516/0.0262	0.1346/0.0667	0.2071/0.1010	0.6583
Average	0.0721/0.0396	0.1755/0.1170	0.2442/0.1541	0.5729

Table 5

Accuracy results of the proposed flow rate estimation method for the TeeJet® AIX110-03 nozzle tip. At the left side of the slash symbol (/), those results obtained employing the high-end microphone (Knowles BL-21994-000). At the right side of the slash symbol (/), those results obtained employing the low-end microphone (CUI CMC-5044PF-A).

Actual flow rate (lpm)	Absolute RMSE (lpm)	Maximum absolute error (lpm)	95% interpercentile range (lpm)	Correlation coefficient
1.15	0.0439/0.0289	0.1179/0.0726	0.1887/0.1094	0.4996
1.35	0.0311/0.0263	0.1038/0.0733	0.1178/0.0956	0.5084
1.55	0.0290/0.0220	0.0785/0.0602	0.1030/0.0815	0.7467
1.70	0.0282/0.0255	0.0687/0.0658	0.1154/0.0931	0.8020
Average	0.0331/0.0257	0.0922/0.0680	0.1312/0.0949	0.6392

results highlight the lack of statistically significant differences between both microphones, at a significance level of $\alpha = 0.05$, for the TeeJet® XRC80-04 and TeeJet® AIX110-03 nozzle tips. Nevertheless, statistically significant differences do appear for the Wilger COMBO-JET® MR80-04 nozzle tip.

3.3. Accuracy comparison for different nozzle-to-microphone distances

In this subsection, an accuracy comparison of the proposed method for different nozzle-to-microphone separation distances is provided while using the low-end microphone (CUI CMC-5044PF-A).

Table 6 shows the accuracies for the Wilger COMBO-JET® MR80-04 nozzle tip at different distances: 6, 12, and 18 cm. Fig. 7 shows the absolute RMSE of the estimation for different flow rates at the three tested distances. In general, a gradual degradation of the accuracy can be observed as distance is increased. This degradation is higher for the lowest flow rates, probably due to the fact that the generated signal has less intensity and the acoustic noise floor masks the signal of interest. Nevertheless, this degradation is almost negligible for the rest of the higher flow rates, as long as the distances are kept close enough.

4. Discussion

This article investigates the feasibility of using microphones as flowmeters for nozzle tips in agricultural sprayers. For this end, a flow rate estimation method is proposed for each individual nozzle tip by processing the generated acoustic signal acquired by a microphone located near the nozzle. The main finding from this article is that accurate real-time flow rate estimation for individual nozzle tips can be achieved by employing acoustic signal processing.

Seven major findings can be highlighted from this study: (i) the nozzle-generated acoustic signal contains enough information to enable accurate flow rate estimation by applying signal processing techniques; (ii) the proposed method can be used to estimate the flow rate of individual nozzles in a low-cost way with a high accuracy in a laboratory environment; (iii) the flow rate estimation becomes less accurate when operating outside the flow range recommended by the nozzle manufacturer; (iv) the proposed method can be used to estimate the flow rate in real time with a demonstrated update frequency of 2 Hz; (v) consistent results can be obtained when using a low-end microphone instead of a more expensive high-end microphone; (vi) the frequency band between 1450 Hz and 1950 Hz provided the best results; and (vii) the nozzle-to-microphone distance is not critical for the method to work accurately, but specific calibrations are required for each distance.

The first finding is that the nozzle-generated acoustic signal contains enough information to enable accurate flow rate estimation. This general conclusion can be derived from the particular results achieved with the proposed method. It is evident that the generated acoustic signal contains information related to the flow rate through the nozzle tip, and many processing techniques can be proposed for this end. Similar conclusions regarding this relationship have been found in previous studies. Jacobs et al. (2015) already proved that the sound of water flowing through a tap can be used to estimate the actual flow rate. Kakuta et al. (2012) demonstrated that a condenser microphone can be used as a vibration sensor in pipelines in order to measure flow rates. Evans et al. (2004) also employed flow-induced mechanical vibrations in the pipe, acquired with an accelerometer, to estimate flow rates. Nevertheless, the present article complements the aforementioned studies by addressing sprayer nozzles where the flow is actually exiting a closed system in a controlled manner.

The second finding is that the proposed method can be used to estimate the flow rate of individual nozzles in a low-cost way with

Table 6
Accuracy results for the Wilger COMBO-JET® MR80-04 nozzle tip using the low-end microphone (CUI CMC-5044PF-A) at different distances.

Distance from nozzle tip to microphone	Actual flow rate (lpm)	Absolute RMSE (lpm)	Maximum absolute error (lpm)	95% interpercentile range (lpm)
6 cm	1.15	0.0689	0.2065	0.2550
	1.25	0.0487	0.1570	0.2201
	1.35	0.0455	0.1291	0.1695
	1.45	0.0462	0.1407	0.1626
	1.55	0.0318	0.0887	0.1353
	1.65	0.0331	0.1028	0.1228
	1.75	0.0280	0.0688	0.1053
	1.85	0.0280	0.0925	0.1150
	1.95	0.0262	0.0667	0.1010
	Average	0.0396	0.1170	0.1541
12 cm	1.15	0.2674	0.6120	0.6815
	1.25	0.0428	0.1699	0.1382
	1.35	0.0724	0.1761	0.2682
	1.45	0.0682	0.1704	0.2696
	1.55	0.0489	0.1682	0.1617
	1.65	0.0311	0.1042	0.1278
	1.75	0.0337	0.1185	0.1302
	1.85	0.0313	0.0860	0.1127
	1.95	0.0372	0.1140	0.1543
	Average	0.0703	0.1910	0.2271
18 cm	1.15	0.2755	0.5863	0.7789
	1.25	0.0885	0.3251	0.2738
	1.35	0.1081	0.2134	0.2964
	1.45	0.1148	0.2178	0.3070
	1.55	0.0503	0.2163	0.2206
	1.65	0.0355	0.1008	0.1369
	1.75	0.0463	0.1435	0.1704
	1.85	0.0344	0.0896	0.1359
	1.95	0.0325	0.1034	0.1435
	Average	0.0873	0.2218	0.2737

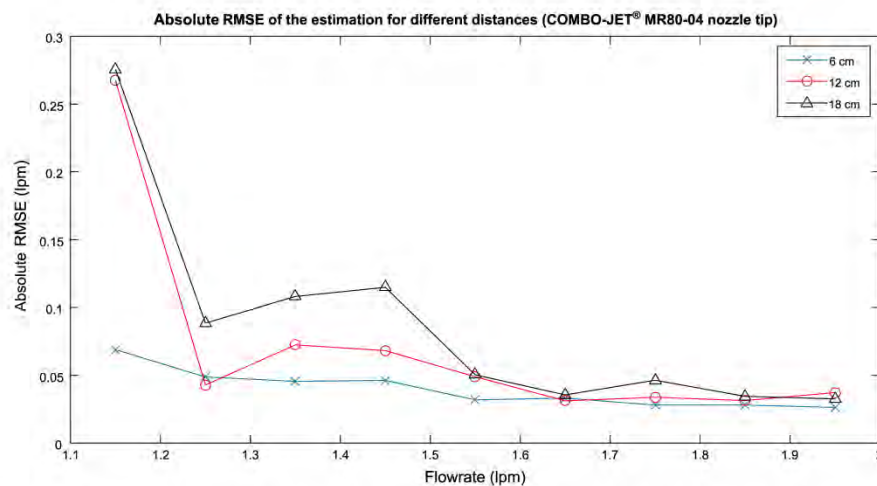


Fig. 7. Comparison of the absolute RMSE estimation accuracy at several flow rates for different nozzle-to-microphone distances using the Wilger COMBO-JET® MR80-04 nozzle tip and the low-end microphone (CUI CMC-5044PF-A).

a high accuracy in a laboratory environment. The results presented in Section 3, mainly Table 2, support this finding, since for all the tested nozzles the average absolute and relative RMSE values are always below 0.08 lpm and 5%, respectively. Moreover, for flow rates lying within the manufacturer recommended operating ranges, the absolute and relative RMSE values are even lower, bounded below 0.05 lpm and 2.5%, respectively. Comparing these results with the ones obtained by Jacobs et al. (2015), significantly better absolute accuracies and slightly better relative accuracies are achieved with the proposed method. However, it is worth noting that both studies are not quite comparable due to the use of nozzle tips versus faucets or taps and also since flow rate ranges are very different in both articles. The flow rate estimation accuracies obtained with the proposed acoustic method are close enough to some of the traditionally used flowmeters, whose relative RMSE errors can reach 4% (Kohlmann, 2004; *Liquid Flowmeters – A Guide for Selecting a Flowmeter for Pressurized Systems*). It should be noted that these studies were conducted in a relatively controlled laboratory environment; thus, the reproducibility of these accuracies in real agricultural settings has yet to be verified.

The third finding is that the flow rate estimation becomes more difficult, *i.e.* the errors increase, for either very low or very high flow rates, when operating outside the flow range recommended by the nozzle manufacturer. This behavior can be noticed in Table 2 for almost every single nozzle. One possible explanation for this behavior is the fact that the spray deposition pattern and output droplet size distribution of the nozzles changes appreciably outside of the manufacturer recommended range, which will consequently change the acoustic signature. The increased difficulty in estimation could also be due to the acoustic signals being more similar in these extreme cases. This effect is even more noticeable for low flow rates due to the inherently lower intensity of the nozzle-generated signal. This lower intensity leads to the acoustic noise floor being relatively stronger with respect to the signal of interest, thus making the estimation more difficult. Nevertheless, it has been checked that, in the recommended operating flow rate ranges given by the nozzle manufacturers, the proposed method presents satisfactory accuracies. No similar findings about lower estimation capabilities for extreme flow rates have been detected in previous studies, to the best of the authors' knowledge. Further

studies should be conducted to provide more insight regarding the reasons behind this behavior.

The fourth finding is that the proposed method can work in real time. This method, when executed in post-processing in MATLAB®, requires less than five seconds to process the 61-second-long recordings for 10 flow rates, where the reported times were obtained in the aforementioned laptop (Dell Latitude E6400). This execution time, less than 0.01 s for each single epoch, shows the feasibility of performing all the necessary tasks between the acquisitions of two consecutive epochs, which is 0.5 s. It is worth remarking that no explicit code optimization was done and the computational efficiency of the method could be further improved for real-time operation.

The fifth finding is that consistent results, with neither significant improvements nor detriments, can be obtained when using a high-end or a low-end microphone. The results presented in Section 3.2 prove that the high-end microphone does not outperform the low-end microphone. Furthermore, the measurements provided by both are coherent (Fig. 6), since moderate (0.40–0.59), strong (0.60–0.79) or very strong (0.80–1.0) positive correlations were found (Tables 3–5). Additionally, the reported p-values from the Welch's *t*-test showed no statistically significant differences between both microphones for two out of the three tested nozzles. The fact that the proposed method is highly independent of microphone quality makes it economically feasible to replicate flow sensors across a large boom with many nozzles. Notwithstanding, this finding should be checked more in detail in later studies, employing a wider variety of high-end and low-end microphones.

The sixth finding is that the frequency band between 1450 Hz and 1950 Hz provided the best accuracies. Several bandwidths were tested, and a bandwidth of 500 Hz was found to be the best because it gave acceptable accuracies and was narrow enough to avoid excessive wideband interferences. Looking over the frequencies from 0 Hz to 50 kHz, the band from 1450 Hz to 1950 Hz contained more information than any other related to the flow rate.

The seventh finding is that the method accuracy does not depend too much on the nozzle-to-microphone distance. The results in Fig. 7 and Table 6 show a tendency of a slow but progressive accuracy degradation as distance is increased. Only distances over 6 cm were tested in order to prevent the microphones from

getting wet and thus being damaged. Moreover, since specific calibrations are required for each distance, it is worth noting that the proposed method will require strict control of microphone location while operating.

The major strength of the proposed method is the low-cost of its design, requiring for its deployment only a low-end microphone and a microcontroller-based computing platform. Another strength of the proposed estimation method is that it can work in real time. Another remarkable feature of the estimation method is the oscillatory behavior observed in Fig. 6, which highlights the possibility of the integral errors in flow rate compensating over time. Thus, an even lower error can be achieved in terms of the cumulative volume applied to the whole plot of land that is being sprayed.

Nevertheless, there are also some limitations to this work. Each nozzle tip requires its own calibration since no singular curve could be fitted accurately for all nozzle tips. Moreover, since the flow rate estimation method is dependent on the nozzle-to-microphone distance, as acoustic power decreases with distance, a new calibration process is mandatory when this distance is varied. However, a simple straightforward calibration can be used in this case, requiring just the determination of the in-band power for highest and lowest flow rates for the normalization stage.

The low-cost sensing method evaluated in this study will bring tremendous benefits to the agricultural chemical application industry. It will be economically feasible to replicate this sensor at every nozzle along a large spray boom to facilitate monitoring and closed-loop control of flow rate from each individual nozzle tip. This will greatly increase the accuracy of placement of chemicals in the field and will prevent much of the errors and inconsistencies currently observed in field application equipment.

Future research related to this article could tackle the evaluation, and almost certainly improvement, of this method in real agricultural settings. More research on how to avoid acoustic interferences in real agricultural settings is needed as well. It is expected that interferences in real agricultural settings, e.g. acoustic noise generated by machinery and wind, can affect the performance of this method. The authors of this paper are currently undertaking new studies in this line of research, investigating about more advanced processing techniques as well as the use of arrays of microphones to avoid the negative effects of unwanted interferences.

Further studies are also required to gain more insight into where the sound enabling flow rate estimation comes from. Five possible sources for the generated acoustic signal have been identified while performing the experiments of this study: (i) turbulences generated by cavities inside the pipe-nozzle interface, (ii) droplet formation in the nozzle-air interface, (iii) acoustic radiation generated by mechanical vibrations of the nozzle or the pipe, (iv) residual elasticity of the nozzle tip outlet that makes its vibration dependent on the flow rate, which acts as an excitation force, (v) finite compressibility of the liquid, and (vi) cross section changes and presence of orifice plates along pipes or the nozzle. This article does not focus on identifying which of these sources have a predominant effect in the observed acoustic signature, but the authors of this paper are working on a follow-up study investigating the sound generation process for nozzle tips by using *Computational Fluids Dynamics (CFD)* simulations.

5. Conclusions

The results from this study support the feasibility of accurately estimating, in real time, the flow rate through agricultural sprayer nozzles based on the acoustic signal recorded in close proximity to them. While employing the proposed method, satisfactory accuracies with relative RMSE values below 5% are obtained under labo-

ratory conditions. Furthermore, the distance from the nozzle tip to the microphone has not been shown to be overly influential, but the shortest distance does generally provide the most accurate results. In addition, the quality of the microphone device seems to have little influence on the overall accuracy of this method. Nevertheless, the results achieved in this article should be confirmed through field tests in agricultural environments. Deeper theoretical insight into acoustic signal generation in nozzle tips and its relationship with flow rate is also needed.

Acknowledgments

The tests conducted in this study could be performed thanks to two three-month-long visiting scholarships granted by the University of Valladolid to both Víctor Martínez-Martínez and Ruben Ruiz-Gonzalez. Furthermore, during all the stages of this study, they were both funded by a Formación de Personal Investigador program grant, financed by the University of Valladolid (Spain) and co-financed by Banco Santander. The authors would also like to express their sincere gratitude to the Writing Center of the University of Kentucky (USA), with a special mention to Leslie C. Davis, for their valuable help with the language editing and proof-reading of the article.

Author contribution

Timothy S. Stombaugh conceived the original idea; Timothy S. Stombaugh, Víctor Martínez-Martínez and Ruben Ruiz-Gonzalez designed the experiments; Ruben Ruiz-Gonzalez performed the experiments; Ruben Ruiz-Gonzalez and Víctor Martínez-Martínez proposed the acoustic estimation method and analyzed the experimental data under the supervision and guidance of Jaime Gomez-Gil and Timothy S. Stombaugh; all four coauthors collaboratively wrote the paper. All authors have approved the final version of this article.

Conflict of interest

The authors declare no conflict of interest.

References

- Cann, G.E., Leehey, P., The acoustic source created by turbulent flow over orifices and louvers. Massachusetts Inst. of Tech., Cambridge.
- CUI CMC-5044PF-A electret microphone datasheet. Available online: <http://www.cui.com/product/resource/cmc-5044pf-a.pdf> (accessed on 18 July 2017).
- Druault, P., Gloerfelt, X., Mervant, T., 2011. Investigation of flow structures involved in sound generation by two- and three-dimensional cavity flows. *Comput. Fluids* 48, 54–67.
- Evans, R.P., Blotter, J.D., Stephens, A.G., 2004. Flow rate measurements using flow-induced pipe vibration. *J. Fluids Eng.* 126, 280–285.
- Gil, E., Llorens, J., Llop, J., Fàbregas, X., Escolà, A., Rosell-Polo, J.R., 2013. Variable rate sprayer. Part 2 – vineyard prototype: design, implementation, and validation. *Comp. Electron. Agric.* 95, 136–150.
- Gopala Pillai, S., Tian, L., Zheng, J., 1999. Evaluation of a flow control system for site-specific herbicide applications. *Trans. ASAE* 42, 863–870.
- Howe, M.S., 2004. Mechanism of sound generation by low Mach number flow over a wall cavity. *J. Sound Vib.* 273, 103–123.
- Hughes, K.L., Frost, A.R., 1985. A review of agricultural spray metering. *J. Agric. Eng. Res.* 32, 197–207.
- Hui, L., Heping, Z., Yue, S., Yu, C., Ozkan, H.E., 2014. Development of digital flow control system for multi-channel variable-rate sprayers. *Trans. ASABE* 57, 273–281.
- Jacobs, H., Skibbe, Y., Booyens, M.J., Makwiza, C., 2015. Correlating sound and flow rate at a tap. *Proc. Eng.* 119, 864–873.
- Kakuta, H., Watanabe, K., Kurihara, Y., 2012. Development of vibration sensor with wide frequency range based on condenser microphone – estimation system for flow rate in water pipes. *World Acad. Sci. Eng. Technol. – Int. J. Mech. Aerosp. Ind. Mechatron. Manuf. Eng.* 6, 2267–2272.
- Knowles BL-21994-000 microphone datasheet. Available online: www.digikey.es/product-detail/es/knowles/BL-21994-000/423-1002-ND/458513 (accessed on 18 July 2017).

- Kobayashi, T., Takami, T., Miyamoto, M., Takahashi, K., Nishida, A., Aoyagi, M., 2009. 3D Calculation with compressible LES for sound vibration of Ocarina. In ArXiv e-prints.
- Kohlmann, M., 2004. Selecting the right flowmeter for the job. *Chem. Eng.* 111, 60–64.
- Liquid Flowmeters – A Guide for Selecting a Flowmeter for Pressurized Systems. Available online: <http://www.ecy.wa.gov/programs/wr/measuring/images/pdf/gsfps.pdf> (accessed on 18 July 2017).
- Loghavi, M., Behzadi Mackvandi, B., 2008. Development of a target oriented weed control system. *Comp. Electron. Agric.* 63, 112–118.
- Michael, R.B., Weber, J.B., Len, R.S., 1990. Efficacy of selected herbicides as influenced by soil properties. *Weed Technol.* 4, 279–283.
- Mulla, D.J., 2013. Twenty five years of remote sensing in precision agriculture: key advances and remaining knowledge gaps. *Biosys. Eng.* 114, 358–371.
- Nordmeyer, H., Hausler, A., Niemann, P., 1997. Patchy weed control as an approach in precision farming. In: *Precision Agriculture 1997*, Proceedings of the 1st European Conference on Precision Agriculture, pp. 307–314.
- Sheen, S.C., 2011. Noise generated by multiple-jet nozzles with conical profiles. *Int. J. Occup. Saf. Ergon.* 17, 287–299.
- Technical Data for Alicat LC & LCR Liquid Flow Controllers. Available online: http://www.alicat.com/documents/specifications/Alicat_Liquid_Controller_Specs.pdf (accessed on 18 July 2017).
- TeeJet® nozzle tips manufacturer webpage. Available online: <http://www.teejet.com/> (accessed on 18 July 2017).
- Testud, P., Aurégan, Y., Moussou, P., Hirschberg, A., 2009. The whistling potentiality of an orifice in a confined flow using an energetic criterion. *J. Sound Vib.* 325, 769–780.
- Testud, P., Moussou, P., Hirschberg, A., Aurégan, Y., 2007. Noise generated by cavitating single-hole and multi-hole orifices in a water pipe. *J. Fluids Struct.* 23, 163–189.
- Wilger Industries Ltd. nozzle tips manufacturer webpage. Available online: <http://www.wilger.net/> (accessed on 18 July 2017).
- Zhang, Z., Mongeau, L., Frankel, S.H., Thomson, S., Park, J.B., 2004. Sound generation by steady flow through glottis-shaped orifices. *J. Acoust. Soc. Am.* 116, 1720–1728.

III Articles out of the compendium

The third chapter of this document presents other published articles outside the three articles comprising the compendium of publications, published as a result of the research. Each section will contain a brief introduction to the article. The articles have been published in JCR-indexed peer-reviewed journals of the first quartile of its category.

Article 4: Vehicle tracking monitoring

This article tackles also the **vehicle tracking monitoring** problem, previously described in chapter “Introduction to the compendium”. The main bibliographic data about this article is shown below:

- Title: A Kalman Filter Implementation for Precision Improvement in Low-Cost GPS Positioning of Tractors.
- Authors: Jaime Gomez-Gil; Ruben Ruiz-Gonzalez; Sergio Alonso-Garcia; Francisco Javier Gomez-Gil
- Journal: Sensors
- Editor: MDPI
- Impact factor: 2.048 (2013)
- Journal Ranking:
 - Q1 on *Instruments & Instrumentation* (10/57).
 - Q2 on *Chemistry, Analytical* (36/76).
 - Q3 on *Electrochemistry* (15/27).
- Date of publication: November 8th, 2013.
- ISSN: 1424-8220.
- Volume (Issue): 13 (11).
- Pages: 15307-15323.
- DOI: 10.3390/s131115307
- URL: <https://www.mdpi.com/1424-8220/13/11/15307>.
- Number of cites: 34.

Article 5: Predictive maintenance monitoring

This article tackles also the **predictive maintenance monitoring** problem, previously described in chapter “Introduction to the compendium”. The main bibliographic data about this article is shown below:

- Title: An Artificial Neural Network based expert system fitted with Genetic Algorithms for detecting the status of several rotary components in agro-industrial machines using a single vibration signal.
- Authors: Víctor Martínez-Martínez; Jaime Gomez-Gil; Francisco Javier Gomez-Gil; Ruben Ruiz-Gonzalez
- Journal: Expert Systems with Applications
- Editor: Elsevier
- Impact factor: 2.981 (2015)
- Journal Ranking:
 - Q1 on *Operations Research & Management Science* (6/82).
 - Q1 on *Engineering, Electrical & Electronic* (27/257).
 - Q1 on *Computer Science, Artificial Intelligence* (19/130).
- Date of publication: April 17th, 2015.
- ISSN: 0957-4174.
- Volume (Issue): 42 (17-18).
- Pages: 6433-6441.
- DOI: 10.1016/j.eswa.2015.04.018
- URL: <https://www.sciencedirect.com/science/article/pii/S0957417415002481>.
- Number of cites: 21.

Bibliography

- Campbell, C., & Cristianini, N. (1998). Simple learning algorithms for training support vector machines. In: University of Bristol.
- Campbell, C., & Ying, Y. R. J. Brachman & T. Dietterich, (Eds.). (2011). *Learning with Support Vector Machines* (1st ed.). San Rafael, CA: Morgan & Claypool Publishers.
- Caron, F., Duflos, E., Pomorski, D., & Vanheeghe, P. (2006). GPS/IMU data fusion using multisensor Kalman filtering: introduction of contextual aspects. *Information Fusion*, 7, 221-230.
- Cortes, C., & Vapnik, V. (1995). Support-vector networks. *Mach. Learn.*, 20, 273-297.
- Ferris, M. C., & Munson, T. S. (2006). Interior-point methods for massive support vector machines. *SIAM J. Optim.*, 13, 783-804.
- Han, T., & Yang, B.-S. (2006). Development of an e-maintenance system integrating advanced techniques. *Computers in Industry*, 57, 569-580.
- Haykin, S. (1998). *Neural Networks: A Comprehensive Foundation* (2nd ed.). New Jersey, USA: Prentice Hall PTR.
- Hsu, C.-W., & Lin, C.-J. (2002). A comparison of methods for multiclass support vector machines. *IEEE Trans. Neural Netw.*, 13, 415-425.
- Jain, A. K., Duin, R. P. W., & Mao, J. (2000). Statistical pattern recognition: a review. *IEEE Trans. Pattern Anal. Mach. Intell.*, 22, 4-37.
- Jardine, A. K. S., Lin, D., & Banjevic, D. (2006). A review on machinery diagnostics and prognostics implementing condition-based maintenance. *Mechanical Systems and Signal Processing*, 20, 1483-1510.
- Kalman, R. E. (1960). A new approach to linear filtering and prediction problems. *Journal of basic Engineering*, 82, 35-45.
- Keicher, R., & Seufert, H. (2000). Automatic guidance for agricultural vehicles in Europe. *Computers and Electronics in Agriculture*, 25, 169-194.
- Kotsiantis, S. B. (2007). Supervised Machine Learning: A Review of Classification Techniques. *Informatica*, 31, 249-268.
- Liakos, K. G., Busato, P., Moshou, D., Pearson, S., & Bochtis, D. (2018). Machine learning in agriculture: A review. *Sensors*, 18, 2674.

- Melendez-Pastor, C., Ruiz-Gonzalez, R., & Gomez-Gil, J. (2017). A data fusion system of GNSS data and on-vehicle sensors data for improving car positioning precision in urban environments. *Expert Systems with Applications*, *80*, 28-38.
- Platt, J. C. (1998). Chapter 12: Fast training of support vector machines using sequential minimal optimization. In B. Schölkopf, C. J. C. Burges & A. J. Smola (Eds.), *Advances in Kernel Methods: Support Vector Learning* (1st ed.). Cambridge: MIT Press.
- Platt, J. C. (Abril 1998). Sequential minimal optimization: A fast algorithm for training support vector machines. In: Microsoft Research.
- Ren, J. (2012). ANN vs. SVM: Which one performs better in classification of MCCs in mammogram imaging. *Knowledge-Based Syst.*, *26*, 144–153.
- Ruiz-Gonzalez, R., Gomez-Gil, J., Gomez-Gil, F. J., & Martínez-Martínez, V. (2014). An SVM-Based Classifier for Estimating the State of Various Rotating Components in Agro-Industrial Machinery with a Vibration Signal Acquired from a Single Point on the Machine Chassis. *Sensors*, *14*, 20713-20735.
- Ruiz-Gonzalez, R., Stombaugh, T. S., Martínez-Martínez, V., & Gomez-Gil, J. (2017). An acoustic method for flow rate estimation in agricultural sprayer nozzles. *Computers and Electronics in Agriculture*, *141*, 255-266.
- Ruiz González, R., Gómez Gil, F. J., Gómez Gil, J., Meléndez Pastor, C., & Feijoo García, F. (2016). Estimación del estado mecánico de maquinaria agrícola en funcionamiento mediante el análisis automático de vibraciones. In E. Velasco Sánchez (Ed.), *XXI CONGRESO NACIONAL DE INGENIERÍA MECÁNICA* (pp. 366-373). Elche (Spain): Universidad Miguel Hernández de Elche.
- Sheather, S. (2009). *A modern approach to regression with R*: Springer Science & Business Media.
- Shilton, A., Palaniswami, M., Ralph, D., & Tsoi, A. C. (2005). Incremental training of support vector machines. *IEEE Trans. Neural Netw.*, *16*, 114-131.
- Smith, L., & Shankar, D. The Top Global Trends Driving The Fourth Agricultural Revolution. Available online: <https://www.planet.com/pulse/top-global-trends-fourth-agricultural-revolution/> (accessed on 29 April 2019).
- Staszewski, W. J. (2002). Intelligent signal processing for damage detection in composite materials. *Composites Science and Technology*, *62*, 941-950.
- Steinwart, I., & Christmann, A. (2008). *Support Vector Machines* (1st ed.): Springer Publishing Company, Inc.
- Tellaeché, A., BurgosArtizzu, X. P., Pajares, G., Ribeiro, A., & Fernández-Quintanilla, C. (2008). A new vision-based approach to differential spraying in precision agriculture. *Computers and Electronics in Agriculture*, *60*, 144-155.
- Unser, M., & Aldroubi, A. (1996). A review of wavelets in biomedical applications. *Proceedings of the IEEE*, *84*, 626-638.
- Vapnik, V. N. (1998). *Statistical Learning Theory*. New York: Wiley.
- White, H. (1988). Economic prediction using neural networks: The case of IBM daily stock returns.

Zhang, N., Wang, M., & Wang, N. (2002). Precision agriculture—a worldwide overview. *Computers and Electronics in Agriculture*, 36, 113-132.